

Design and Performance of Highly Skewed Deck Girder Bridges

Pinar Okumus, Ph. D.
Mauricio Diaz Arancibia
University at Buffalo, the State University of New York

Michael G. Oliva, Ph. D.
University of Wisconsin, Madison

WisDOT ID no. 0092-16-05

May 2018



RESEARCH & LIBRARY UNIT



WISCONSIN HIGHWAY RESEARCH PROGRAM

WISCONSIN DOT
PUTTING RESEARCH TO WORK

DISCLAIMER

This research was funded through the Wisconsin Highway Research Program by the Wisconsin Department of Transportation and the Federal Highway Administration under Project 0092-16-05. The contents of this report reflect the views of the authors who are responsible for the facts and accuracy of the data presented herein. The contents do not necessarily reflect the official views of the Wisconsin Department of Transportation or the Federal Highway Administration at the time of publication.

This document is disseminated under the sponsorship of the Department of Transportation in the interest of information exchange. The United States Government assumes no liability for its contents or use thereof. This report does not constitute a standard, specification or regulation.

The United States Government does not endorse products or manufacturers. Trade and manufacturers' names appear in this report only because they are considered essential to the object of the document.

TECHNICAL REPORT DOCUMENTATION PAGE

1. Report No. 0092-16-05	2. Government Accession No.	3. Recipient's Catalog No.	
4. Title and Subtitle Design and Performance of Highly Skewed Deck Girder Bridges		5. Report Date May 2018	
		6. Performing Organization Code	
7. Author(s) Pinar Okumus, Michael G. Oliva, Mauricio Diaz Arancibia		8. Performing Organization Report No. If applicable, enter any/all unique numbers assigned to the performing organization.	
9. Performing Organization Name and Address University at Buffalo, the State University of New York University of Wisconsin, Madison		10. Work Unit No.	
		11. Contract or Grant No. Project No 0092-16-05	
12. Sponsoring Agency Name and Address Wisconsin Department of Transportation Research & Library Unit 4802 Sheboygan Ave. Rm 104, Madison, WI 53707		13. Type of Report and Period Covered Final Report November 2015-May 2018	
		14. Sponsoring Agency Code	
15. Supplementary Notes N/A			
16. Abstract <p>High skew alters load paths and creates unique performance problems. Acute corner deck cracking, bridge racking, overloading or uplifting at bearings, changes in shear and moment reactions can result due to live or thermal loads. This project investigates the performance of bridges in Wisconsin with high skew to identify limits for simplified analysis methods, to evaluate and recommend design details and practices that can mitigate negative impacts of skew on decks and bearings.</p> <p>A literature review, including review of practices in other states, was conducted. Selected bridges were inspected to identify problems unique to skew. One prestressed concrete and one steel girder were tested in-situ to collect data that can validate finite element analyses. Long term (1-year) data were collected on the prestressed concrete bridge. 2-D analyses validated with test data were run to evaluate AASHTO LRFD Bridge Design Specifications girder-line analyses for bridges with varying geometry and details. Analyses were also run to understand displacements and stresses under long term loading.</p> <p>Bridge inspections showed that not all bridges with skew have the problems to the same extent. Although skew increased maximum skew and decreased maximum moments, AASHTO specifications with WisDOT exceptions were able to predict load distribution, albeit with minimal safety margin for some cases. Bridges should be designed to accommodate racking and expansion joint displacements, which can be calculated from longitudinal displacements using geometry. Using mixed bearings over a single pier significantly reduces bridge horizontal displacements and helps control deck cracking. Restraint of deck through full-depth end diaphragms, laterally restrained bearings, or additional reinforcement are expected to worsen deck cracking.</p>			
17. Key Words Load distribution, racking, acute corner cracks, deck cracking, long term loading, analysis methods, girder line, modeling, load testing, mixed bearing, horizontal displacements, bearing forces		18. Distribution Statement No restrictions. This document is available through the National Technical Information Service. 5285 Port Royal Road Springfield, VA 22161	
19. Security Classif. (of this report) Unclassified	20. Security Classif. (of this page) Unclassified	21. No. of Pages 120	22. Price

EXECUTIVE SUMMARY

Objective

The objective of this project is to understand the effects of large skew on bridge analysis, design and service performance. Bridge analysis is affected because large skew alters distribution of loads from deck to girders in girder-deck type bridges. Performance is affected because either loads that cause volumetric changes in superstructure create large deformations at girder ends, or restraint against these volumetric changes create stresses in superstructure. Design details that can control skew effects were investigated.

Problems Associated with Skew

A literature review, interviews with Wisconsin regional bridge maintenance engineers, a survey to New York State bridge maintenance engineers and field inspections revealed the following related to high skew:

- Skew bridge geometries can affect girder live load distribution due to modified load paths. Due to the skewed geometry, the shortest path to supports becomes the region joining obtuse corners of a span. Higher shear forces are seen near obtuse corners, while reduced shear forces are found near acute corners, possibly leading to uplift. In addition, girder moments are reduced with increasing skews. Torsion and negative moments at bridge ends also develop in skewed geometries.
- Superstructure horizontal movements are mainly caused by long-term loading (mainly temperature and shrinkage). These movements have two perpendicular components: longitudinal and lateral movements, and translate into alternative axes components such as parallel-to-(racking) and normal-to- expansion joints. When deformations are allowed, extensive deformations may deteriorate bearing performance, completely close expansion joints, push girders to bear against abutment backwall, break keeper bars attached to bearing plates to prevent lateral movements, and misalign bridges with approach slabs (racking). In addition, substructure deformation directions may not follow that of superstructure. Figure A presents some of these problems.
- When deformations due to volumetric changes are restricted, additional stresses created in superstructure may cause deck cracks, crack abutment girder seats with end diaphragms that restrain lateral movements, or distress bearings. Figure A presents examples of some of these problems.



Figure A. Misaligned girder (left), bent keeper bar (middle, left) misaligned parapet wall and closed expansion joint (middle, right), diagonal acute corner deck cracks (right). [1]

A field inspection of 4 similar bridges with and without skew (0° and 52° skew prestressed concrete; and 3° and 30° skew steel girder) showed that not all bridges with skew have these performance problems.

The scan of state DOT bridge manuals compared to AASHTO LRFD Bridge Design Specifications (BDS) revealed that multiple DOT's disallow moment reduction. Some DOT's limit bulb-tee girders to low skew bridges. Differences are also in deck reinforcement alignment and design methods (traditional vs isotropic).

Field Data and Analytical Model Validation

Experimental data was collected on two girder-deck type bridges to understand bridge behavior and for 2-D finite element analysis (FEA) validation. These bridges were the HAST bridge and the Chippewa Bridge.

The HAST Bridge: The HAST bridge is a prestressed concrete girder bridge with 64° skew, a horizontal curvature, and a mix of expansion and fixed bearings over the same pier. Two types of data were collected on this bridge: 1) under live load, 2) under long-term loading.

- 1) Bending and shear strains on three girders; and bending strains and temperatures in the acute deck corner were measured under live load. These data were compared to 2-D FEA. Due to the small magnitude of strains ($< 25 \mu\epsilon$ for girder shear, $< 50 \mu\epsilon$ for girder bending, and $< 15 \mu\epsilon$ for deck bending), typical for stiff prestressed girders, small deviations in FEA from test data translated into percentage errors as large as 90% and 78% for bending and shear peak strains, respectively. However, when data was converted to “load distribution between tested girders”, FEA was within 30% of test data for peak bending and shear distribution values. Refinements to the validated model included addition of end, pier and intermediate diaphragms, flexible supports, and measured material properties. These refinements lead to FEA being within 20% and 28% of the peak raw strain data for bending and shear, and within 23% and 21% of peak values of bending and shear “load distribution to instrumented girders”, respectively. Figure B (left) is an example comparison of test and FEA results for the validated model for bending strains.
- 2) Girder end displacements at bearings and deck strains were measured over a 1-year period. Maximum girder end displacements were 0.82 in. (at 4 °F) and 0.28 in. (at 87 °F) in the longitudinal and transverse direction of girders, respectively. Installation temperature was 45 °F. Longitudinal displacement data correlated well with temperature fluctuations, unlike transverse displacements. The lack of correlation between temperature and transverse displacements may be due to the small magnitudes for displacements in this direction. With such small magnitudes of displacements, additional factors such as shrinkage, temperature gradients (as opposed to uniform temperature changes), bearing stiffness, stiffness of the reference frames for displacement sensors can dominate the displacement behavior over uniform temperature changes. From simple geometry, large longitudinal displacements have a large component in the racking direction because racking is proportional to the sine of the skew angle, which increases with increasing skew.

At the time of live load testing, the bridge deck did not exhibit visible cracks. However, after one year, some transverse and longitudinal cracking at bridge ends were detected. Measured deck strains during the observation period were highly correlated to temperature, which indicated free deformations taking place at the instrumented points. With the exception of the gage closer to the bridge end, detected cracking showed that monitoring points were not located where restraining stresses developed.

Deck strain measurements displayed that maximum compression and tension strains in the deck were less than $850 \mu\epsilon$ and less than $150 \mu\epsilon$, corresponding to cooling (up to $-4 \text{ }^\circ\text{F}$) and heating (up to $+99 \text{ }^\circ\text{F}$).

The Chippewa Bridge: The Chippewa bridge was a 23-year-old steel girder bridge with 47° skew. This bridge was tested under static live load to understand load distribution and level of composite action. For all girders near load, where measurable strains were collected, neutral axis positions matched theoretical calculations. For all loading configurations, load distribution was lower than predicted by AASHTO LRFD BDS. FEA predicted load distribution well. An example to this is shown in Figure B (right).

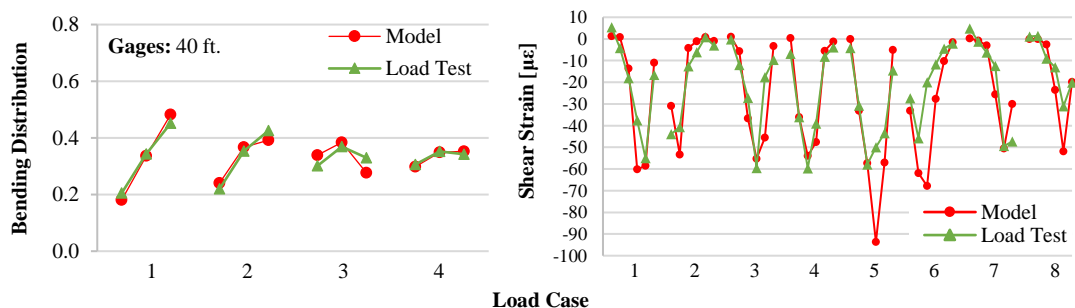


Figure B. Load distribution from FEA and test for HAST bridge (left) and for the Chippewa bridge (right).

Evaluation of AASHTO Load Distribution Factors (1-D modeling)

AASHTO LRFD load distribution factors (girder-line analysis), including WisDOT exceptions, were evaluated for a larger group of bridges with varying skew, secondary bridge elements, and geometry, using

the validated FEA models. These models were created using one of the concrete bridges inspected, and the Chippewa bridge.

Concrete Bridge Inspected as the Base Model: Variables were 0°, 15°, 30°, 45° and 60° skew, end and intermediate diaphragms. For the 60° skew case with no secondary elements, the following were also variables: number of spans, bridge width, girder depth, girder spacing, and deck thickness. The results showed that the maximum reduction in moment and the maximum increase in shear with increasing skew was insignificant (less than 10%), and moderate (less than 29%), respectively. Contribution of end and intermediate diaphragms on load distribution was not significant (less than 4% in bending and 12% in shear). For all geometric parameters studied, AASHTO predicted load distribution 21% and 12% higher than models did for moment on interior and exterior girders, respectively. For shear on interior and exterior girders, AASHTO predicted load distribution factors to be 37% more and 2% less than models did. On exterior girders, shear load distribution factors of AASHTO were slightly un-conservative for several cases, as shown in Figure C (left).

The Chippewa Bridge as the Base Model: Bridges created using the Chippewa bridge as a base model had the same parameters as bridges created using the concrete bridge inspected as the base model. In addition, impact of continuous composite action across span was also investigated. FEA showed that the greatest reduction in moment and increase in shear with increasing skew were less than 17% and 19%, respectively. Secondary bridge member contribution was small (less than 6% in bending and 7% in shear). Load distribution factors predicted by AASHTO, for bridge geometries investigated, were on average 18% and 14% higher than the ones predicted by models, for moment on interior and exterior girders, respectively. AASHTO predictions of load distribution factors was 51% and 34% more than model predictions, for shear on interior and exterior girders, respectively. Figure C (right) shows the shear load distribution factor comparison between FEA and AASHTO as an example.

Even though prestressed concrete and steel bridge base models were slightly conservative since they did not include secondary components (i.e., end and intermediate diaphragms), the need to supplement AASHTO distribution factors with 2-D models of highly skewed bridges was clear to achieve both economical and safe designs.



Figure C. Load distribution comparison between AASHTO and FEA for bridges with varying parameters for the concrete bridge (left) and Chippewa bridge (right).

Evaluation of Displacements under Long-Term Loading

Long-term effects were evaluated using the validated FEA, on the same bridges for which load distribution factors were evaluated. Long-term loading on bridge models consisted of seasonal temperature changes applied to the superstructure only. Negative temperature changes were applied to both prestressed concrete and steel bridges.

Effects of Bridge Skew Angle: Bridge skew angle effects on superstructure horizontal displacements at girder end bearings were investigated on the inspected prestressed concrete and the Chippewa bridges. Skew angles were varied from 0° to 60°, in 15° increments. It was found that increasing skew angles could lead to greater transverse displacements. In addition, rotation tendency on skewed bridges with regular support arrangements over piers was towards obtuse corners for negative changes in temperature, and the opposite for positive changes.

Effects of Bridge Details and Geometry: Effects of bridge details and geometry on girder end displacements (at bearings) were studied on the prestressed concrete bridge inspected and the Chippewa bridge as base models (case 0). Variables studied were the same as ones studied under short-term loading. These bridges were named as cases 1-9. A general trend was not observed in displacement patterns with changing parameters.

Effects of Bearing Fixity Arrangements: The effect of six bearing arrangements on girder end (bearing) displacements were investigated using the HAST bridge and the Chippewa bridge as the base models. Figure D compares displaced shapes. These analyses showed that the mixed bearing fixity arrangement used in the design of HAST bridge (arrangement 6 and 5 in Figure D for HAST and Chippewa, respectively) was the most effective in controlling bearing transverse displacements.

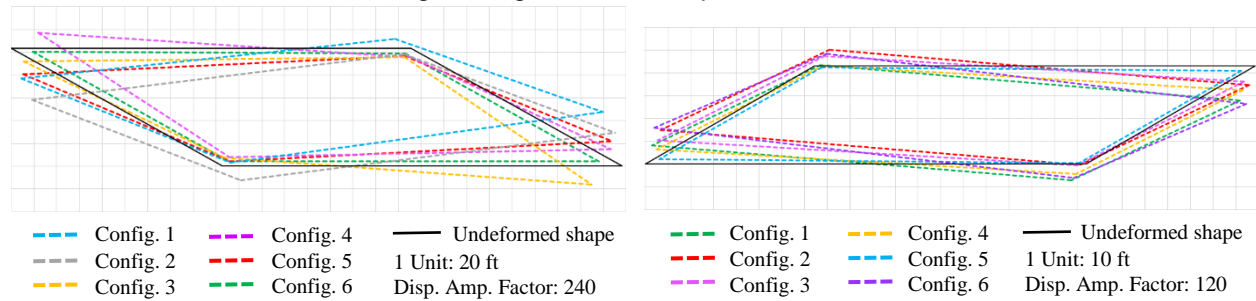


Figure D. Displaced shapes for HAST (left) and Chippewa (right) bridges for varying bearing fixities.

Mixed Bearing Fixity Arrangement Performance: The effect of bridge skew angle, pier stiffness, and length-to-width ratios on the performance of the mixed bearing fixity arrangement was evaluated. The base bridge for this study was the Chippewa Bridge, modified to include this bearing configuration. Results showed that this special fixity arrangement performs better (i.e., leads to greater reductions in transverse displacements) at high skew angles, is less effective when the bridge features hammerhead piers, and that is particularly efficient for moderate length-to-width ratios.

Evaluation of Lateral Bearing Forces under Long-Term Loading

Lateral forces at fixed girder bearings, induced by temperature loading applied to the superstructure, were evaluated using validated bridge models. The effects of different modeling approaches on bearing force predictions, and effects of selected bridge details on peak bearing forces were investigated. Base bridges were the HAST and inspected prestressed concrete bridges.

Modeling Techniques Affecting Fixed Bearing Force Predictions:

It was determined that including pier stiffness and application of thermal changes to piers in the models had the greatest influence on predictions of forces at fixed bearings. For instance, representing piers as infinitely rigid in the models lead to overly conservative bearing forces, and assuming equal thermal changes occurring in both superstructure and piers caused smaller forces in bearings than with models that assumed temperature changes in superstructure only.

Bridge Details Affecting Maximum Forces at Fixed Bearings:

Bridge variables considered were bridge skew angle (0°-60° in 15° increments), bridge geometries studied under short-term loading, and the mixed support configuration. FEA results showed that fixed bearing forces increase with increasing skew angles, that considerably wide bridges may lead to large fixed bearing forces, and that the mixed bearing arrangement did not cause important increases in bearing forces relative to forces on a bridge with regular fixity configuration over piers.

Evaluation of Stresses under Long-Term Loading

Deck stresses were evaluated to understand acute corner deck cracks under shrinkage loading. Temperature strains alone were shown to be too small to initiate cracking and were not considered. Details investigated were end diaphragm and lateral end restraint type, bridge skew angle, and deck reinforcement amount and orientation. The results showed that details that restrain decks (full depth end diaphragms and lateral restraint at bearings) create a larger deck area with plastic strains (indicator for cracking) as shown in Figure E.

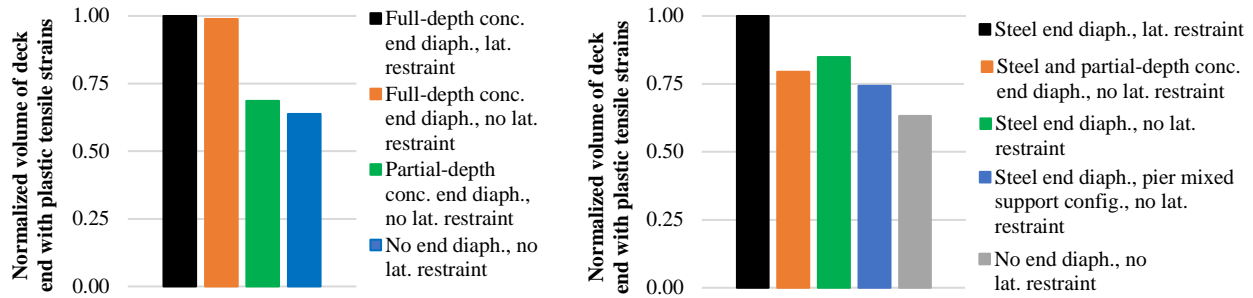


Figure E. Volume of deck elements with plastic strains for concrete (left) and steel girder (right) bridges.

Partial-depth concrete end diaphragms disconnected from the deck, as a crack control measure, did not lead to significant improvements. The severity of cracking was found to increase with greater skew angles. Analysis results showed that orienting reinforcement in skew direction or doubling the reinforcement area caused higher strains in the deck, indicating a higher cracking risk.

Conclusions and Summary

Skew can increase maximum shear and decrease maximum moment in girders. It can cause large horizontal displacements that effect bearings and expansion joints. When these deformations are restrained, deck acute corner cracks may occur.

Bridge load testing showed that load distribution to girders are conservatively estimated by AASHTO using girder-line analyses for both prestressed concrete and steel bridges. 2-D FEA can accurately predict load distribution. Refinements such as addition of secondary members, using 3-D analyses, flexible supports help improve FEA predictions for strains.

Longitudinal girder end displacements correlate well with temperature and were more than 5 times that of transverse displacements with the mixed bearing arrangement used on the HAST bridge. Large longitudinal displacements alone, without transverse displacements, can translate into large racking and expansion joint displacements due to high skew. Bearing pads and expansion joints should be designed using the largest longitudinal displacements calculated using temperature changes. Deck strains are mainly caused by temperature and shrinkage, and not due to live load.

AASHTO girder-line analyses are valid for a group of bridges with 60° skew, and with varying parameters, for prestressed concrete and steel bridges. FEA showed a small decrease in moments and also a small increase in shear reactions in girders with increasing skew. Secondary bridge elements did not contribute to load distribution significantly.

Analysis of bridges with varying geometry under temperature loading did not reveal a consistent change in displacement patterns with changing bridge geometries. On the other hand, bearing arrangements over supports made a significant difference in displacements. Overall, for both prestressed concrete and steel bridges, the mixed bearing arrangement used in the HAST bridge resulted in the smallest transverse displacements.

Predictions of fixed bearing forces on highly skewed bridges featuring the mixed bearing arrangement over piers can be influenced by pier stiffness, and difference in temperatures of superstructure and substructure. High skew angles, and significantly wide bridges can lead to large forces at fixed bearings. The mixed bearing arrangement does not cause important increments in peak bearing forces, in comparison to forces on bridges with regular fixity configurations.

Shrinkage was the main cause of typical diagonal deck cracking on high skew bridges. Temperature changes alone were unable to create deck cracking. The models showed that avoiding bridge details that restrain shrinkage deformations was the best approach to reduce the severity of diagonal cracking. Partial-depth concrete end diaphragms disconnected from the deck did not lead to significantly improved cracking behavior. High skew angles can significantly increase the severity of cracking. Orienting deck reinforcement with skew or increasing deck reinforcement amount adversely affected deck cracking.

Design Recommendations

The following are the design recommendations:

- Girder line analyses of AASHTO LRFD BDS, with WisDOT exceptions, predicted load distribution to girders well for bridges up to 60° skew angle and can be used. For some cases, girder-line analyses did not provide a margin of safety. For this reason, 2-D bridge analyses should be considered to complement girder-line analyses.
- Excluding secondary components and, for steel bridges, non-composite action over piers from 2-D bridge models leads to slightly conservative and similar load distribution predictions, respectively. These components can be excluded for preliminary design.
- WisDOT practice of excluding moment skew correction factors is reasonable and should continue.
- Bearing transverse displacements at high skew angles can be several times the ones occurring in non-skewed bridges. The use of 2-D bridge models is recommended to accurately predict amplified superstructure transverse movements.
- Bridge displacements in racking and normal-to-expansion joint directions should be calculated from geometry using the longitudinal girder displacements obtained from temperature loadings. Girder bearing plates and expansion joints should be large enough to prevent unseating of girders and closing of expansion joints, respectively. In addition, a sufficiently large gap that can accommodate temperature displacements should be left between girder ends and abutment back wall to prevent girders being pushed laterally by the abutment back wall.
- Since racking displacements are proportional to larger longitudinal displacements and the sine of the skew angle, these displacements can be minimized by using prestressed girders that have smaller temperature displacements than steel girders. However, the higher stiffness of prestressed girders may worsen cracking in deck under shrinkage loading.
- For both prestressed concrete and steel bridges, a mixed bearing arrangement over the same pier (half expansion and half fixed, as used in the HAST bridge) should be used to minimize transverse superstructure movements. The following recommendations should be considered when this bearing arrangement is used:
 - The mixed bearing arrangement should be employed on highly skewed bridges (>30°), reviewed on a project-by-project basis for bridges with low skew angles (<30°), and avoided on non-skewed bridges.
 - Pier stiffness can affect the performance of the special fixity arrangement. Including piers in 2-D models is recommended in order to have a reasonable prediction of the mixed arrangement performance. For high skew angles, control of bearing transverse displacements is expected to be significant regardless of pier type with the use of the mixed bearing arrangement. Hammerhead piers benefit from the mixed bearings the least among all pier types investigated.
 - The mixed bearing configuration should be evaluated on a project-by-project basis for significantly wide or long bridges, as these bridges benefit from the mixed bearing arrangements less than other bridges do. Nevertheless, at high skew angles, the mixed bearing arrangement was effective for all bridge geometries.
- Bridge models that exclude piers to estimate fixed bearing forces should be avoided since they could lead to overly conservative bearing forces. Where appropriate, pier flexibility should be included in bridge models to reduce lateral bearing forces to realistic magnitudes. Assuming that superstructure and piers are subject to equal thermal changes may lead to significantly smaller bearing lateral forces. Since this assumption is not conservative, it should be verified.
- Diagonal cracking on highly skewed bridges may be controlled by incorporating the following recommendations:

- The main contributor to diagonal cracking is shrinkage. Concrete mixes and construction practices that control shrinkage are recommended.
- Bridge details that restrain the volumetric concrete contraction caused by shrinkage should be avoided. Full-depth concrete end diaphragms and laterally restrained expansion bearings provide such restraints.
- The mixed bearing arrangement over the same piers improved deck cracking; and should be considered as a crack control method in three-span girder bridges.
- Increasing deck reinforcement amount or orienting deck reinforcement along skew are not effective methods to control diagonal cracking and should not be considered. In fact, increased deck reinforcement may lead to more cracking, since reinforcement also restrains shrinkage.

TABLE OF CONTENT

1. INTRODUCTION	1
1.1. MOTIVATION AND OBJECTIVES.....	1
1.2. SKEW EFFECTS	1
1.3. SCOPE OF THE PROJECT.....	2
1.4. ORGANIZATION OF THE REPORT.....	2
2. LITERATURE REVIEW	4
2.1. SKEW EFFECTS ON BRIDGES.....	4
2.1.1. IMPACT ON LOAD PATHS AND ANALYSIS	4
2.1.2. IMPACT ON BRIDGE DISPLACEMENTS	5
2.1.3. IMPACT ON DECK PERFORMANCE	7
2.1.4. CONSTRUCTABILITY OF STEEL GIRDER BRIDGES	8
2.2. FEEDBACK FROM WISCONSIN BRIDGE MAINTENANCE ENGINEERS.....	8
2.3. FEEDBACK FROM NEW YORK BRIDGE MAINTENANCE ENGINEERS.....	9
2.4. MITIGATING MEASURES FOR SKEW EFFECTS	10
2.4.1. SKEW RELATED PROVISIONS OF AASHTO LRFD BDS.....	10
2.4.2. DIFFERENCES BETWEEN AASHTO LRFD BDS AND STATE DOT PRACTICES	10
2.5. SUMMARY AND CONCLUSIONS.....	13
3. FIELD INSPECTIONS	15
3.1. FIELD INSPECTION OF BRIDGES WITH AND WITHOUT SKEW	15
3.1.1. COMPARISON OF DECK PERFORMANCE	15
3.1.2. COMPARISON OF BRIDGE HORIZONTAL MOVEMENTS	16
3.1.3. COMPARISON OF SUBSTRUCTURE CONDITIONS	19
3.2. FIELD INSPECTION OF LOAD TESTED BRIDGES.....	19
3.3. SUMMARY AND CONCLUSIONS.....	21
4. LOAD TESTING OF HIGHLY SKEWED GIRDER BRIDGES	22
4.1. LOAD TESTING AND MONITORING OF THE PRESTRESSED CONCRETE BRIDGE	22
4.1.1. BRIDGE DESCRIPTION.....	22
4.1.2. SHORT-TERM LOAD TESTING.....	23
4.1.3. LONG-TERM MONITORING	29
4.2. LOAD TESTING OF THE HIGHLY SKEWED STEEL BRIDGE	36
4.2.1. BRIDGE DESCRIPTION.....	36
4.2.2. SHORT TERM LOAD TESTING	37
4.3. SUMMARY AND CONCLUSIONS.....	43
5. FINITE ELEMENT MODELING METHODS AND VALIDATION	46
5.1. FINITE ELEMENT BRIDGE MODELING TECHNIQUES	46
5.1.1. 1-D (Girder-Line) MODELING APPROACH	46
5.1.2. THE GRILLAGE METHOD	46
5.1.3. 2-D BRIDGE MODELING APPROACH	46
5.1.4. 2.5-D BRIDGE MODELING APPROACH	47
5.1.5. 3-D BRIDGE MODELING APPROACH	47
5.1.6. BRIDGE PIERS.....	48
5.2. MATERIAL PROPERTIES	48
5.2.1. CONCRETE MATERIAL PROPERTIES.....	48
5.3. LOADING	48
5.3.1. SHORT-TERM LOADING	48
5.3.2. LONG-TERM LOADING	49
5.4. FINITE ELEMENT MODEL VALIDATION	50
5.4.1. VALIDATION OF PRESTRESSED CONCRETE GIRDER BRIDGE MODELS	50
5.4.2. VALIDATION OF STEEL GIRDER BRIDGE MODELS	53
5.5. IMPACT OF MODEL REFINEMENTS ON ANALYSIS RESULTS.....	55
5.5.1. REFINEMENTS BY SECONDARY BRIDGE MEMBERS AND MATERIAL PROPERTIES	55
5.5.2. REFINEMENTS THROUGH MODELING TECHNIQUES	57
5.6. CONCLUSIONS AND SUMMARY	58

6.	EVALUATION OF GIRDER LINE ANALYSIS METHODS	60
6.1.	PARAMETRIC STUDIES ON PRESTRESSED CONCRETE BRIDGES	60
6.1.1.	EFFECT OF SKEW ANGLE AND SECONDARY BRIDGE ELEMENTS	60
6.1.2.	EFFECT OF BRIDGE GEOMETRY	61
6.2.	PARAMETRIC STUDIES ON STEEL GIRDER BRIDGES	63
6.2.1.	EFFECT OF SKEW ANGLE AND SECONDARY BRIDGE ELEMENTS	63
6.2.2.	EFFECTS OF BRIDGE GEOMETRY	64
6.3.	SUMMARY AND CONCLUSIONS	66
7.	BEARING DISPLACEMENTS UNDER LONG-TERM LOADING.....	67
7.1.	BRIDGE SKEW ANGLE.....	67
7.1.1.	PRESTRESSED CONCRETE BRIDGES WITH VARYING SKEW ANGLES	67
7.1.2.	STEEL BRIDGES WITH VARYING SKEW ANGLE	68
7.2.	BRIDGE DETAILS AND GEOMETRY	69
7.2.1.	PRESTRESSED CONCRETE BRIDGES WITH VARYING BRIDGE DETAILS AND GEOMETRY	69
7.2.2.	STEEL BRIDGES WITH VARYING DETAILS AND GEOMETRY	70
7.3.	BEARING FIXITY ARRANGEMENTS	71
7.3.1.	PRESTRESSED CONCRETE BRIDGES WITH VARYING BEARING FIXITY ARRANGEMENTS.....	72
7.3.2.	STEEL BRIDGES WITH VARYING FIXITY ARRANGEMENTS	73
7.3.3.	FACTORS AFFECTING MIXED BEARING FIXITY ARRANGEMENT PERFORMANCE	73
7.4.	SUMMARY AND CONCLUSIONS.....	76
8.	BEARING FORCES UNDER LONG-TERM LOADING.....	78
8.1.	MODELING TECHNIQUES AFFECTING FIXED BEARING FORCE PREDICTIONS	78
8.1.1.	SUPPORT RIGIDITY	78
8.1.2.	PIER FOUNDATION EFFECTS.....	79
8.1.3.	CAP BEAM AND FIXED BEARINGS CONNECTION EFFECTS	79
8.1.4.	EXPANSION BEARINGS STIFFNESS EFFECTS	80
8.1.5.	PIER TEMPERATURE CHANGE EFFECTS.....	80
8.2.	BRIDGE DETAILS AFFECTING MAXIMUM FIXED BEARING FORCES	81
8.2.1	VARYING SKEW ANGLE	81
8.2.2	VARYING BRIDGE DETAILS AND GEOMETRY	81
8.2.3	VARYING BEARING FIXITY ARRANGEMENTS.....	82
8.3.	SUMMARY AND CONCLUSIONS.....	83
9.	DECK CRACKING UNDER LONG-TERM LOADING.....	84
9.1.	DECK CRACKS	84
9.2.	DECK CRACKING ANALYSIS METHOD AND PARAMETERS	84
9.3.	LOADING	84
9.4.	EFFECT OF BRIDGE END DETAILS ON DECK CRACKS	85
9.4.1.	PRESTRESSED CONCRETE BRIDGES WITH VARYING BRIDGE END DETAILS... 85	
9.4.2.	STEEL BRIDGES WITH VARYING BRIDGE END DETAILS	88
9.4.3.	DISCONNECTED PARTIAL-DEPTH CONCRETE END DIAPHRAGM	90
9.5.	EFFECT OF BRIDGE SKEW ANGLE ON DECK CRACKS	91
9.5.1.	SKEW EFFECTS ON DECK CRACKING OF PRESTRESSED CONCRETE BRIDGES	91
9.5.2.	SKEW EFFECTS ON DECK CRACKING OF STEEL BRIDGES	93
9.6.	EFFECT OF DECK REINFORCEMENT ON DECK CRACKS	95
9.6.1.	PRESTRESSED CONCRETE BRIDGES WITH VARYING DECK REINFORCEMENT 95	
9.6.2.	STEEL BRIDGES WITH VARYING DECK REINFORCEMENT	98
9.7.	SUMMARY AND CONCLUSIONS.....	101
10.	CONCLUSIONS AND RECOMMENDATIONS	102
10.1.	CONCLUSIONS	102
10.1.1.	CONCLUSIONS BASED ON THE LITERATURE REVIEW AND FIELD INSPECTIONS	102
10.1.2.	CONCLUSIONS BASED ON LOAD TESTING.....	102

10.1.3. CONCLUSIONS BASED ON FINITE ELEMENT MODELING METHODS AND VALIDATION.....	103
10.1.4. CONCLUSIONS FOR LOAD DISTRIBUTION UNDER SHORT-TERM LOADS.....	103
10.1.5. CONCLUSIONS FOR GIRDER BEARING DISPLACEMENTS UNDER LONG-TERM LOADS.....	103
10.1.6. CONCLUSIONS FOR DECK CRACKING UNDER LONG-TERM LOADING	104
10.2. DESIGN RECOMMENDATIONS	104
11. REFERENCES	106

1. INTRODUCTION

1.1. MOTIVATION AND OBJECTIVES

Skew is defined as the angle between a line perpendicular to bridge superstructure and supports. In Wisconsin, 30% of bridges built between 1995-2014 had a skew angle larger than 20° [1]. Twenty-two of these bridges had skew angles larger than 60° (Figure 1.1). Although it is well known among the bridge community that the behavior of bridges with high skew is more complex than bridges with no skew; for many bridge projects with tight geometric constraints, skewed supports are the only design solution. As transportation demands increase and undeveloped lands continue to shrink, skew bridges will likely be in higher demand in the future. It is, therefore, important to understand implications of skew on bridge behavior and develop strategies to accommodate skew effects in design.

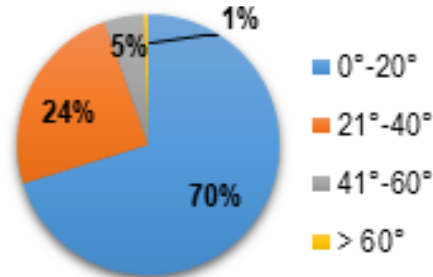


Figure 1.1. Bridges with skew, 1995-2014.

The objective of this project is to understand the effects of large skew on bridge analysis, design and service performance. Bridge analysis is affected because skew alters distribution of loads from deck to girders. Performance is affected because either loads that cause volumetric changes in superstructure create large deformations at girder ends or restraint against these volumetric changes create stresses in superstructure. Finally, design of bridges with high skew is dependent on the bridge community's understanding of structural effects of skew. This project contributed to this understanding to incorporate skew in design.

1.2. SKEW EFFECTS

Skew effects can be categorized into two: 1) effects on load distribution, 2) effects on service performance.

- Effect on load distribution: Skew can affect live load distribution from deck to girders, creating increased shear reactions in girders near obtuse corners and uplift of girders near acute corner. Girder moments are reduced due to change in shortest path to supports. Torsion and negative moments may also be generated in superstructure, even near simple supports. These effects are described in more detail in Chapter 2.1: Skew Effects on Bridges.
- Effects on service performance: Long-term loading such as shrinkage and temperature causes superstructures to deform. When deformations are allowed and are excessive, they may deteriorate bearings, completely close expansion joints or misalign bridges with approach slabs (racking). When deformations are restricted, additional stresses created in superstructure may cause deck to crack, crack end diaphragms with shear keys, or distress bearings. A balance between deformations and stresses is needed to control performance issues. Additional details of long-term effects are discussed in Chapter 2.1: Skew Effects on Bridges. Figure 1.2 displays some of these performance problems.



Figure 1.2. Misaligned girder (left), misaligned parapet wall and closed expansion joint (middle) of B-13-228, diagonal acute corner deck cracks (right) of B-09-212. [1]

1.3. SCOPE OF THE PROJECT

The goal of the project was to reveal impact of skew on analysis, design and performance of bridges. The scope of this project included the following:

- Conduct a literature review on skew effects on bridges, including review of practices of other Departments of Transportation (DOT).
- Document the visible effects of skew on bridge performance by bridge inspections, and scan of bridge inspection data of WisDOT.
- Load test and monitor a prestressed concrete girder bridge and load test a steel girder bridge to understand skew effects and to collect data for analytical model validation.
- Build finite element models of high skew bridges, and validate models using test data.
- Study load distribution on a group of bridges with varying details and geometry using the finite element models. Determine the applicability limits of 1-D (girder-line) and 2-D modeling techniques.
- Study deformations on a group of bridges with varying details and geometry using finite element models. Determine causes of deformations, and identify maximum displacements that can be expected at expansion bearings or joints.
- Study stresses created by restraint against deformations on a group of bridges with varying details and geometry using finite element models. Determine causes of stresses, and identify maximum stresses that can be expected at bearings and decks.
- Study the impact of design details (secondary bridge elements, deck reinforcement details, girder end restraints including mixed bearings over the same support) on deformations and stresses.
- Make design recommendations to account for or control skew effects.

1.4. ORGANIZATION OF THE REPORT

This report is composed of 10 Chapters.

Chapter 2 provides a literature review on skew effects on concrete and steel girder bridges. It also presents an overview of DOT design practices as documented in their bridge design manuals. These practices are compared to provisions of AASHTO LRFD BDS related to skew to identify state exceptions to AASHTO LRFD BDS.

Chapter 3 summarizes the results of field inspections on four similar bridges with and without skew. Two of these bridges had prestressed concrete girders. The other two had steel girders. In addition, observations on high skew prestressed concrete and steel bridges that were load tested are included in this chapter.

Chapter 4 presents load test and monitoring of a 64° skew prestressed concrete bridge (called the HAST bridge) and load test of a 47° skew steel girder bridge (called the Chippewa Bridge). Bending and strain data under live load are given for both bridges. Deck strain and girder end deformation data collected over 1 year are presented for the prestressed concrete bridge.

Chapter 5 gives the details of finite element methods employed in this study, validation of finite element models of tested HAST and Chippewa Bridges, refinements to models needed to achieve better correlation with test data, and a discussion on balance between accuracy and computational efficiency.

Chapter 6 presents finite element results on a large group of bridges under short-term loading. Bridge models were created using one of the prestressed concrete bridges inspected in Chapter 3 and the steel Chippewa Bridge as base bridges. Variables included varying skew angles, secondary elements (end diaphragms, intermediate diaphragms), bridge geometry and deck-concrete composite action. Included is an evaluation of AASHTO LRFD BDS load distribution factors for these bridges.

Chapter 7 includes bearing displacements at girder ends obtained by finite element results on a large group of bridges under long-term loading. The same bridges studied in Chapter 6 were subjected to temperature loads. Variables also included bridge skew angle, and different bearing fixity arrangements. Bridge details that could affect the performance of the mixed bearing arrangement are investigated.

Chapter 8 evaluates fixed bearing forces caused by thermal loading on highly skewed prestressed concrete bridges. Modeling techniques that could affect bearing force estimates are assessed. Parametric studies to determine the role of bridge skew angle, varying bridge geometry, and bearing fixity arrangement over piers on maximum fixed bearing forces are performed.

Chapter 9 is devoted to investigating deck diagonal and acute corner cracking. Nonlinear finite element models were created for selected bridges. Bridge details studied were diaphragm and lateral restraint details at bearings, bridge skew angle, reinforcement orientation and amount. A comparison of deck strains with varying details is provided in this chapter.

Chapter 10 provides conclusions and design recommendations of this study.

2. LITERATURE REVIEW

2.1. SKEW EFFECTS ON BRIDGES

High skew angles affect load distribution, performance and constructability by: 1) altering internal reaction forces in girders and supports, 2) causing horizontal movement of superstructure, resulting in bearing misalignment, 3) causing deck cracking, 4) creating constructability issues for steel girders. These factors reduce the accuracy of simple analytical models or cause performance, maintenance or constructability issues. Each of these skew effects is described in this section, together with potential causes. Skew effects are also documented through visuals obtained from bridge inspections.

2.1.1. IMPACT ON LOAD PATHS AND ANALYSIS

2.1.1.1. GIRDER INTERNAL FORCES

In bridges with no skew, load paths follow the longitudinal bridge direction toward the supports as shown in Figure 2.1a. In skewed bridges, this load path runs through the area connecting the obtuse corners as forces follow the shortest path to supports as shown in Figure 2.1b. Although, this is more pronounced in concrete slab bridges than in deck-girder bridges where girders also serve as load paths toward the supports [2; 3], the effects are considerable after 30° of skew [4-6] in deck-girder bridges.

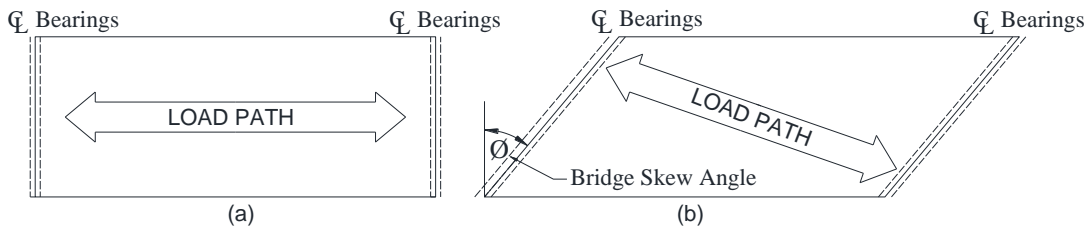


Figure 2.1. Load paths in (a) non-skewed and (b) skewed bridges.

Increasing values of bridge skew angle reduces moment in girders along the span and at supports. Shear forces at simply supported [7] and continuous [8] girder ends can increase significantly at obtuse corners with high skew. Shear at simply supported girder ends decrease at acute corners and at interior girders compared to counterparts with smaller skew angles [7]. Analytical studies [9] proposed varying shear forces along the length of girders, as well as varying girder end shears along support lines. A linear decrease of shear from ends to mid-span and from obtuse corner to acute corner can be considered to account for varying shear.

Huang et al. [10] investigated transverse bending moment distribution on highly skewed steel girder bridges. They instrumented and load tested a two-span, deck-on-steel bridge with a skew angle of 60°. Load distribution was evaluated by comparing load test results with live load distribution factors obtained from AASHTO. Researchers concluded that for bridges similar to the one tested, AASHTO distribution factors are conservative for positive moments and un-conservative for negative moments.

2.1.1.2. REACTIONS AT BEARINGS

At the abutments of skewed bridges, bearing reactions measured at the obtuse corners were found to be greater than those at the acute corners or at interior bearings [7]. Reactions at pier supports were found to be highly dependent on the ratio of lengths of different spans in a bridge. Support reactions were similar at bearings over a pier for bridges with two equal spans, regardless of the skew angle. For skewed bridges with two unequal continuous spans, increasing skew angles led to greater reactions at exterior girders and smaller reactions at interior girders [8]. Highly skewed bridges with simply supported ends may experience uplift at the acute corners due to decreasing reaction forces.

2.1.1.3. NEGATIVE MOMENT AND TORSION AT BRIDGE ENDS

Torsion and negative moments at bridge ends can be induced by high skew angles, even for bridges where bearings are detailed as roller supports [11]. Consistent with the gravity load paths on skewed bridges, bridge ends rotate around an axis parallel to bridge supports as shown in Figure 2.2. Unexpected negative moments on top of deck at bridge ends and torsion on beams can be formed.

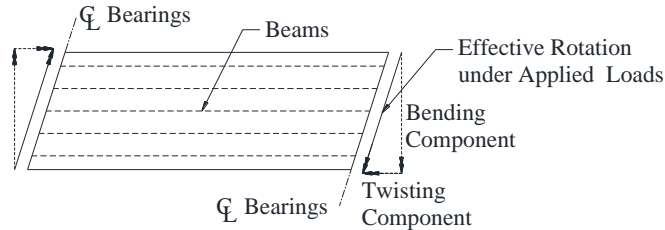


Figure 2.2. Effective rotation of girder ends.

2.1.2. IMPACT ON BRIDGE DISPLACEMENTS

Displacements due to skew may have three sources [12; 13]: 1) thermal expansion or contraction, 2) shrinkage of deck, and 3) interaction of thermal expansion and shrinkage with certain types of abutments. Skewed bridges expand non-uniformly across their cross section under thermal loads and shrinkage as shown in Figure 2.3a, where the largest deformation is along the longest distance, along a line connecting the acute corners. Superstructure and substructure members can be distressed due to thermal expansion, when substructure components provide restraint against expansion.

Thermal expansion between the acute corners causes lateral and longitudinal movements at bridge ends. When skewed bridges have integral or semi-integral abutments, these movements are restrained and additional backfill pressure develops at abutments. Due to skew angle, the resultants of these forces are not collinear and may rotate the bridge further towards the acute corners or counter clockwise direction as shown in Figure 2.3b.

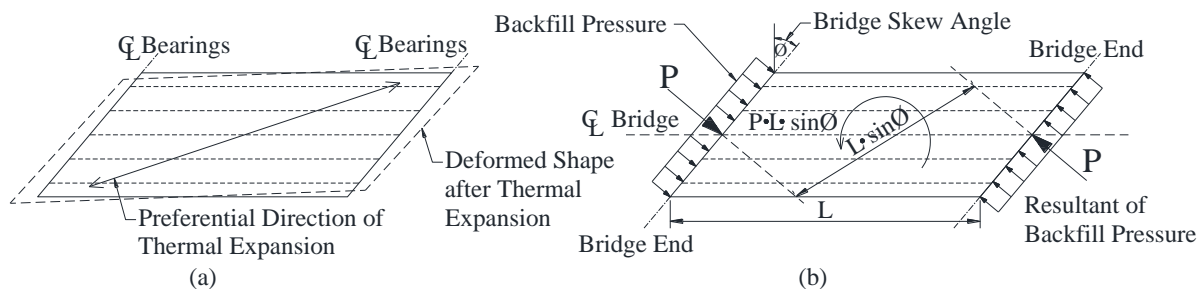


Figure 2.3. (a) Thermal expansion, and (b) backfill reactions due to thermal expansion. [13]

Horizontal movements are documented in Figure 2.4 – Figure 2.6. These figures are taken from an inspection of a three-span continuous prestressed concrete deck-girder bridge with a skew angle of 30°, sill abutments with semi-expansion seats and elastomeric bearing pads. Even though the bridge skew angle is moderate, displacements of the superstructure are significant. Bridge rotation is documented by cracks in abutments at girder seats in Figure 2.4a since the full depth concrete end diaphragm does not allow superstructure to freely rotate. Bridge rotation is also seen through vertical joint opening between adjacent bridges in Figure 2.4b, and misalignment of parapet wall over the abutment in Figure 2.5. This kind of rotation towards the acute corners could have been caused by thermal expansion.

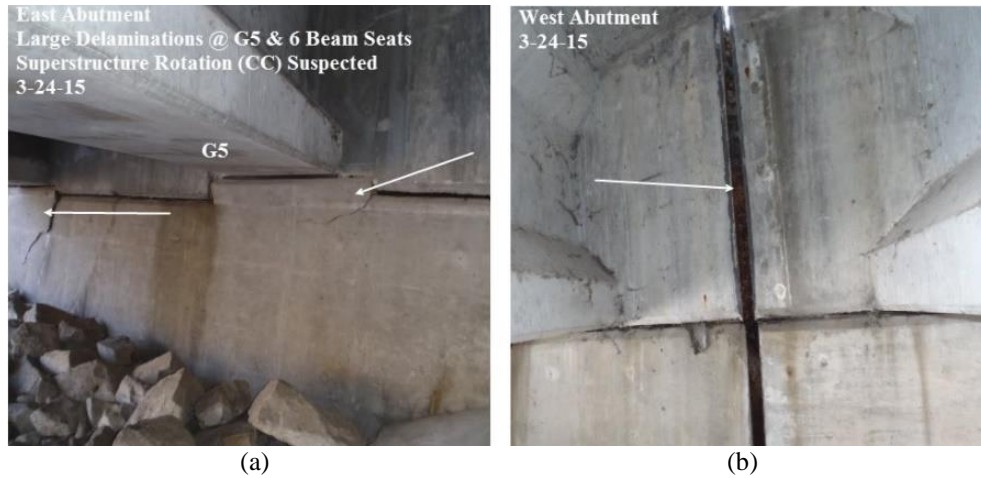


Figure 2.4. (a) Cracks at girder seats at the acute corner, and (b) open joint between adjacent bridges at the obtuse corner. [1]

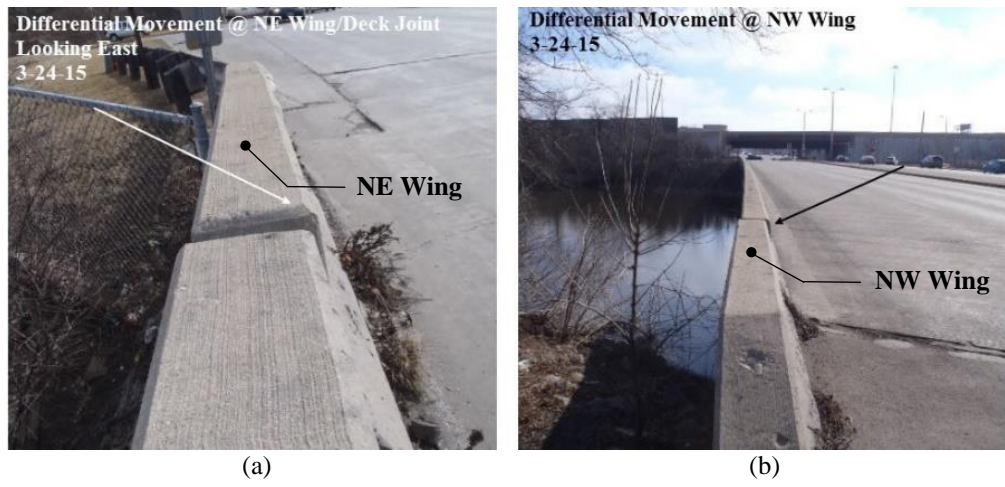


Figure 2.5. Misalignment of wingwall and bridge parapet wall at (a) acute, and (b) obtuse corners. [1]

Similarly, Figure 2.6 was taken from the inspection of a four-span continuous prestressed concrete deck-girder bridge with a skew angle of 51°, semi-retaining abutments and steel laminated elastomeric bearings. It shows one of the several bearings in the obtuse corner that rotated toward the acute corner, possibly due to thermal expansion and torsion at the obtuse corner.



Figure 2.6. Bearing rotation at the obtuse corner. [1]

2.1.3. IMPACT ON DECK PERFORMANCE

Cracking in concrete decks and possible solutions to it have been investigated for several decades. However, in these studies, skew effects on deck cracking were either tangentially investigated or not addressed. Therefore, the role of skew on deck cracking is not yet fully understood.

Larson et al. [14] conducted an investigation into the causes of and possible solutions to concrete deck deterioration. They observed that simple span steel bridges exhibited greater frequencies of transverse cracking with increasing skews. Schmitt and Darwin [15] conducted field surveys in continuous steel girder bridges to evaluate levels of deck cracking (crack density), that were later compared to identify correlations with several variables in order to establish their role in bridge deck cracking. They found no apparent relationship between cracking and skew in bridges with monolithic decks. For bridges with two-layer decks (decks with bonded concrete overlays), cracking tendency was higher with greater skew angles. Krauss and Rogalla [16] investigated the occurrence of early transverse deck cracking, through theoretical analyses, field instrumentation and laboratory research, to determine the major factors contributing to deck cracking. They stated that skew has a minor effect on transverse cracking, but may lead to slightly higher stresses near corners. Saadeghvaziri and Hadidi [17] used statistical analysis, finite element modeling, and bridge response measurements to study the causes of transverse concrete deck cracking in bridges and to propose control measures for implementation in design. Through their statistical analysis, they found no direct relation between transverse cracking occurrence and bridge skew angle. Mokarem et al. [18] studied the performance of nineteen bridge decks built with high performance concrete, located in different climates and in service for 5 to 10 years. Based on a detailed survey of deck cracking condition, they concluded that when skewed supports were part of the structural system, diagonal cracks near supports were likely to occur. Stringer and Burgueno [19] found through nonlinear finite element modeling that the skew angle could increase the amount of restraint in jointless steel girder bridges subject to early-age shrinkage, and lead to more deck cracking near abutments under such loading. They recommended to avoid large skew angle configurations when possible.

Unlike the researchers cited above, Fu et al. [3] concentrated their efforts on skewed bridges, and studied the causes of deck corner cracking. They instrumented the deck of two girder-type bridges. One of the bridges had steel I-girders and 49° of skew, while the other had AASHTO prestressed concrete girders and 46° of skew on the instrumented span. Deck strains, deck temperature, ambient temperature and humidity were recorded under short-term and long-term loading. Using the data together with finite element models, they hypothesized that deck corner cracking is caused by thermal loading and shrinkage during concrete hydration, and that fatigue loading caused by traffic may widen the cracks. Additional reinforcement in corner regions was recommended. Examples of this type of cracking are displayed in Figure 2.7 that shows the top and bottom of the deck of the bridges documented in Figure 2.6, Figure 2.4 and Figure 2.5, respectively.

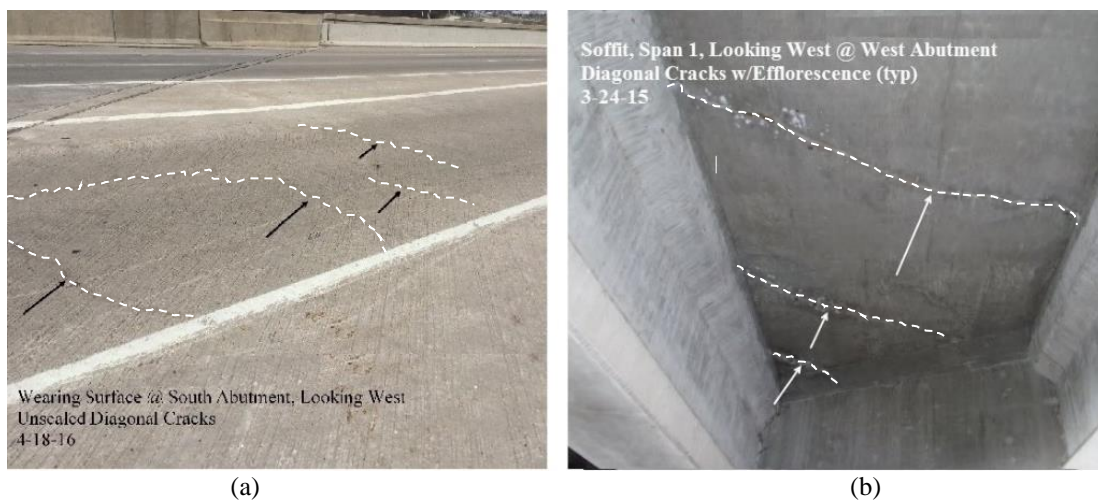


Figure 2.7. Diagonal cracks on the (a) top and (b) bottom faces of the deck at the acute corners. [1]

In spite of the limited research on the role of skew on deck cracking, field observations have also shown that concrete deck diagonal cracks at acute corners may be associated with skewed bridges, and that they occur on top and bottom faces of the deck, typically oriented orthogonal to the skewed end support lines. Diagonal cracking extending well beyond acute corner regions in highly skewed bridges has also been observed and recorded on field inspection reports [20]. Research on the causes of this type of extending cracking were not available in literature. The impact of skew angle, among other variables, on deck cracking is investigated in Chapter 9.5 of this report.

2.1.4. CONSTRUCTABILITY OF STEEL GIRDER BRIDGES

Bridge skew angle may affect construction of steel deck-girder bridges [21]. Under non-composite loads, girders are subjected to differential deflections. In the presence of intermediate cross-frames, which are usually perpendicular to beam centerlines and have high in-plane stiffness, differential deflections lead to torsion and flange lateral bending on beams. The use of skewed intermediate cross-frames does not eliminate induced torsion, in spite of connecting points of similar deflection.

Torsion in girders has also been reported at piers and abutments, caused by the resistance of end cross-frames to get distorted after the application of non-composite loads. This may result in girders being out-of-plumb during deck pour and compromise strength. In addition, bearings may carry additional lateral forces. Prestressed concrete girders have higher lateral stiffness and require fewer cross-bracings than steel girders. Therefore, they are less susceptible to reaction forces described here.

2.2. FEEDBACK FROM WISCONSIN BRIDGE MAINTENANCE ENGINEERS

To collect additional information on field performance of Wisconsin bridges with high skew, Wisconsin regional bridge maintenance engineers of the five regions were contacted. The following is a summary of their feedback:

- The North Central region reported horizontal bridge movements, missing keeper bars and acute corner deck cracking with bridges over approximately 30 degree of skew. They think that steel bridges may have more problems than prestressed concrete because they are older and they have lighter superstructures that can move more easily.
- The North East region reported that they do not see any obvious issues with bearings. They see more prevalent diagonal cracking in decks with high skew, but they do not see a general correlation between deck cracking and increasing skew angles.
- The North West region reported common acute deck corner cracks with or without end diaphragms, and even on bridges that are not yet open to traffic. Approximately 70% of bridges built after 2000 and with skew larger than 10 degrees had deck cracking. Exterior girder heating before the other girders may be one reason for acute corner deck cracks. Snow plowing in the opposite direction of skew may cause problems at the expansion joint. They reported pier diaphragm cracks when concrete girders are enclosed in cast in place concrete diaphragms. They also stated that old structures have larger horizontal displacements and new bridges have fewer skew related problems in general. Example bridges with performance issues reported are B-16-95 and B-09-0212.
- The South East region reported that they tend to see more problems on bridges with three spans, and bridges with unequal spans. They also stated that end diaphragms, when they restrain the lateral movement of the bridge, could cause substructure and beam pedestal cracking.
- The South West region reported acute deck corner cracking and horizontal bridge movements as evident from missing keeper bars or beam seats shearing off in concrete diaphragms. Even on moderate skews, when girder ends are too close to abutment backwall, due to lateral movement girders push off against the abutment backwall, which then further moves bearings laterally eventually misaligning girders with bearing centerlines. B-13-228 is an extreme example of racking eventually closing the expansion joint. They did not report a correlation between any bridge characteristic and skew effects.

2.3. FEEDBACK FROM NEW YORK BRIDGE MAINTENANCE ENGINEERS

In this section, the results of a survey distributed to the regional maintenance engineers of the New York State Department of Transportation (NYSDOT) regarding the skew effects on bridges are presented. Of the 23 engineers surveyed, 22 observed that skewed bridges performed worse, and 1 indicated that this is not be the case when they are properly designed. Among the 22 engineers, 1 mentioned that skewed bridges would perform worse only if they had a concrete superstructure.

Figure 2.8 summarizes the problems NYSDOT maintenance engineers commonly experience on bridges with high skew. Problems reported by the majority included lateral movements, parapets misalignments, acute corner cracking, and to a lesser extent overall angled deck cracking. Some engineers mentioned premature joint failures and broken bearings in the “others” category.

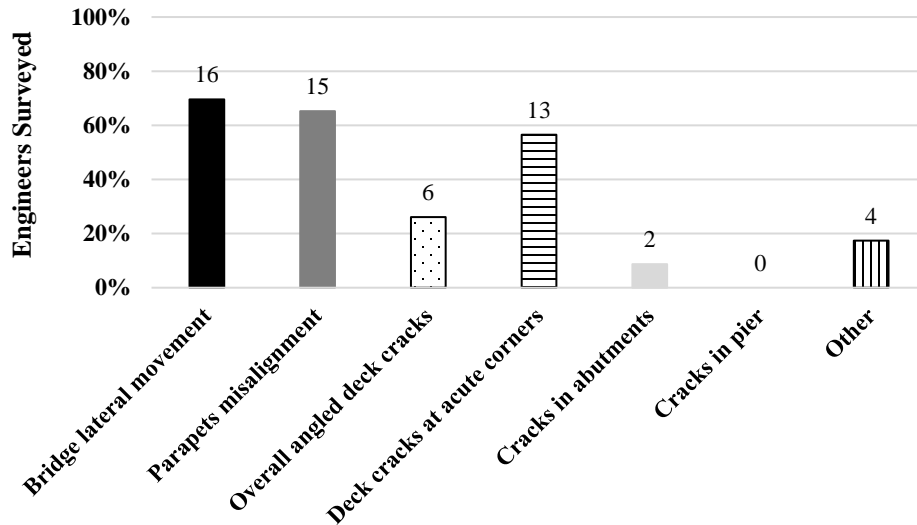


Figure 2.8. Problems commonly associated with high skew by NYSDOT maintenance engineers.

Engineers were also asked which bridge component or detail they associate with the aforementioned problems. Results are presented in Figure 2.9. The bridge details most commonly associated with skew were uneven span lengths and elastomeric bearings. Some believed that the use of continuous, concrete superstructures aggravates skew effects. Among “other” details, combination of skew with longitudinal grades and joint-free details were mentioned.

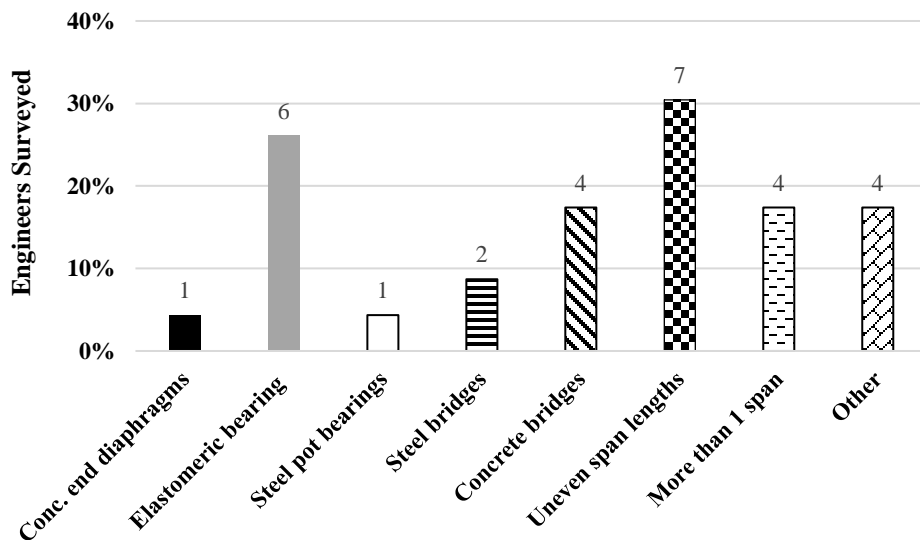


Figure 2.9. Bridge elements that worsen skew-related problems.

2.4. MITIGATING MEASURES FOR SKEW EFFECTS

The AASHTO LRFD BDS [22] and current bridge design manuals of several State Departments of Transportation (DOT) were reviewed to see if the effects of bridge skewness were acknowledged and included in the design of deck-girder type bridges. The state DOT's whose bridge design practices were reviewed included Wisconsin [23], New York [24], Connecticut [25], Minnesota [26], Ohio [27], Michigan [28], Vermont [29], Massachusetts [30], New Jersey [31], Indiana [32], New Hampshire [33], Maine [34], Illinois [35], Pennsylvania [36], Rhode Island [37], Texas [38], and Washington [39]. Most of the states were selected to be in the Northeastern region of the US, as these regions have harsh environmental conditions causing faster bridge deterioration. Differences between AASHTO LRFD BDS and DOT practices are reported. The review provided here is limited to design practices of prestressed concrete girders and concrete decks.

2.4.1. SKEW RELATED PROVISIONS OF AASHTO LRFD BDS

2.4.1.1. PROVISIONS RELATED TO GIRDERS

AASHTO LRFD BDS [22] provides live load distribution factors for typical deck-girder type bridges to simplify analysis for typical bridges to 1-D girder-line analyses, largely based on NCHRP 12-26 [6] and NCHRP 12-62 [40] projects. To account for the altered load paths due to skew, Section 4.6.2.2 provides correction factors to live load distribution factors. AASHTO LRFD BDS C4.6.2.2.3c indicates that large skews produce significant torsional effects that invalidate the use of load distribution factors, i.e. the bridge can no longer be considered "regular".

Section 4.6.2.2.2e allows reduction of girder bending moments due to skew. Correction factors for bending moments may be applied to all girders and throughout the beam length. Skew angles below 30° are treated negligible, except for bridges with box beams. Moments are not reduced further for skew angles above 60°.

Section 4.6.2.2.3c requires an increase in shear forces due to skew. Correction factors for shear are applied to exterior girders at the obtuse corner and the first interior girders only when girders can be assumed to behave as a unit. Otherwise, shear correction factors apply to all interior girders and exterior girders at the obtuse corners. Between the obtuse corner support and mid-span, correction factors can be decreased linearly with a value of 1.0 at mid-span. Requirement that considers the variation of shear along exterior girder span seems to be developed by NCHRP 20-7/Task 107 [9]. NCHRP 20-7/Task 107 also recommended a linear decrease of shear correction factor from the obtuse corner to 1.0 at the acute corner, however, this was not included in AASHTO LRFD BDS. Negative values of correction factors can be used to calculate uplift of exterior girders at acute corners due to skew. Correction factors for skew greater than 60° are not available or provided in AASHTO LRFD BDS.

2.4.1.2. PROVISIONS RELATED TO DECKS

AASHTO LRFD BDS Commentary C4.6.2.1.1 and C4.6.3.2.1 recognize that skewed supports are responsible for a number of detrimental effects such as negative moments at corners, large torsion in the end zones due to differential deflection and significant redistribution of reaction forces. Although consideration of these in design is recommended, no explicit design guidance is provided in this section.

AASHTO LRFD BDS section 9.7.2.5 presents a crack control provision dealing with end zone torsional cracks caused by differential deflections, observed in bridges with skew angles larger than 25°. For skew angles beyond this value, the provision requires the deck reinforcement, as determined by the empirical design method, to be doubled for end zones and in both directions. End zones extend a distance equal to the effective length of the deck per AASHTO LRFD BDS 9.7.2.3.

AASHTO LRFD BDS section 9.7.1.3 states that primary reinforcement of the deck could be placed in the direction of skew for skew angles smaller than 25°. This provision seems to aim at facilitating deck construction, as inferred from the commentary to this section, and not mitigating skew effects.

2.4.2. DIFFERENCES BETWEEN AASHTO LRFD BDS AND STATE DOT PRACTICES

2.4.2.1. PRACTICES RELATED TO GIRDERS

Review of state practices on girder analysis revealed a general agreement between DOT's and AASHTO LRFD BDS. Table 2.1 summarizes the differences between DOT practices and AASHTO LRFD BDS. The

table also provides additional specifications, if any, given by DOT's for the analysis of girders for bridges with large skew. Main deviations of DOT's from AASHTO LRFD BDS are highlighted below:

- Even though the reduction in bending moments caused by skew is acknowledged, some DOT's do not reduce moments to be conservative.
- Several DOT's apply correction factors for shear to all girders and across the entire span. Others allow the application of correction factors to shears at the support and reactions at the obtuse corner of only the exterior girders.
- Additional specifications (i.e., not included in AASHTO) consist of limitations of certain types of girders, such as prestressed concrete bulb-tee or I-girders, for varying skew angle limits.

Table 2.1. Deviations of DOT practices from AASHTO LRFD BDS on girders.

State	Different from AASHTO LRFD BDS		Additional Specifications
	4.6.2.2.2e	4.6.2.2.3c	
WI [23]	17.2.8: Moment reduction not allowed.	17.2.8: Shear correction for all girders, and entire span.	No
NY [24]	No	No	No
CT [25]	No	No	No
MN [26]	No	4.2.2.1: Shear correction for all girders, and entire span.	No
OH [27]	No	No	No
MI [28]	No	No	No
VT [29]	No	No	No
MA [30]	No	No	2.3.5.4: Northeast bulb-tees and similar girders avoided for skew > 45°.
NJ [31]	No	No	No
IN [32]	No	406-12.10(01): For shear at obtuse corner of exterior girders. Below 30°, shear correction disregarded.	No
NH [33]	No	No	No
ME [34]	No	No	No
IL [35]	3.3.1: Moment reduction not allowed.	3.3.1: Shear correction applied to all girders at non-continuous ends. Optional simplified correction factors proposed.	No
PA [36]	Structures C4.6.2.2.2e: Moment reduction not allowed.	Structures 4.6.2.2.3c: Shear correction for end shear of exterior girders at the obtuse corner.	Structures 5.14.1.1: Prestressed concrete PA bulb-tee and I-girders with a skew limit of 60°.
RI [37]	No	No	No
TX [38]	No	No	No
WA [39]	No	No	5.6.2: Prestressed concrete girders not allowed for skew > 45°.

2.4.2.2. PRACTICES RELATED TO DECKS

State DOT's acknowledge the effect of skew angle on bridge decks, in general, similar to AASHTO LRFD BDS. Table 2.2 presents the differences between DOT practices and AASHTO LRFD BDS for concrete bridge decks and present guidance given by DOT's in addition to AASHTO LRFD BDS, if any. Main deviations of DOT practices from AASHTO LRFD BDS are as below:

- In relation to the provision on end zone torsional crack control, differences mainly are on the skew angle, beyond which additional reinforcement is required, and the amount, configuration and extension of this reinforcement.
- The skew angle below which primary reinforcement could be placed in the direction of the skew differs from AASHTO LRFD BDS for several DOT's.
- Additional guidance provided by DOT's include limits for the use of isotropic reinforcement, guidance for edge beam design and deck transverse reinforcement detailing in skewed bridges.

Table 2.2. Deviations of DOT practices from AASHTO LRFD BDS for concrete decks (rf = reinforcement).

State	Different from AASHTO LRFD BDS		Additional Specifications
	9.7.1.3	9.7.2.5	
WI [23]	17.5.3.1: The limit is 20°.	No	No
NY [24]	5.1.5.1, 5.1.5.2: The limit is 30°. Traditional deck rf included.	5.1.5.1: The limit is 30°. Girder spacing used, instead of effective deck length.	5.1.5.1: Traditional instead of isotropic rf for skew > 45°.
CT [25]	8.1.2.5.1: The limit is 20°.	8.1.2.5.1: The limit is 20°. Additional rf in skew direction only (#5@9").	No
MN [26]	9.2.1: The limit is 20°.	9.2.1: No limit given. Additional rf in skew direction (2 #5@5"), radial transverse rf and bent corner bars.	No
OH [27]	302.2.4.2: The limit is 15°.	No	No
MI [28]	7.02.20 E: The limit is 20°.	No	No
VT [29]	No	No	No
MA [30]	No	No	No
NJ [31]	20.5: Main rf ⊥ to girders regardless of skew angle. A portion of it should be fanned extending into the acute deck corner.	No	No
IN [32]	No	No	404-3.03: Transverse edge beams should not include top transverse deck steel for skews > 25°.
NH [33]	No	No	No
ME [34]	No	No	No
IL [35]	3.2.3: The limit is 15°. Additional span length constraint.	No	3.2.2.1: Guidance on the design of edge beams, based on skew.
PA [36]	Structures 9.7.1.3 and C9.7.1.3: The limit is 15°.	Structures 9.7.2.5 and C9.7.2.5: The limit is 15°.	Appendix G, C1.4.2.5: Deck transverse rf ⊥ to girders extend inside end-diaphragm and terminate as close as possible to its back face.
RI [37]	9.6.3: The limit is 30°.	No	No
TX [38]	Chapter 3, Section 2 (Pg. 3-4): The limit is 15°. For skew > 15°, rf should include corner breaks.	No	No
WA [39]	5.7.2: Rf is always ⊥ to bridge centerline.	No	No

2.5. SUMMARY AND CONCLUSIONS

This section presented analysis, performance and constructability issues related to high skew in bridges, through a review of published literature, and a review of AASHTO and State DOT practices. Literature review on analysis methods of bridges with high skew angles showed that skew may alter gravity load paths, change shear and moment distribution to girders, and create negative moment and torsion at bridge ends. Intermediate and end diaphragms can restrain movement and can cause lateral moment and torsion due to differences in deflections of adjacent beams under gravity loading.

Service problems related to high skew angles include deck cracking and bearing movements. Some of the service problems are attributed to shrinkage and temperature loading. Diagonal cracks at acute corners of concrete decks of skewed bridges are not directly addressed by AASHTO LRFD BDS as it does not link acute corner cracking with non-mechanical loading (i.e., shrinkage and temperature loading). Instead, AASHTO LRFD BDS section 9.7.2.5 only considers end zone cracking caused by torsion due to differential deflections.

AASHTO LRFD BDS and current DOT practices were in general agreement. Several states do not allow moment reductions and apply shear correction to all girders for conservatism. Some states limit the use of bulb-tee girders, I-girders or all prestressed girders for high skew bridges. For deck reinforcement, there is some variability between state practices about direction of deck reinforcement.

3. FIELD INSPECTIONS

Several deck-girder type Wisconsin bridges with prestressed concrete and steel girders were visually inspected to identify performance issues unique to high skew bridges. Four of these bridges were selected so that they had similar design characteristics, but different skew angle. It was also ensured that these bridges had details that are not outdated in practice. Current common details include elastomeric bearings, semi-retaining abutments and strip seal expansion joints. In addition, inspections from the two highly skewed concrete and steel girder bridges that were load tested are included in this chapter.

3.1. FIELD INSPECTION OF BRIDGES WITH AND WITHOUT SKEW

The four girder bridges included in this section are similar in girder material, year built, span length, span-length-to-deck-width ratio, number of spans, but different in skew angle. Table 3.1 and Table 3.2 present information on the inspected prestressed concrete and steel girder bridges, respectively. Inspection results are compared to understand performance issues observed in similar bridges with different skew angles.

Table 3.1. Characteristics of inspected prestressed concrete bridges (L=span length, W= deck width).

Girder type	Skew	L/W	Pier type	Abutment type	Bearing type	No. spans	Span length	Year built
70" bulb-tee girder (B-40-399)	52°	3.0	Multi-column	Semi-retaining	Steel laminated elastomeric pad (abutments), elastomeric pad (pier)	2	130'	2001
		–					147'	
54" I-girder (B-20-066)	0°	3.2					100'	1995
		–					100'	
		3.2						

Table 3.2. Characteristics of inspected steel bridges (L=span length, W= deck width).

Girder type	Skew	L/W	Pier type	Abutment type	Bearing type	No. spans	Span length	Year built
66" Plate girder (B-67-166)	30°	2.7	Multi-column	Semi-retaining	Metallic assembly (abutments and pier)	2	133'	1976
		–					133'	
50" Plate girder (B-59-070)	3°	3.0					110'	1979
		–					105'	
		2.8						

3.1.1. COMPARISON OF DECK PERFORMANCE

3.1.1.1. DECK PERFORMANCE OF PRESTRESSED CONCRETE BRIDGES

Contrary to the expectations of the research team, no visible cracks were detected in the acute corners of the bridge with 52° skew on the bottom or top surfaces of the deck (Figure 3.1a). No cracks were visible on the remaining of the deck surfaces. On the other hand, the bridge with 0° skew, had a significant number of transverse and longitudinal deck top surface cracks, sealed previously. Several longitudinal cracks were spread spaced at 8 ft over abutments as shown in Figure 3.1b. In addition, transverse cracks spaced between 1ft and 8 ft were spread between the pier and midspan. No cracks were visible on the deck bottom surface.



Figure 3.1. (a) Lack of cracking on deck bottom surface for 52° skew, and (b) longitudinal cracks for 0° skew near the abutment.

3.1.1.2. DECK PERFORMANCE OF STEEL BRIDGES

Deck inspection of the bridge with 30° skew revealed a wearing surface with patches, reflective and transverse cracks over the pier distributed at approximately 4 ft and 7 ft, respectively. As in the prestressed concrete skewed bridge, there was no visible acute corner cracks. Concrete spalled with exposed reinforcement on the bottom face of the concrete deck near girder field splices on the north span (Figure 3.2a). The deck of the bridge with 3° skew had longitudinal cracks (Figure 3.2b). There were small transverse un-sealed cracks over the pier and on deck bottom surface. In general, the asphalt overlay obstructed crack detection.



Figure 3.2. (a) Concrete spalling on deck bottom surface for 30° skew, and (b) longitudinal sealed cracks on deck top surface for 3° skew.

3.1.2. COMPARISON OF BRIDGE HORIZONTAL MOVEMENTS

3.1.2.1. HORIZONTAL DISPLACEMENTS OF PRESTRESSED CONCRETE BRIDGES

Bridge movement was inspected by measuring expansion joint openings and bearing pad deformations. Expansion joint openings were measured at an ambient temperature of 31 °F and are given in Table 3.3. Expansion joint openings were the same in all four corners for each bridge, indicating insignificant racking for both bridges.

Movements of bearings in the direction of girders measured over the two abutments were consistent with ones created by thermal contraction for both bridges. Figure 3.3 shows example bearing pad movement in the direction of girders for 52° skew. Bearing pad displacements of the bridge with 0° skew were smaller than the one with 52° skew, likely due to 30% to 50% shorter span lengths in the 0° skew bridge.



Figure 3.3. Longitudinal displacement of an interior bearing for 52° skew.

In addition to bearing pad movement in the direction of girders, the bridge with 52° skew also had a small (less than 0.25 in.) transverse horizontal movement towards the centerline of the bridge at the obtuse corners of the bridge abutments (Figure 3.4a). This could be an indication of bridge rotation toward acute corners. However, similarity in expansion joint openings at all corners contradicts this conclusion. In addition, a rotation around an axis parallel to the bridge centerline was observed on an acute corner bearing (Figure 3.4b). This may be attributed to torsion at one end of the bridge. However, this type of bearing movement was not observed on the acute corner at the other bridge end. Although both types of bearing movements shown in Figure 3.4 are acknowledged, they were too small to conclude a relationship to skew. Inspection results related to prestressed concrete bridge movements are summarized in Table 3.3.



Figure 3.4. (a) Lateral displacement, and (b) rotation of the bearing for 52° skew.

Table 3.3. Horizontal bridge movements of inspected prestressed concrete bridges.

Skew	Expansion joint openings at 31°F	Longitudinal bearing movements	Transverse bearing movements
52°	2.13" at all four corners	Abutment bearings moved towards pier	Small movements towards bridge centerline at abutment bearings near obtuse corners
0°	2.50" at all four corners	Abutment bearings moved towards pier	Unnoticeable

3.1.2.2. HORIZONTAL DISPLACEMENTS OF STEEL BRIDGES

At 31 °F, expansion joint openings for both bridges are given in Table 3.4. Expansion joint openings were similar at acute and obtuse corners, indicating horizontal displacements were not significant for either bridge.

On the bridge with 30° skew, bearing movements over the abutments were evident from missing or bent keeper bars or from gaps between bearing and keeper bars (Figure 3.5). Bearing movement was in the transverse direction of the bridge and all bearings displaced toward the longitudinal centerline of the bridge. Bearing movements for the bridge with 3° skew were imperceptible. However, in some cases bearings had slightly bent keeper bars. Rust was present on bearings and anchor bars of these two bridges. Inspection measurements of steel bridge movements are summarized in Table 3.4.



Figure 3.5. (a) Bent interior keeper bar and (b) gap between bearing and exterior keeper bar of obtuse corner bearing at north bridge end for 30° skew.

Table 3.4. Horizontal bridge movements of inspected steel bridges.

Skew	Expansion joint openings at 31°F	Longitudinal bearing movements	Transverse bearing movements
30°	2.38" at acute and obtuse corners of south end, and 2.00" at acute and obtuse corners of north end	Unnoticeable	Transverse movement towards bridge centerline at most abutment bearings. Several abutment bearings had broken or bent keeper bars
3°	2.00" (acute) and 1.88" (obtuse) at east end corners, and 2.13" (obtuse) and 2.50" (acute) at west end corners	Unnoticeable	Mostly unnoticeable. A few abutment bearings had slightly bent keeper bars

3.1.3. COMPARISON OF SUBSTRUCTURE CONDITIONS

3.1.3.1. SUBSTRUCTURE CONDITIONS OF PRESTRESSED CONCRETE BRIDGES

Abutments of both bridges had vertical cracks typically located at the level of beam centerline or beam pedestal edges, some of which ran along the entire abutment height. Figure 3.6 compares the abutments of the bridges with 52° (a) and 0° (b) skew. In addition, the bridge with 0° skew had a small area of spall at the concrete diaphragm over the pier.



Figure 3.6. Vertical abutment cracks for bridges with (a) 52° skew, and (b) 0° skew.

3.1.3.2. SUBSTRUCTURE CONDITIONS OF STEEL BRIDGES

Vertical cracks on the abutments were observed on both bridges (Figure 3.7). However, the severity of cracking, concrete efflorescence and rust stains seemed more significant on the bridge with 30° skew. In addition, this bridge presented regions with concrete spalling (Figure 3.7a).



Figure 3.7. Vertical cracks on the abutments of bridges with (a) 30° skew, and (b) 3° skew.

3.2. FIELD INSPECTION OF LOAD TESTED BRIDGES

Field inspection information was also gathered from the two girder bridges load tested by the research team. These are two highly skewed prestressed concrete and steel girder bridges that will be fully described in Chapter 4: Load Testing. In this report, they are referred to as the HAST bridge and the Chippewa bridge for prestressed concrete and steel bridges, respectively. Table 3.5 and Table 3.6 provide a summary that allows a comparison with the other bridges presented in this chapter.

Table 3.5. Characteristics of load tested prestressed concrete bridge (L=span length, W= deck width).

Name (WisDOT Bridge ID)	Girder type	Skew	L/W	Pier type	Abutment type	Bearing type	No. spans	Span length	Year built
The HAST bridge (B-40-870)	54" W-girder	64°	1.2	Multi-column	Semi-retaining	Steel laminated elastomeric pad (abutments and piers), metallic assembly (piers)	3	109.2'	2016
			–					125.4'	
			1.3					–	
			–					85.8'	
			0.9						

Table 3.6. Characteristics of load tested steel bridge (L=span length, W= deck width).

Name (WisDOT Bridge ID)	Girder type	Skew	L/W	Pier type	Abutment type	Bearing type	No. spans	Span length	Year built
The Chippewa bridge (B-09-177)	33" W-girder	47°	1.1	Multi-column	Sill	Steel laminated elastomeric pad (abutments and pier), metallic assembly (pier)	3	47'	1993
			–					69.5'	
			1.6					–	
			–					47'	
			1.1						

3.2.1. DECK PERFORMANCE OF LOAD TESTED BRIDGES

At the time of load testing of the prestressed concrete HAST bridge, which took place 28 days after the placement of deck concrete, there were no visible cracks in the deck. However, after one year, several transverse (approx. perpendicular to bridge centerline) and some diagonal cracking at the bridge ends were observed on the deck bottom face of the bridge. Figure 3.8 shows a crack map of the deck bottom face at the exterior east span of the bridge.

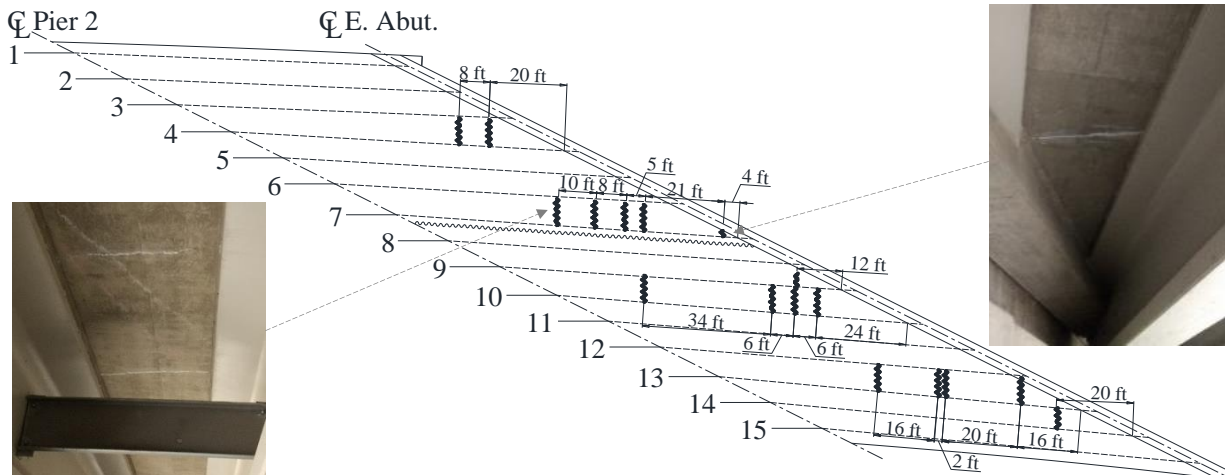


Figure 3.8. Deck bottom face crack map at the east span of the load tested prestressed concrete bridge.

Similarly, the deck of the steel Chippewa bridge had numerous deck bottom face cracks running in the transverse direction (approx. perpendicular to bridge centerline), and diagonal cracking at the acute corners at the intersection of girders and supports at bridge ends (Figure 3.9).



Figure 3.9. Deck bottom face: (a) transverse cracking on west span, and (b) typical acute corner cracking at bridge ends of the load tested steel bridge.

3.2.2. HORIZONTAL DISPLACEMENTS OF LOAD TESTED BRIDGES

Expansion joint openings are not available for any of the tested bridges as expansion joints were not accessible. Both bridges had longitudinal bearing pad movements consistent with thermal loading, and imperceptible transverse bearing movements. Lack of transverse bearing movements may be due to the temperatures on the day of inspection (48 °F and 65 °F) for the HAST (concrete) and Chippewa (steel) bridges, respectively) being close to installation temperature. Prestressed concrete bridge with a skew of 64° had a special bearing fixity arrangement, which might also have helped minimize transverse displacements.

3.3. SUMMARY AND CONCLUSIONS

The main goal of the field inspections was to compare similar bridges with and without skew to identify performance problems specific to skew. Contrary to expectations, the comparison showed that condition of bridges with high skew was not worse than the ones with no skew. Although some bearing movements were visible in bridges with skew, they were not significant or consistent enough to directly relate them to skew. In fact, it was observed that the deck of bridges with no skew could have significantly more cracking than their counterparts with high skew. On the other hand, the two highly skewed girder bridges load tested had transverse cracks along the span and at bridge ends. This included the HAST bridge that had a special bearing fixity arrangement, designed to minimize superstructure horizontal displacements. These observations show that not all bridges with high skew experience problems with skew to the same degree. This may be due to presence of some bridge characteristics that mitigate or worsen the negative effects of skew for some bridges, or the temperature during inspection. The impact of bridge details and geometry on load distribution, deck cracking and bridge movements are investigated in Chapter 6 to Chapter 9.

4. LOAD TESTING OF HIGHLY SKEWED GIRDER BRIDGES

Bridge load testing and long-term monitoring were used to evaluate bridge behavior. The goal of the load tests was to understand and assess bridge response under short and long-term loading, and to generate data to validate numerical models that are later employed to study bridge performance. Two load tests were performed: a load test on a prestressed concrete girder bridge, and a load test on a steel girder bridge.

4.1. LOAD TESTING AND MONITORING OF THE PRESTRESSED CONCRETE BRIDGE

The tested bridge was selected due to its high skew and distinctive mixed support fixity arrangement over the piers; a feature designed to minimize horizontal lateral movements. The investigation addressed the most common problems with skewed bridges: load distribution, superstructure horizontal movements and deck corner cracking, using short-term and long-term loading schemes. Short-term loading consisted of truck loading under controlled conditions, and was used to generate shear and bending strain data. These data were used to validate finite element models employed for parametric studies. Long-term loading was composed of temperature loads, shrinkage and traffic load. Under these loads, bearing horizontal movements and deck strains at critical locations were continuously monitored for approximately 5 and 12 months, respectively, to gain a better understanding of how highly skewed bridges move and how deck cracking develops.

4.1.1. BRIDGE DESCRIPTION

The tested structure is B-40-870, also known as the HAST bridge because it carries the Interstate Highway 94 East-Bound traffic over the Hank Aaron State Trail (HAST) in Milwaukee County, Wisconsin. All three spans are deck-on-prestressed concrete-girders, continuous for live load and superimposed loads. The bridge has a skew of 64°. General characteristics and geometry of the bridge are presented in Table 4.1 and Figure 4.1, respectively.

Table 4.1. The HAST bridge, Bridge B-40-870, general features.

Name (WisDOT Bridge ID)	Skew	Span lengths	Pier type	Ave. deck width	Girder type	Abutment type	Bearing types	Year built
The HAST bridge (B-40-870)	64°	109.2' – 125.4' – 85.8'	Multi-column	94.9'	54" wide flanged prestressed girder	Semi-retaining	Elastomeric (abutments and piers), metallic assembly (piers)	2016

The bridge has fifteen prestressed concrete girders on each span, with varying or flared spacing due to a horizontal curvature of 4,300 ft of radius. The cast-in-place deck is 8-in thick, fully composite with girders by means of #4 shear connectors at stirrup spacing. Transversely, girders are connected through steel intermediate diaphragms, and through full depth cast-in-place concrete diaphragms over piers. The concrete diaphragms are not in contact with pier caps or girder bearing pads. The specified compressive strength of concrete for deck and substructure is 4 ksi. Pretensioned concrete girders have a specified concrete strength of 8 ksi, with 270 ksi ultimate strength strands. Mild steel reinforcement has a specified yield strength of 60 ksi.

The bridge has a unique configuration of bearing fixity. Bearings over each pier are a mixed arrangement of both expansion and fixed bearings. Bearings over the abutments are expansion bearings only, as shown in Figure 4.1d. This special bearing arrangement was designed to keep thermal and shrinkage displacements at expansion joints and at parapet expansion joint cover plates under the limits specified on section 28.3.4 of the WisDOT Bridge Manual (BM) [23].

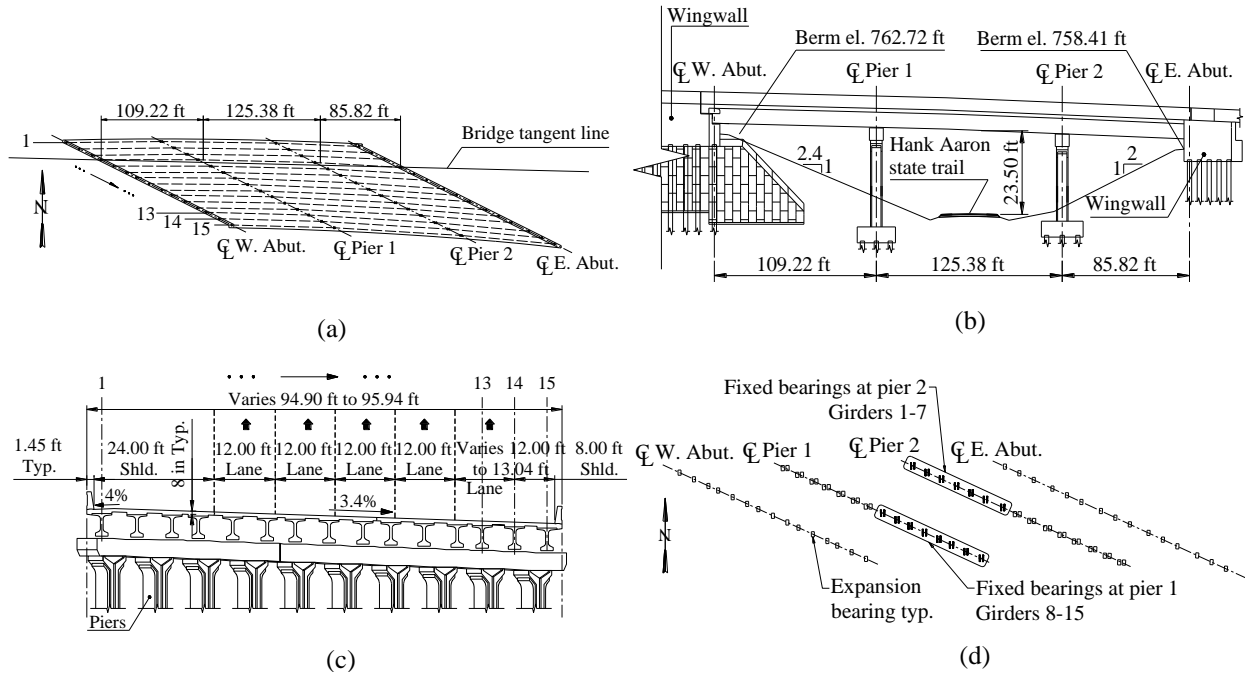


Figure 4.1. Bridge geometry: (a) plan view; (b) elevation (looking north); (c) cross section (looking east); (d) bearing layout shown on plan view.

4.1.2. SHORT-TERM LOAD TESTING

4.1.2.1 LOADING FOR SHORT-TERM LOAD TEST

Loading to collect short-term data consisted of two dump trucks, positioned in series or parallel, moving at crawl speeds (i.e., less than 5 mph) to simulate a pseudo-static load. Dimensions and axle weights of the two trucks used are shown in Figure 4.2. The middle and rear axles were assumed to equally share the measured weight of both axles together.

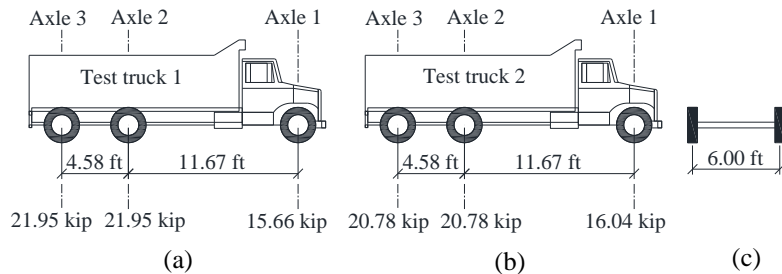


Figure 4.2. Load test trucks dimensions and axle weights: (a) test truck 1; (b) test truck 2; (c) front view showing axle width.

The short-term test had four load cases (Figure 4.3). In all load cases, the trucks moved from west to east. Each load case was run twice to ensure the results were repeatable. During some runs, the trucks came to a full stop at predefined positions to achieve actual static loading. Each load case was selected to maximize response at a selected bridge member, or to understand live load distribution when one or more lanes were loaded. Table 4.2 presents the details of truck stops and the purpose of each test.

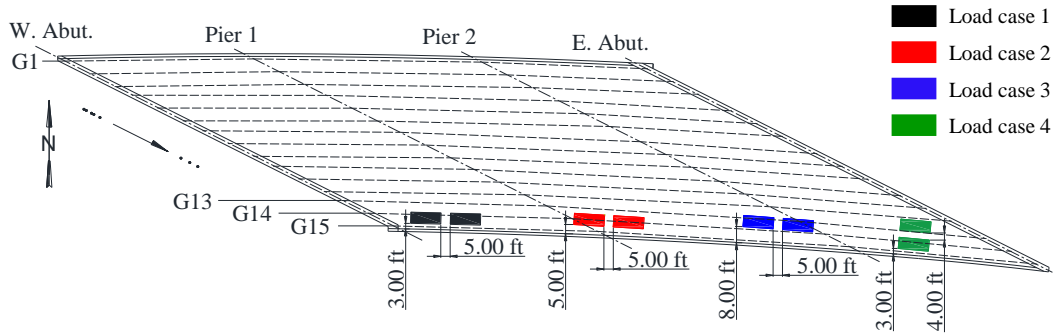


Figure 4.3. Load test load cases.

Table 4.2. Truck stops per load case.

Load case	Load case was run to maximize the response of	Run	Stops		
			Span 1 at mid-span (west)	Span 2 at mid-span	Span 3 at mid-span (east)
1	exterior girder under 1-lane loading	1	Yes	Yes	-
		2	-	-	-
2	deck under 1-lane loading.	1	Yes	Yes	-
		2	-	-	-
3	interior girder under 1-lane loading	1	-	Yes	-
		2	Yes	Yes	Yes
4	exterior girder under 2-lane loading.	1	Yes	Yes	-
		2	-	-	-

4.1.2.2 INSTRUMENTATION FOR SHORT-TERM LOAD TEST

Instrumentation for Girder Bending Strains

Bending strains were measured through uniaxial resistance strain gages attached on the surface of prestressed concrete girders on the west span (span 1). These gages were installed in pairs on the bottom face of the three girders (girders 13, 14 and 15 in Figure 4.1a and Figure 4.4) near the south side, and at three points along their span (at 15 ft, 40 ft and 80 ft from the west end of girders). Two gages were used at each gage location for redundancy against potentially malfunctioning sensors.

Instrumentation for Girder Shear Strains

A second set of strain gages was used on the west end of the same girders (girders 13, 14 and 15) to measure shear strains at girder ends on the west span (span 1). These sensors are located near the obtuse corner where maximum shear response is expected on a skewed bridge. The gages were placed at mid-height of girder webs, where strains reach measurable values (i.e., close to the location of maximum shear strain). For this purpose, three strain gages were arranged in a 45-degree rosette layout, with the central one aligned with the horizontal axis of the girder. Vertical shear strains were calculated using two diagonally oriented gages of the three gages. The horizontal gage served as a redundant gage. The layout of bending and shear strain gages is presented in Figure 4.4 shown on plan view.

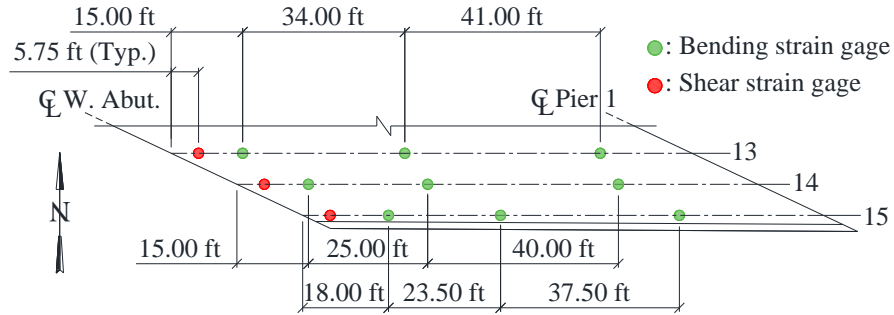


Figure 4.4. Bending and shear strain gage layout shown on plan view of south-west corner.

Instrumentation for Deck Strains

These gages were used to evaluate short and long-term loading effects. A total of twelve vibrating wire strain gages were installed in the concrete deck. Eleven were embedded in the deck, near the south-east corner of the bridge. The twelfth vibrating gage was used to measure shrinkage and temperature effects. This “stress-free” control gage was installed inside an unloaded, “stress free” concrete cylinder cast with the concrete used in the deck (Figure 4.5). The cylinder with the gage inside was placed near the bridge so that it is exposed to similar environmental conditions as the deck. Each of the vibrating wire gages was connected to a solar powered data logger that allowed remote access to the information. All vibrating wire gages also measured temperature.



Figure 4.5. “Stress free” concrete cylinder.

Vibrating wire strain gages in the concrete deck were arranged along two lines: at deck mid-span between girders 14 and 15 (oriented in longitudinal and transverse directions), and along the edge of the top flange of girder 14 (oriented in transverse direction). All gages were attached to the top deck reinforcement, except for two along the latter line that were attached to the bottom reinforcement. Gages on the top layer and bottom layer deck reinforcement were at an average depth of 4 in. and 6 in. from the deck top surface, respectively. The layout of vibrating wire strain gages is shown in Figure 4.6. The acute corner region of the bridge was selected for instrumentation in order to better understand the development and progress of the typical diagonal concrete deck cracks that are regularly reported for skewed bridges.

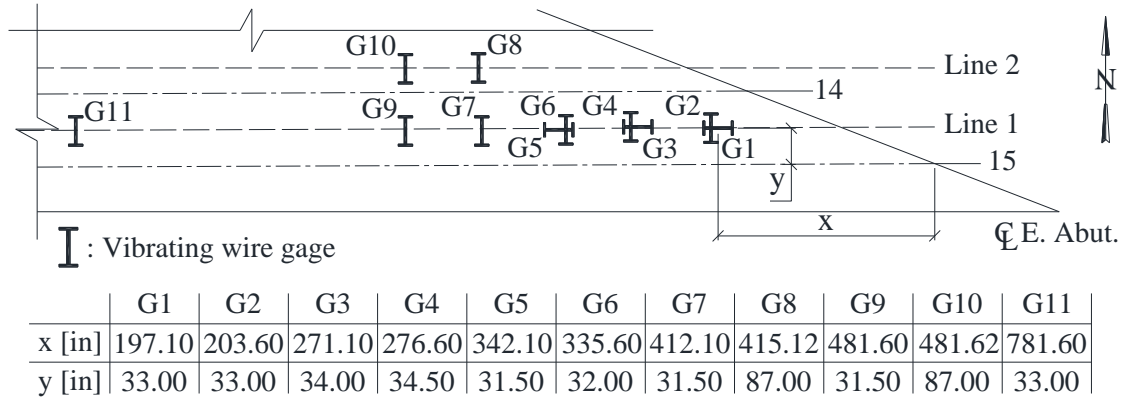


Figure 4.6. Deck vibrating wire strain gages layout shown on plan view.

Instrumentation for Bearing Pad Vertical Displacements

Displacement transducers were placed at the bearing pads of four selected girders near the acute corner to measure the vertical displacement of elastomeric bearing pads (Figure 4.7). Even though these displacements were expected to be small, the intent was to understand the proportion of the live load (assumed proportional to bearing pad displacement) that goes to each of the instrumented girders. Each bearing pad had four displacement transducers (one at each bearing pad corner). The transducers were attached to metallic plates on top of the elastomeric bearing pad using magnets. A better choice for measuring girder end reaction would be load cells. However, load cells were deemed cost-prohibitive since large reaction forces were expected (56 kip) and since load cells installed under bearing pads cannot be removed or reused. The displacement transducers were attached one day before the load test.



Figure 4.7. Displacement transducers installed on west abutment expansion bearing.

Instrumentation for Vertical Displacements on Central Span

Displacement targets were placed at mid-span of three selected girders to measure girder displacements using an optical instrument (a total station). Displacement targets were glued on the bottom surface of prestressed concrete girders approximately one month prior to load testing. The intention with displacements measurements was to understand load distribution between instrumented girders. Figure 4.8 shows displacement targets.



Figure 4.8. Optical displacement targets on girders of bridge central span.

4.1.2.3 PRELIMINARY EVALUATION OF SHORT-TERM LOAD TEST DATA

All measurements, including shear strains, bending strains, deck strains, bearing pad displacements, superstructure mid-span displacements, were reviewed for errors before data were analyzed further. The patterns and magnitudes of shear and bending strains were as expected. In addition, girder and deck strains measured through duplicate gages and/or load cases were the same as the ones originally measured. These evaluations showed that strain measurements were reliable.

On the other hand, bearing pad displacement measurements were deemed erroneous and discarded because duplicate measurements were not the same as the originals, and magnitudes of measurements were not consistent with loading. Data collected by displacement transducers were inconsistent due to the sensitivity of very small displacements (expected to be less than 0.012 in.) to unintended movements in displacement transducers and the limited precision of the transducers (0.004 in.). These measurements were discarded. Similarly, duplicated load cases did not result in the same girder mid-span displacements. Low precision of total station and displacement targets, compared to the very small measurement targets (less than 0.28 in. over 125.38 ft span) likely caused error in these measurements. Mid-span displacement measurements were also discarded.

4.1.2.4 RESULTS OF SHORT-TERM LOAD TEST

Shear Strain Influence Lines

Shear strain influence lines were created using the approximate locations of trucks along the span. Figure 4.9 shows the influence line for shear strains on the three instrumented girders for the four load cases. Girders 13, 14 and 15 were adjacent. Girder 15 is the exterior girder as shown in Figure 4.4 Since only three girders were instrumented, shear load distribution cannot directly be calculated from load testing.

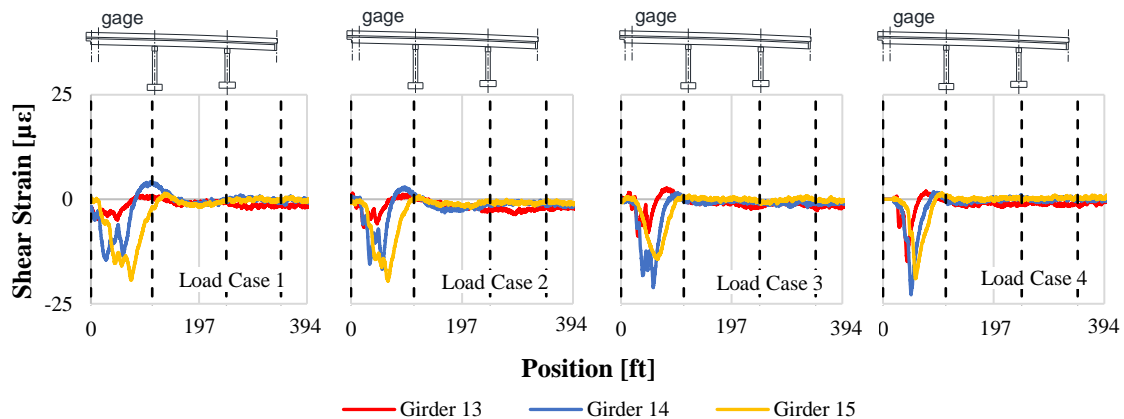


Figure 4.9. Shear strain influence lines for girders 13, 14 and 15 for load cases 1-4.

Bending Strain Influence Lines

Bending strain influence lines for the instrumented girders are shown in Figure 4.10 for each load case, and for each gage location. These influence lines are an indicator for how bending moments were distributed among the three instrumented girders that were located closest to loading.

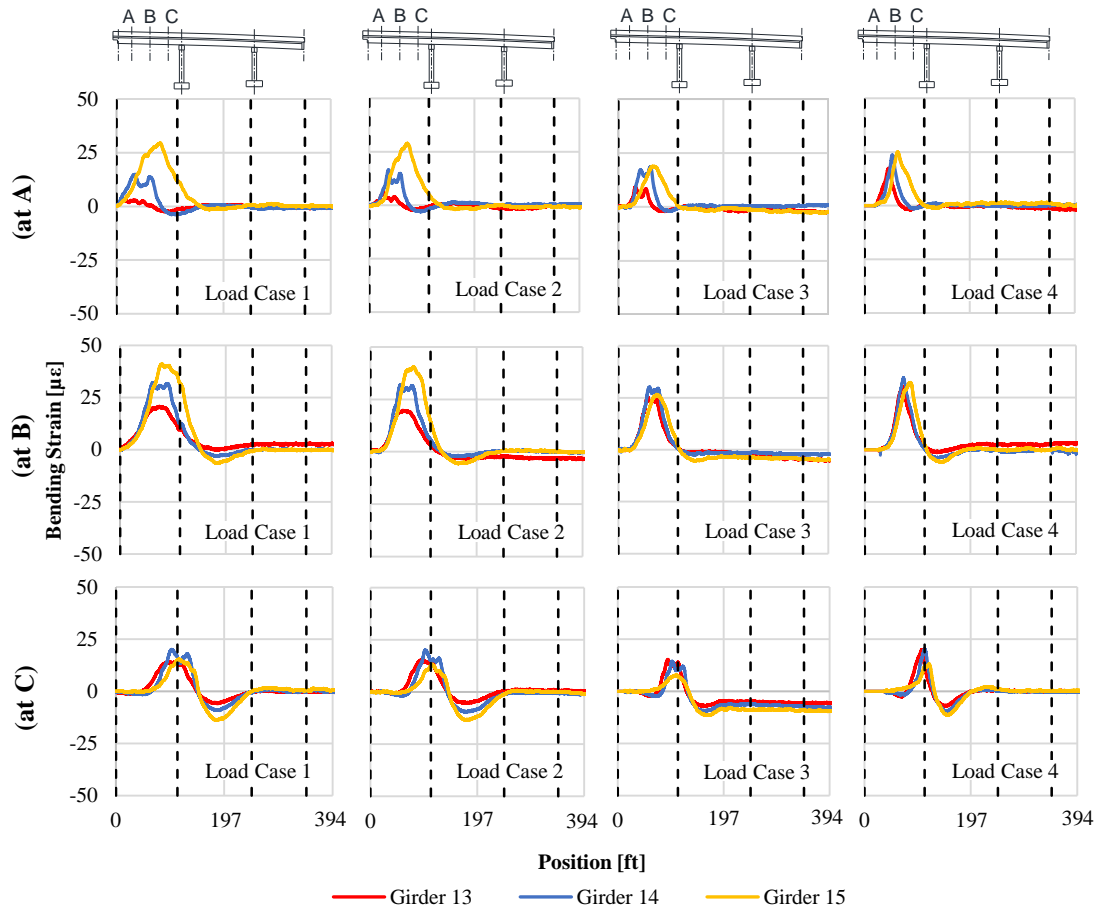


Figure 4.10. Bending strain influence lines for girders 13, 14 and 15 for load cases 1-4. Tension: (+); compression: (-).

Deck Strains during Load Test

Change in deck strains were small during load testing under all load cases. Figure 4.11 shows the maximum strain measured at each gage during load testing. The figure also shows the maximum strains measured at the “stress-free” cylinder gage. Deck strains created by truck loading in the deck were small and, in various cases, comparable to the ones created by small temperature changes that took place during the load test (in approximately 4 hours) as measured by the “stress-free” cylinder gage.

Vibrating wire gages were embedded in concrete and therefore did not measure the maximum tensile and compression stresses at extreme fibers of the deck. The average depth of gages in deck, measured from the top surface of the deck, was approximately 4.4 in., close to the mid-height of the deck. The maximum extreme fiber strains were calculated from the measured strains, assuming a linear axial strain profile along the deck height. The absolute values of these strains are shown in parentheses for each gage location in Figure 4.6. The maximum strain at the extreme fiber was measured along the longitudinal direction of the bridge, was 100 micro-strains and was smaller than the theoretical cracking strain of the deck.

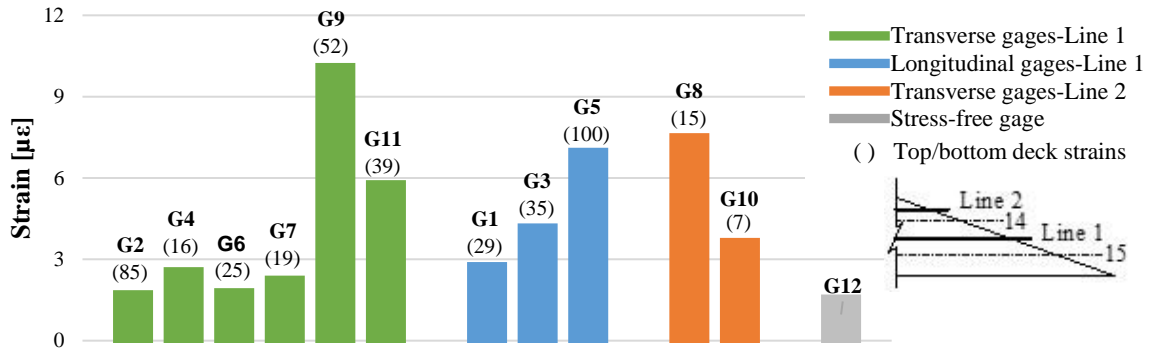


Figure 4.11. Maximum deck strains from all load cases at all gages and at deck extreme fibers for all gage locations (absolute values).

4.1.3. LONG-TERM MONITORING

4.1.3.1 LOADING FOR LONG-TERM MONITORING

Long-term loading was composed of temperature loads, shrinkage and traffic load.

4.1.3.2 INSTRUMENTATION FOR LONG-TERM MONITORING

Instrumentation for Girder End Displacements

The displacement sensors were wireless devices that have two components; the displacement sensing element and the wireless transmitter (Figure 4.12). The displacement sensing element had a mechanical stroke length of 3 in. It is connected (i.e., wired) to the wireless transmitter that sends displacement readings, at pre-set time intervals, to a solar powered data collector that allows storage of and remote access to the information. Displacement sensors also measure temperature.

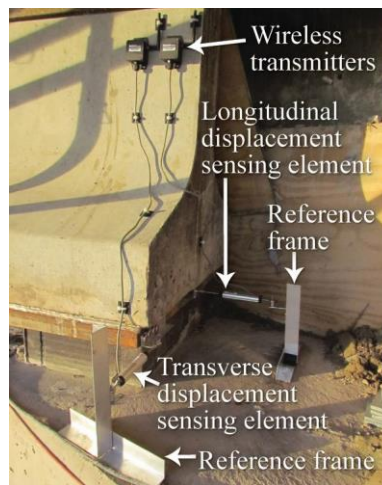


Figure 4.12. Displacement sensors as installed on the girder bearing at the S-E corner over the abutment.

Five displacement sensors were installed on the bridge to understand the global displacement behavior of the bridge in the horizontal space. Girder bearings near the north-west and south-east corners over the abutments had two displacement sensors each (Figure 4.12). One sensor was placed on the girder near the south-west corner over the abutment. Having two sensors at a particular bearing, one in the longitudinal and the other in the transverse bridge directions, and under the assumption of small rotations on the horizontal plane enabled the computation of the relative change of bearing position with time. This was not possible with the single sensor near the south-west abutment corner. However, this sensor still provided important bearing transverse displacement measurements. The acute corners of the bridge were chosen to be instrumented for displacements because they may experience significant movements. Figure 4.13 presents the layout of displacement sensors.

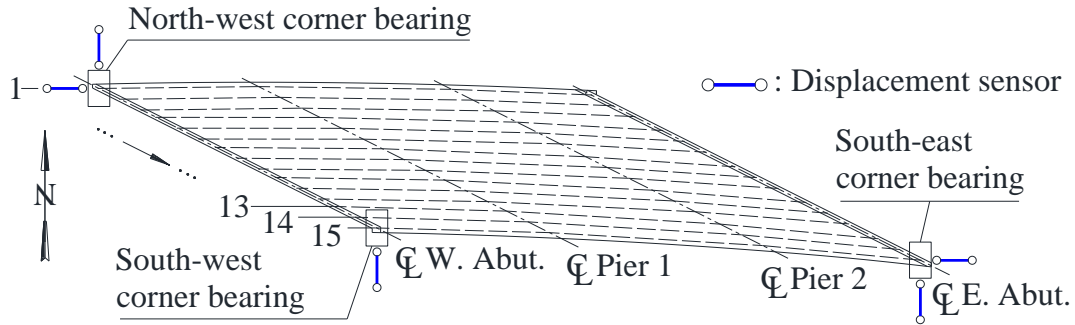


Figure 4.13. Displacement sensor layout shown on plan view.

Instrumentation for Deck Strains

The same vibrating wire strain gages used for deck short term strain measurements were used to collect strain and temperature data under long term loading.

4.1.3.3. RESULTS OF LONG-TERM MONITORING

Displacement Sensors Results

Data collection from displacement sensors started on November 13, 2016, shortly after construction, and continued for a year. Several disturbances to sensors resulted in loss of data during a number of data collection periods. Data until May 16, 2017 are presented in Figure 4.14 -Figure 4.15, as an example. Gaps on these graphs correspond to periods (i.e., approx. one month) with no data. Reported displacement values are relative to bearing positions at the beginning of data recording. Since data recording started shortly after construction, displacements at the beginning of recording are expected to be virtually zero. Results after the data gaps assume that no changes in displacement occurred during the period when no data were recorded. The displacement results are presented in two directions: in transverse (i.e., perpendicular to bridge axis) and longitudinal (i.e., along bridge axis) directions, and in parallel-to-expansion joint (racking) and normal-to-expansion joint directions.

Transverse and Longitudinal Displacements

Figure 4.14a - Figure 4.14b display the bearing displacements and the average internal temperature of the corresponding pair of sensors at the bridge acute corners. Figure 4.14c shows the transverse displacements in the south-west corner bearing and temperature, measured by a single sensor. In Figure 4.14c, potential impact of longitudinal displacements on transverse displacement measurements, which cannot be captured due to the lack of a second sensor, was neglected.

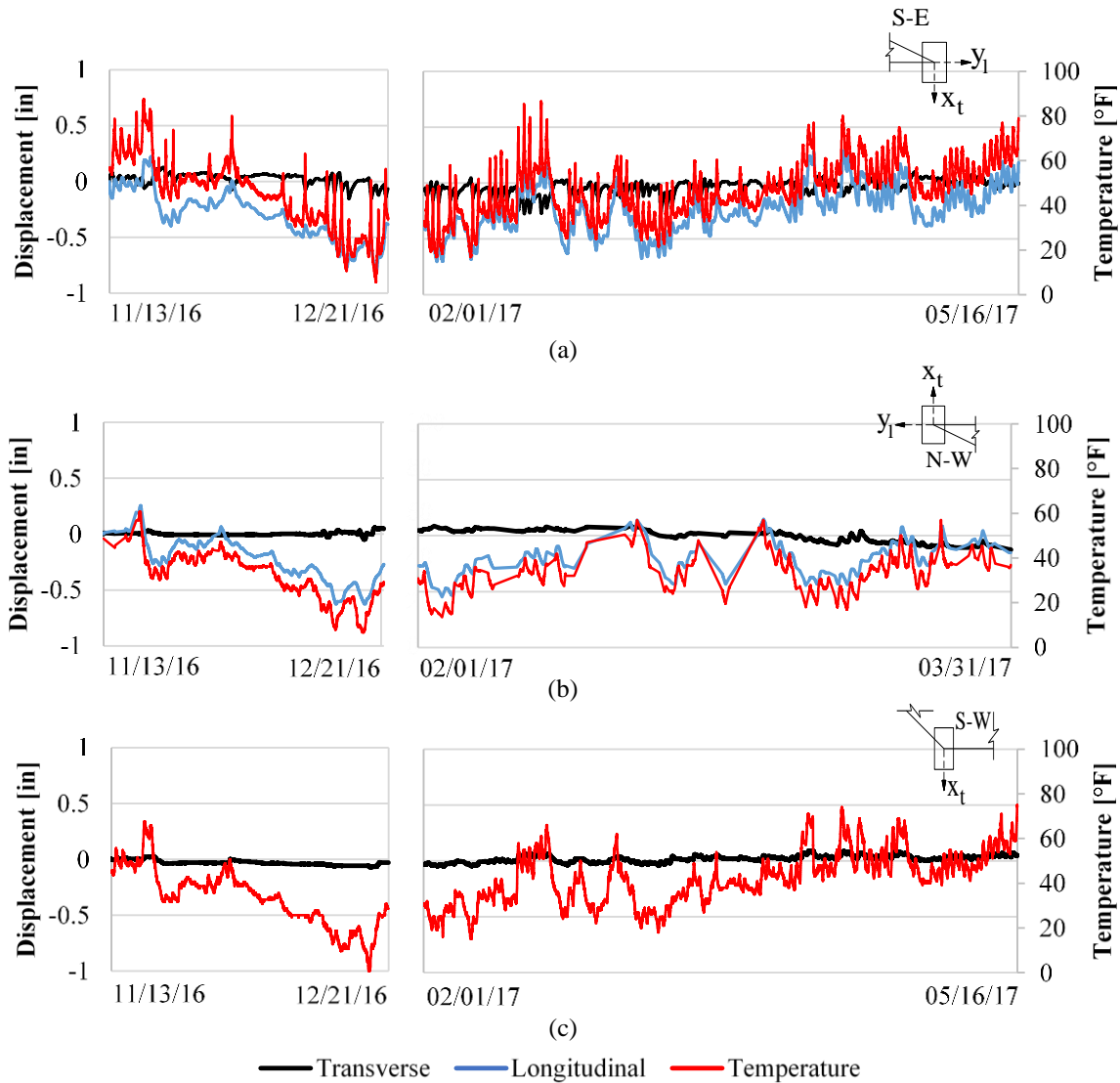


Figure 4.14. Bearing transverse and longitudinal displacements, and temperature on the: (a) south-east corner; (b) north-west corner; (c) south-west corner.

Results in Figure 4.14a and Figure 4.14b show that longitudinal displacements were much larger than transverse displacements (up to 5 times) at both acute corner bearings. In all locations, transverse displacements were smaller than 0.28 in. It is also interesting to note that longitudinal displacements on the south-east bearing are larger than the ones observed on the north-west bearing, even though the expansion length for the latter is longer, as shown in Figure 4.1a. This can be explained by the horizontal curve of the bridge causing the effective expansion length for the south-east bearing to be approximately 10 ft longer than the north-west bearing.

Figure 4.14a and Figure 4.14b show that the longitudinal displacements correlated well with temperature, indicating that temperature change is the main reason for longitudinal bridge displacements. In fact, the Pearson's correlation coefficient, which indicates for a pair of variables how strong their linear association is (i.e., ± 1 : perfect linear relationship, 0: no linear correlation) [41], between longitudinal displacements and temperature for both bearings and periods had a strong positive correlation with values above 0.90.

Pearson correlation coefficients for temperature and transverse displacements on acute corner bearings were below 0.25. Such low coefficients show that transverse displacements and temperature on acute corners did not correlate linearly and that factors other than temperature may have a more important role

on transverse displacements. In contrast to this finding, transverse displacements and temperature on the obtuse corner had a strong positive linear association with correlation coefficients of 0.90. This may imply that transverse bearing movements also depend on location. Nevertheless, it is clear from the small lateral bearing displacements that any lateral translation or rotation on the bridge was very small, and that the thermal movements of the bridge are predominantly due to longitudinal expansion or contraction.

Table 4.3 summarizes maximum values of transverse and longitudinal displacements ($\delta_{\max(+)}$ and $\delta_{\max(-)}$) since the beginning of data recording (construction), in both positive and negative directions according to the sign conventions shown in Figure 4.14.

Table 4.3. Maximum bearing displacements in transverse and longitudinal directions.

Location	Period	Transverse direction		Longitudinal direction	
		$\delta_{\max(+)}$ [in]	$\delta_{\max(-)}$ [in]	$\delta_{\max(+)}$ [in]	$\delta_{\max(-)}$ [in]
S-E corner	1	0.13	-0.15	0.23	-0.82
	2	0.10	-0.28	0.29	-0.70
N-W corner	1	0.06	-0.05	0.25	-0.63
	2	0.09	-0.13	0.15	-0.55
S-W corner	1	0.07	-0.02	N/A	N/A
	2	0.05	-0.09	N/A	N/A

Parallel-to-Expansion Joint (racking) and Normal-to-Expansion Joint Displacements

Results presented in the previous section seem to show that the unique support fixity arrangement (Figure 4.1d) led to small transverse displacements as intended by design. Figure 4.15 shows parallel-to-expansion joint and normal-to-expansion joint displacements, calculated from transverse and longitudinal displacements based on bridge geometry. Parallel-to- and normal-to- joint displacements at the south-west corner cannot be calculated since only a single sensor was used at this location.

When Figure 4.14a and Figure 4.14b are compared with Figure 4.15, it can be seen that bearing displacements in parallel-to-joint and normal-to-joint directions are mainly caused by longitudinal movements of the bridge. In fact, given the high skew of the bridge (i.e. 64°), approximately 90% and 40% of the bearing longitudinal displacement translates into the parallel-to-joint displacement, and normal-to-joint displacements, respectively. In general, parallel-to-joint displacements are larger than normal-to-joint displacements.

Parallel-to-joint displacements at both corners presented a strong positive linear relationship with temperature, with correlation coefficients beyond 0.90. Furthermore, normal-to-joint displacements at both corners exhibited a less strong, still positive, linear correlation, with coefficients between 0.76 and 0.96. As expected, these results confirm the major influence of longitudinal bearing movements on these displacement components. During the seasonal warming period, the linear correlation between displacements and temperature was less strong than the one in the seasonal cooling period, indicating that temperature is more predominant during the cooling period.

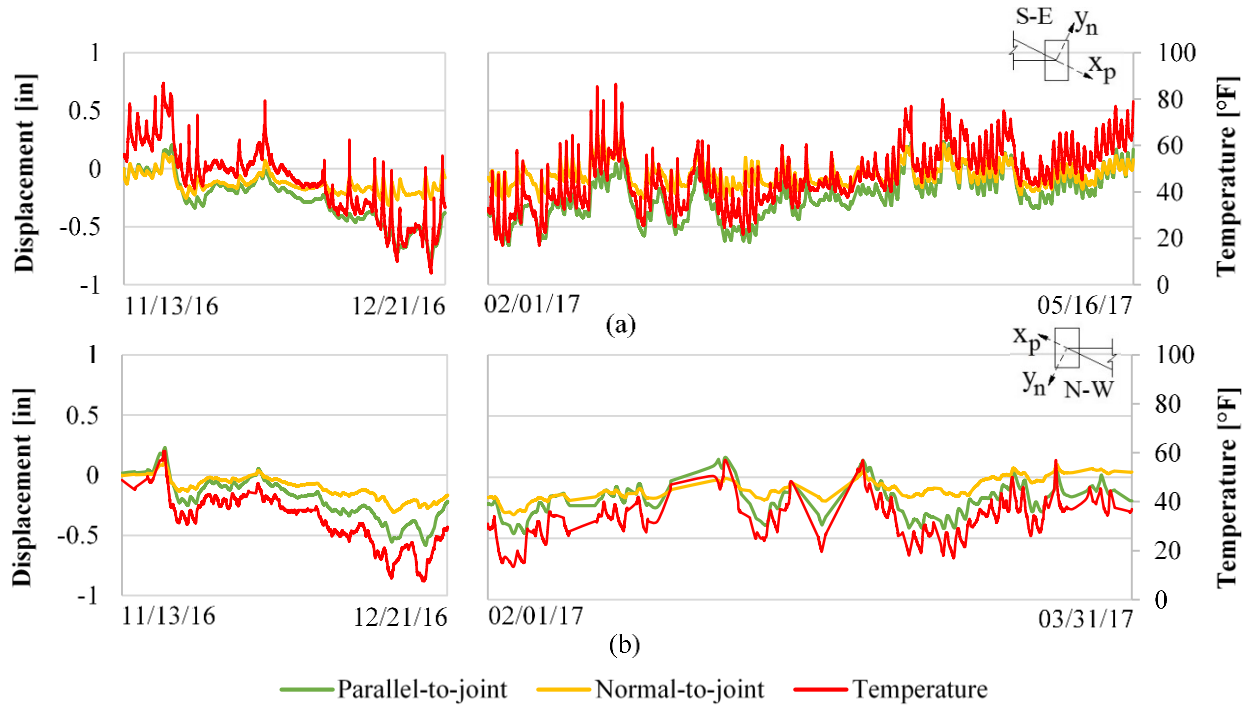


Figure 4.15. Bearing parallel-to-joint and normal-to-joint displacements, and temperature on the: (a) south-east corner; (b) north-west corner.

Table 4.4 presents maximum values of parallel-to- and normal-to- expansion joint displacements ($\delta_{\max(+)}$ and $\delta_{\max(-)}$) recorded since the beginning of data acquisition, in both positive and negative directions according to the sign conventions shown in Figure 4.15.

Table 4.4. Maximum bearing displacements in parallel-to- and normal-to- joint directions.

Location	Period	Parallel-to-joint direction		Normal-to-joint direction	
		δ_{\max} [in]	δ_{\min} [in]	δ_{\max} [in]	δ_{\min} [in]
S-E corner	1	0.20	-0.78	0.12	-0.31
	2	0.23	-0.66	0.30	-0.29
N-W corner	1	0.23	-0.58	0.11	-0.31
	2	0.16	-0.46	0.10	-0.31

Vibrating Wire Strain Gages Results

Recording of deck strains began on October 18, 2016 (i.e., 85 hours after deck pour), and was in progress for one year. Deck strains and strains of a “stress-free” cylinder gage were measured.

Total Strains

Figure 4.16 and Figure 4.17 present strain and temperature data up to October 16, 2017. Figure 4.16 displays total deck strains along lines 1 and 2 and for the “stress-free” cylinder gage. Figure 4.17 shows temperature on the “stress-free” control gage, and the average of temperature from all deck sensors. Temperatures on deck sensors were similar.

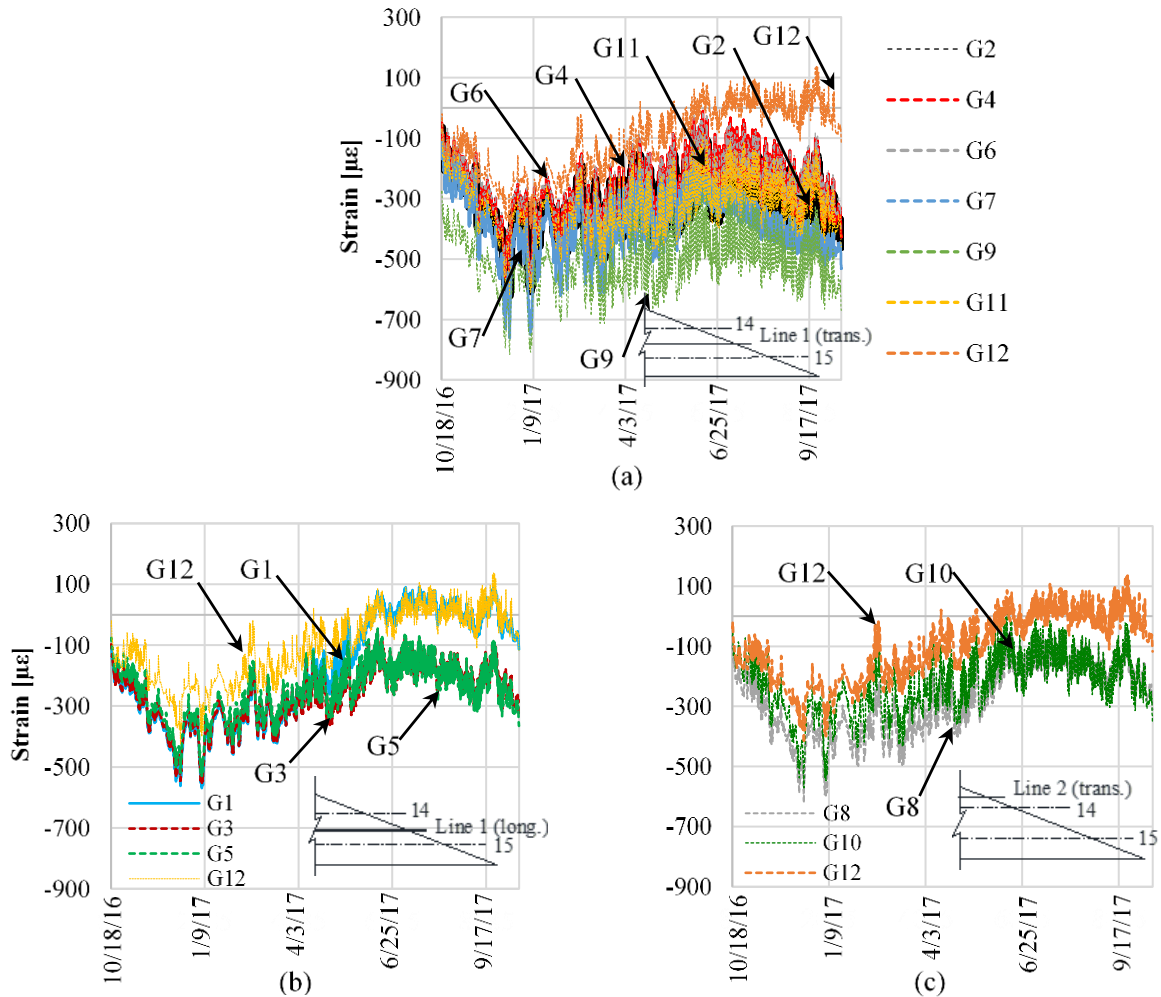


Figure 4.16. Deck strains: (a) total transverse strains on line 1; (b) total longitudinal strains on line 1; (c) total transverse strains on line 2. Tension: (+); compression: (-).

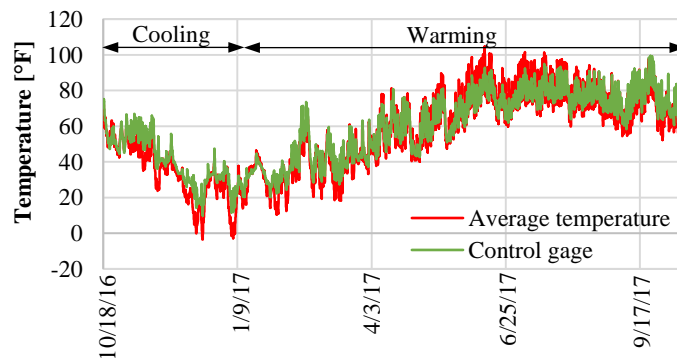


Figure 4.17. Average temperature of all gages in the deck and temperature in the “stress-free” cylinder control gage.

Table 4.5 shows maximum strains (ϵ_{\max}) from all gages, and corresponding temperatures ($T_{\epsilon_{\max}}$) from the cooling and heating periods. In addition, initial temperatures (T_0) that correspond to the beginning of data collection are given. Differences in strains in the deck may be caused by temperature gradients through the bridge depth. The difference between deck and “stress-free” cylinder gage measurements, in addition to strains created by external loading and restraining effects, can be explained as follows. The temperature changes measured in the deck and “stress-free” gage can be different, since the “stress-free” cylinder was

stored under the deck. All strains measured include shrinkage effects, which may be larger in the deck than it is in the “stress-free” cylinder gage due to the larger exposed area of the deck.

Table 4.5. Maximum strains and corresponding temperatures for the deck and the “stress-free” cylinder gage. Tension: (+); compression: (-) for strains.

Gage	T _o	Cooling		Heating		Gage direction (referring to bridge direction)
		ε _{max.c}	T at ε _{max.c}	ε _{max.h}	T at ε _{max.h}	
	[°F]	[με]	[°F]	[με]	[°F]	
1 (deck)	74	-569	-2	91	99	Longitudinal
2 (deck)	74	-621	-3	-65	74	Transverse
3 (deck)	73	-559	-3	-48	106	Longitudinal
4 (deck)	72	-590	-5	-10	106	Transverse
5 (deck)	72	-530	-3	-45	105	Longitudinal
6 (deck)	72	-577	-4	-1	105	Transverse
7 (deck)	73	-762	-5	-113	73	Transverse
8 (deck)	69	-621	-1	-32	98	Transverse
9 (deck)	74	-816	-4	-250	108	Transverse
10 (deck)	69	-571	-1	19	98	Transverse
11 (deck)	73	-621	-4	-66	73	Transverse
12 (“stress-free”)	72	-423	10	137	99	N/A

Figure 4.18 supplements Figure 4.16, and presents the total change in strain during the data recording period as a function of gage position along lines 1 and 2. It shows that change in transverse strains along line 1 are significant and around -400 μstrain. Changes in longitudinal strains on line 1 increased towards the pier.

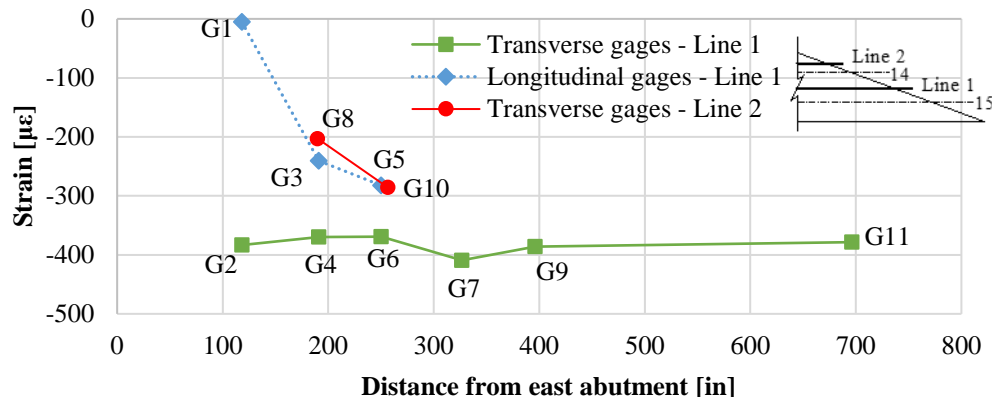


Figure 4.18. Total change in strain along gage lines 1 and 2 during data recording period. Tension: (+); compression: (-).

Residual Strains

Figure 4.19 shows deck strains after the “stress-free” cylinder control gage (gage 12) strains are subtracted. This figure indicates that after the removal of strains captured by the control gage, which are interpreted to be temperature and shrinkage strains, this region of the deck gradually and almost linearly accumulated compressive strains. This is likely due to the effects of the actual temperature distribution in the superstructure, and higher shrinkage strains in the deck than the “stress-free” cylinder gage due to differences in exposure conditions, which were not completely excluded from the results.

Longitudinal gage 1 on line 1 (Figure 4.19b) was the exception and displayed a rapid increase in tensile strains that started roughly on March 2017. After three months, the tendency changed to tensile strains. This gage is closer to the end of the bridge, and may be crossed by transverse or diagonal paths of high tensile stresses that lead to typical deck acute corner cracking, after which concrete experiences tension softening, explaining the reduction in tensile strains on gage 1 towards the end of the observation period.

Strains in Figure 4.19 represent strains due to external load and restraining effects. The corresponding stresses, that may induce cracking, can be obtained by multiplying these strains with the modulus of elasticity of concrete.

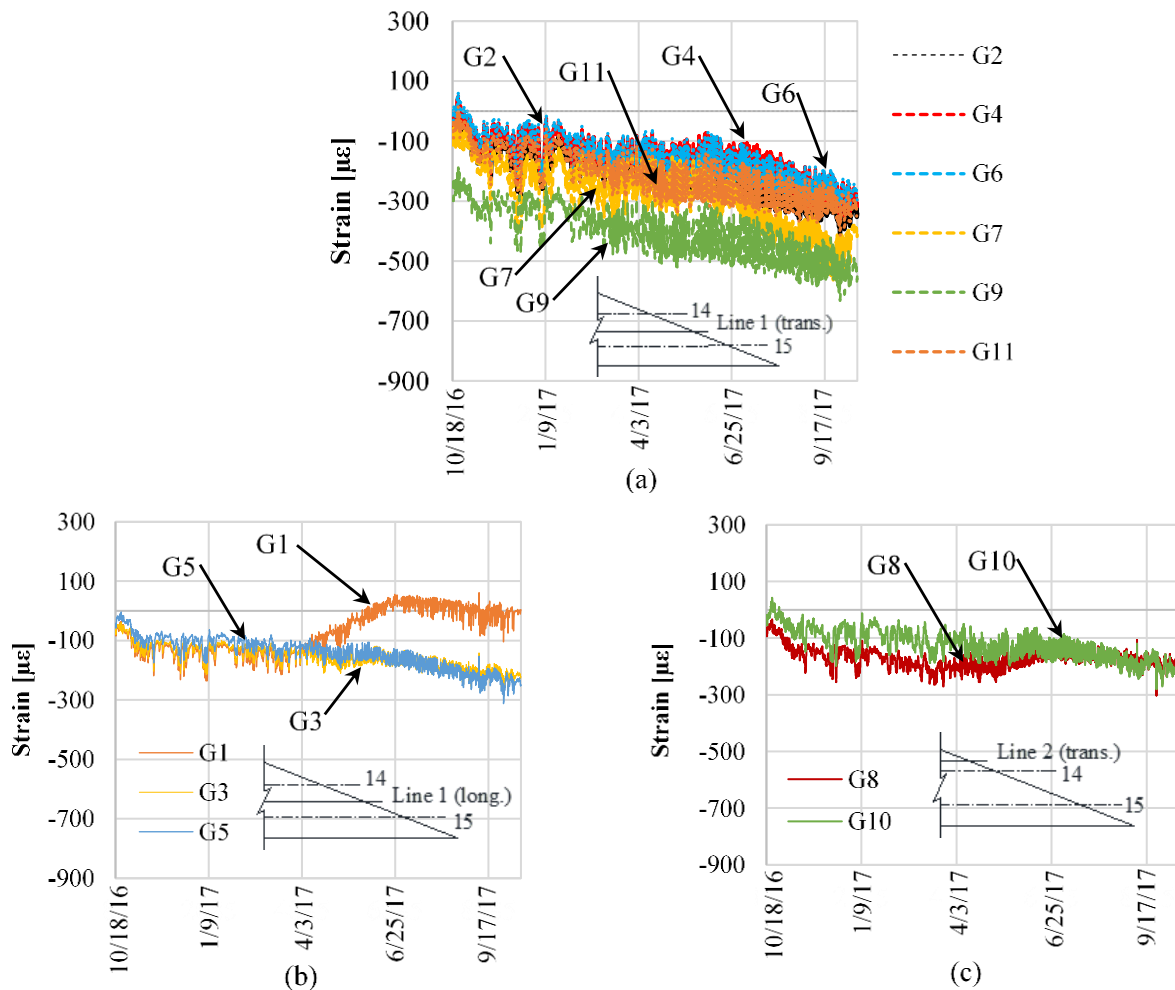


Figure 4.19. Deck strains minus strains from gage 12: (a) transverse strains on line 1; (b) longitudinal strains on line 1; (c) transverse strains on line 2. Tension: (+); compression: (-).

4.2. LOAD TESTING OF THE HIGHLY SKEWED STEEL BRIDGE

A 23-year-old, medium-span, steel girder bridge was load tested on May 12, 2017 to assess load distribution and composite action between girders and deck. This bridge is named as the Chippewa bridge in this report. Existing cracks in the deck provided an opportunity to understand the impact of deck cracks on load distribution. Test results were also used to validate finite element models that were later employed for a parametric study. Unlike the prestressed concrete girder bridge, this bridge was only tested for short term loading.

4.2.1. BRIDGE DESCRIPTION

Bridge B-09-177 carries State Highway 29 West-Bound traffic over County Highway “X” on Chippewa County, Wisconsin. The structure is a three-span, continuous, concrete deck-on-steel W-girders bridge with a skew angle of 47°. General design information and geometry are presented in Table 4.6 and Figure 4.20, respectively.

Table 4.6. The Chippewa bridge, Bridge B-09-177, general features.

Name (WisDOT Bridge ID)	Skew	Span lengths	Pier type	Deck width	Girder type	Abutment type	Bearing types	Year built
The Chippewa bridge (B-09-177)	47°	47.0' – 69.5' – 47.0'	Multi-column	42.2'	W33×130	Sill	Elastomeric (expansion), metallic (fixed)	1993

The straight superstructure has a concrete, 8.0-in. thick cast-in-place deck, composite with girders except for a distance 7.25 ft and 7.5 ft towards exterior and central spans, respectively, over the piers. The concrete deck rests on six steel beams with a constant spacing of 7.25 ft. Beams are connected transversely through channel-shaped (MC18×42.7) steel diaphragms along spans, over piers and abutments. The specified concrete compressive strength for the deck and substructure is 4 ksi and 3.5 ksi, respectively. Girders and diaphragms are A572 Grade 50 and A36 steel, respectively. Mild steel reinforcement has a specified yield strength of 60 ksi.

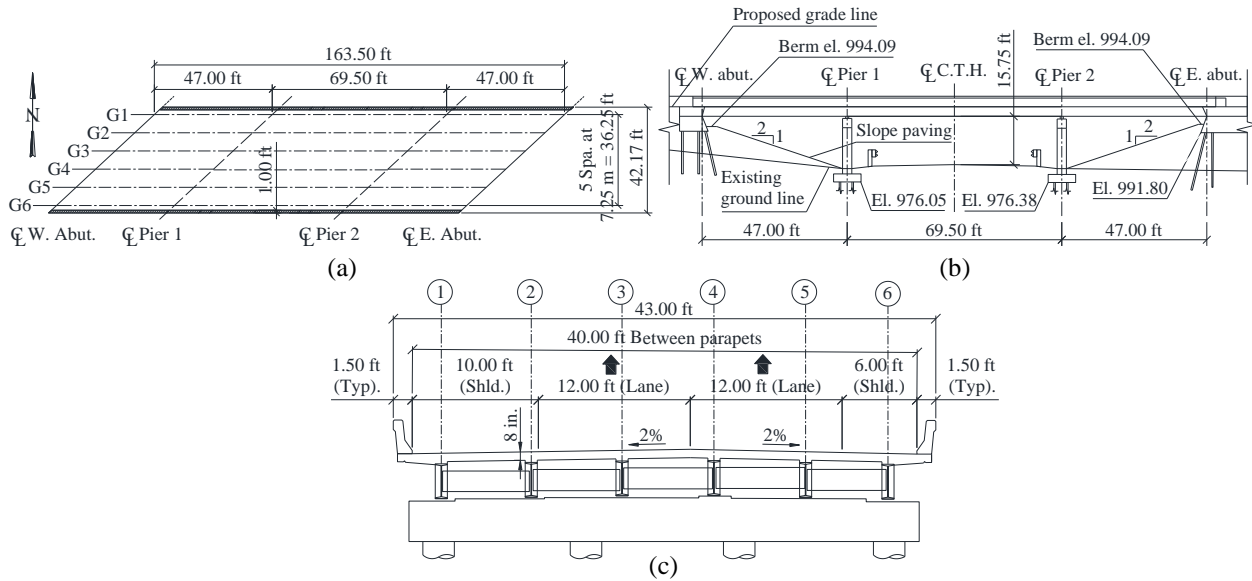


Figure 4.20. Bridge geometry: (a) plan view; (b) elevation (looking north); (c) cross section (looking east).

4.2.2. SHORT TERM LOAD TESTING

4.2.2.1 LOADING FOR SHORT TERM LOAD TEST

Short-term loading consisted on dump trucks moving from east to west abutments at crawl speed (i.e., less than 5 mph) to simulate a static loading on the bridge. Dimensions and axle weights of test trucks are shown in Figure 4.21.

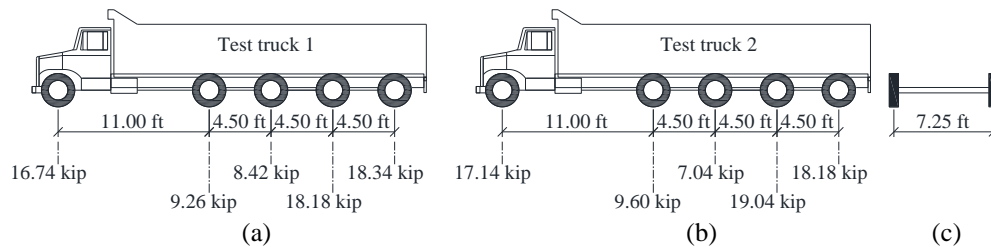


Figure 4.21. Load test truck dimensions and axle weights: (a) test truck 1; (b) test truck 2; (c) front view showing axle width.

Eight load configurations were planned for the load test. These configurations covered several locations across the bridge width and had test trucks arranged either in series or in parallel. During each pass, trucks stopped at approximately mid-span of the instrumented span (i.e., west exterior span) to achieve a fully static loading at a known position. Load configurations (LC) are displayed in Figure 4.22.

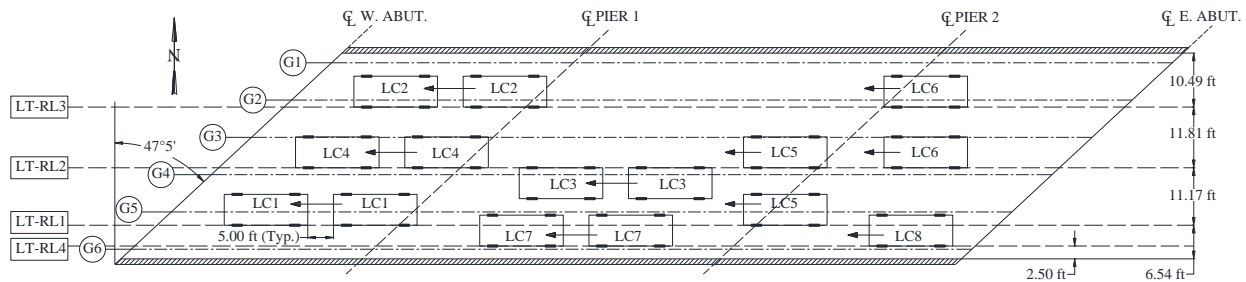


Figure 4.22. Load test load configurations (LC).

4.2.2.2 INSTRUMENTATION FOR SHORT-TERM LOAD TEST

Girder bending and vertical shear strains were measured at several locations on the west exterior span of the bridge using uniaxial resistance strain gages attached to the surface of girders. Bending strains were monitored on all six girders, and at three sections located 12 ft., 22 ft., and 31 ft. from the west abutment (Figure 4.23a). At each location, bending strains were recorded on the girder bottom face, and on the web, 9 in. above the bottom of the girder (Figure 4.23b). Such arrangement and assuming a linear distribution of strains along the girder height made possible the evaluation of the neutral axis position. Vertical shear strains were also measured on all six girders, but at a single section located 5 ft. from the same abutment (Figure 4.23a). A pair of strain gages attached at mid-height of girder webs and oriented 45° above and below the horizontal was needed to evaluate shear strains (Figure 4.23b).

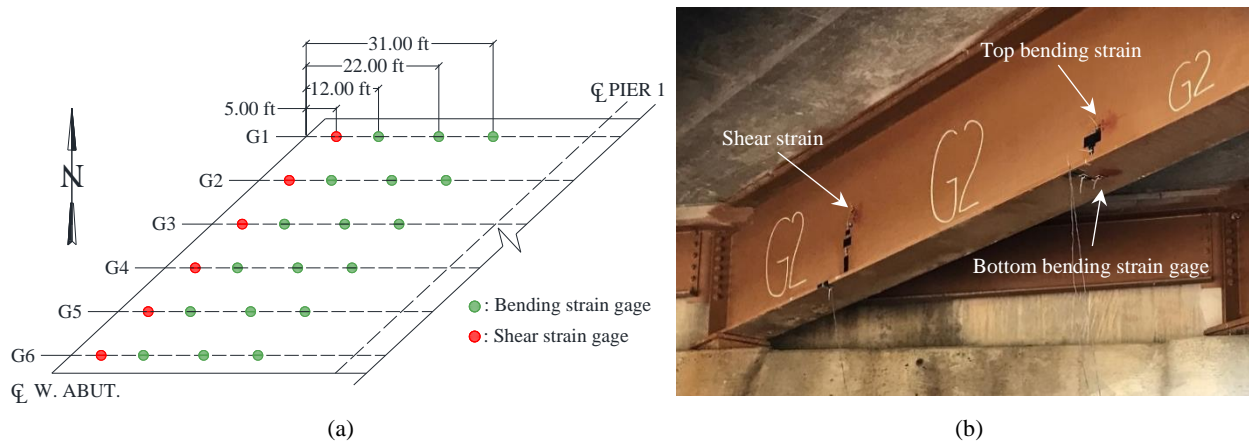


Figure 4.23. (a) Bending and shear strain gage layout shown on plan view; (b) bending and shear gages.

4.2.2.3 RESULTS OF SHORT-TERM LOAD TEST

Bending Strains

Bending strains under load configurations 2, 4 and 5 are plotted against time for trucks to move along the bridge in Figure 4.24 and in Figure 4.25 for bottom and top bending strains, respectively, as examples. This information provides insight on the load distribution characteristics of the tested bridge. In general, the highest bending and shear were carried by the three girders closest to the load.

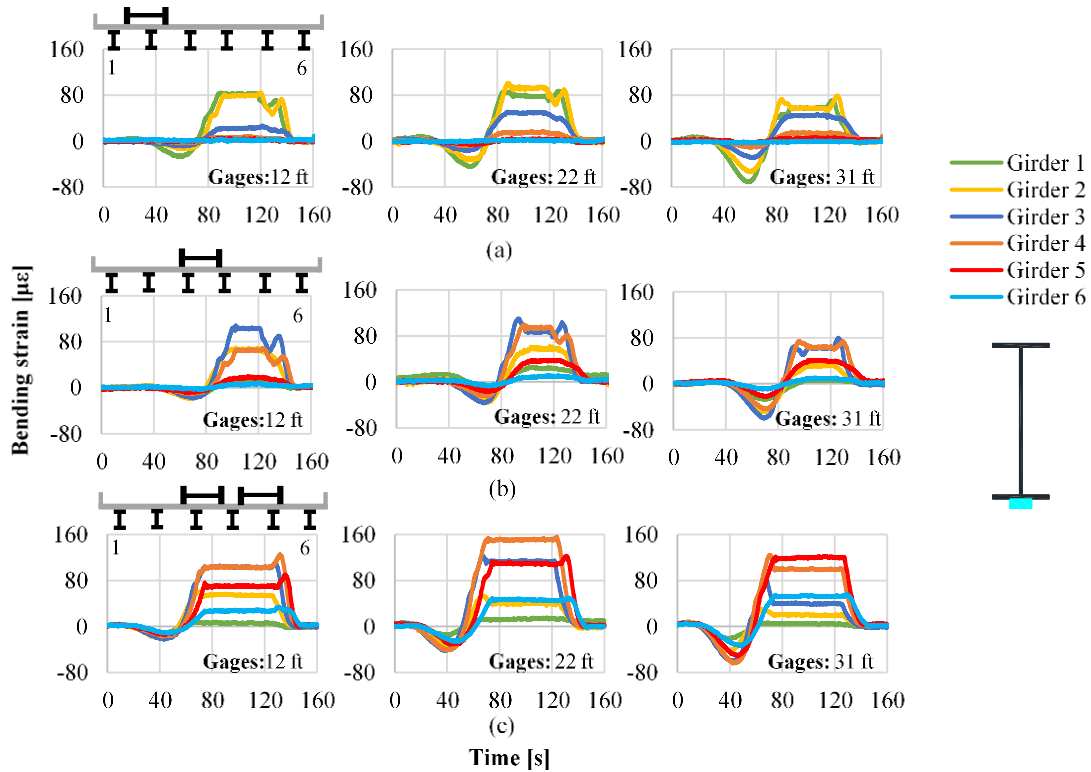


Figure 4.24. Bottom bending strain time histories for: (a) load configuration 2; (b) load configuration 4; (c) load configuration 5. Tension: (+); compression: (-).

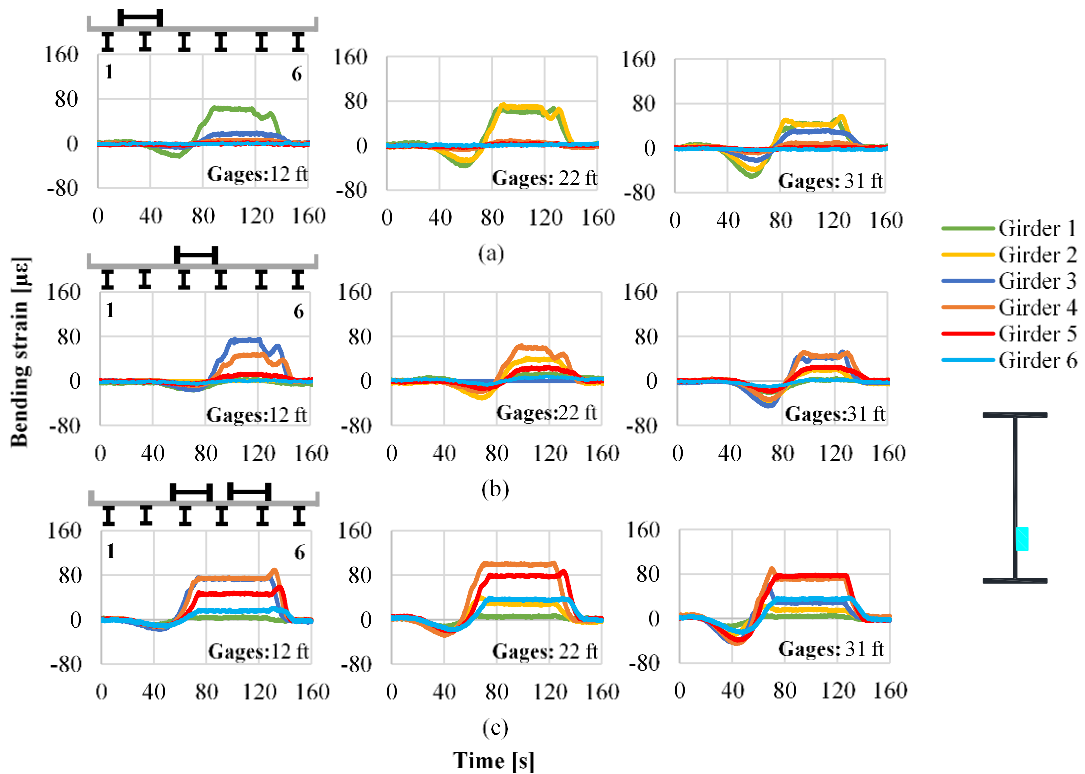


Figure 4.25. Top bending strain time histories for: (a) load configuration 2; (b) load configuration 4; (c) load configuration 5. Tension: (+); compression: (-).

Shear Strains

Similar to bending strains, shear strains under the load configurations 2, 4 and 5 are plotted against time for trucks to move along the bridge in Figure 4.26, as examples. The results show that the majority of shear was carried by the three girders closest to the load.

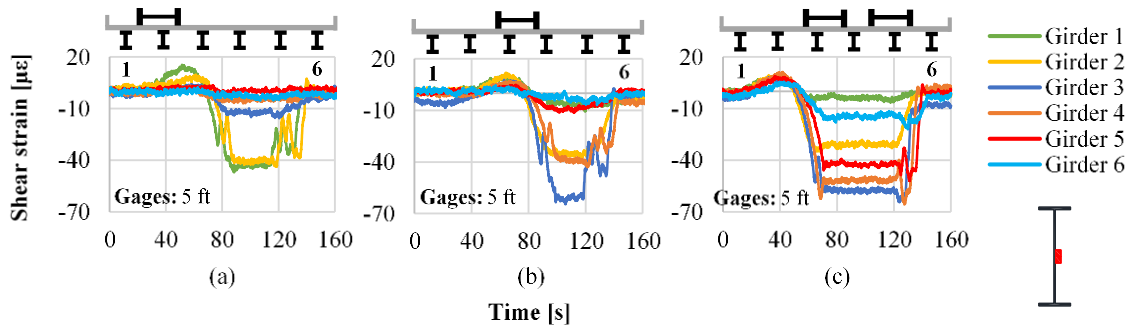


Figure 4.26. Vertical shear strain time histories for: (a) load configuration 2; (b) load configuration 4; (c) load configuration 5.

Neutral Axis Positions

Figure 4.27 compares measured and theoretical neutral axis positions for load configurations 1-8. Theoretical neutral axis positions were calculated from bending strains measured at two locations along girder height. Calculations assumed deck and steel girders were fully-composite, and included the contribution of parapets for exterior girders and steel reinforcement in the deck and parapets. The theoretical neutral axes lie at 32.5 in. and 38.6 in. from the bottom of girders for interior and exterior girders, respectively.

Field results for almost all load configurations had small deviations between measured and theoretical neutral axes of girders close to the loading location. For example, in load configuration 2 (Figure 4.27b), the measured and theoretical neutral axis locations are within 4% of each other, indicating that girders close to loading are fully-composite with the deck. However, girders further from the load have larger deviations between measured and theoretical neutral axes. In addition, some measured neutral axes lead to unrealistic results for girders further away from loading. The deviations indicate amplification of errors in measurement of very small strains on girders away from loading. For these measurements, strains were not large enough to achieve the level of accuracy needed to calculate neutral axis location. Therefore, for the rest of this report, all girders of this bridge were assumed to be fully composite with the deck.

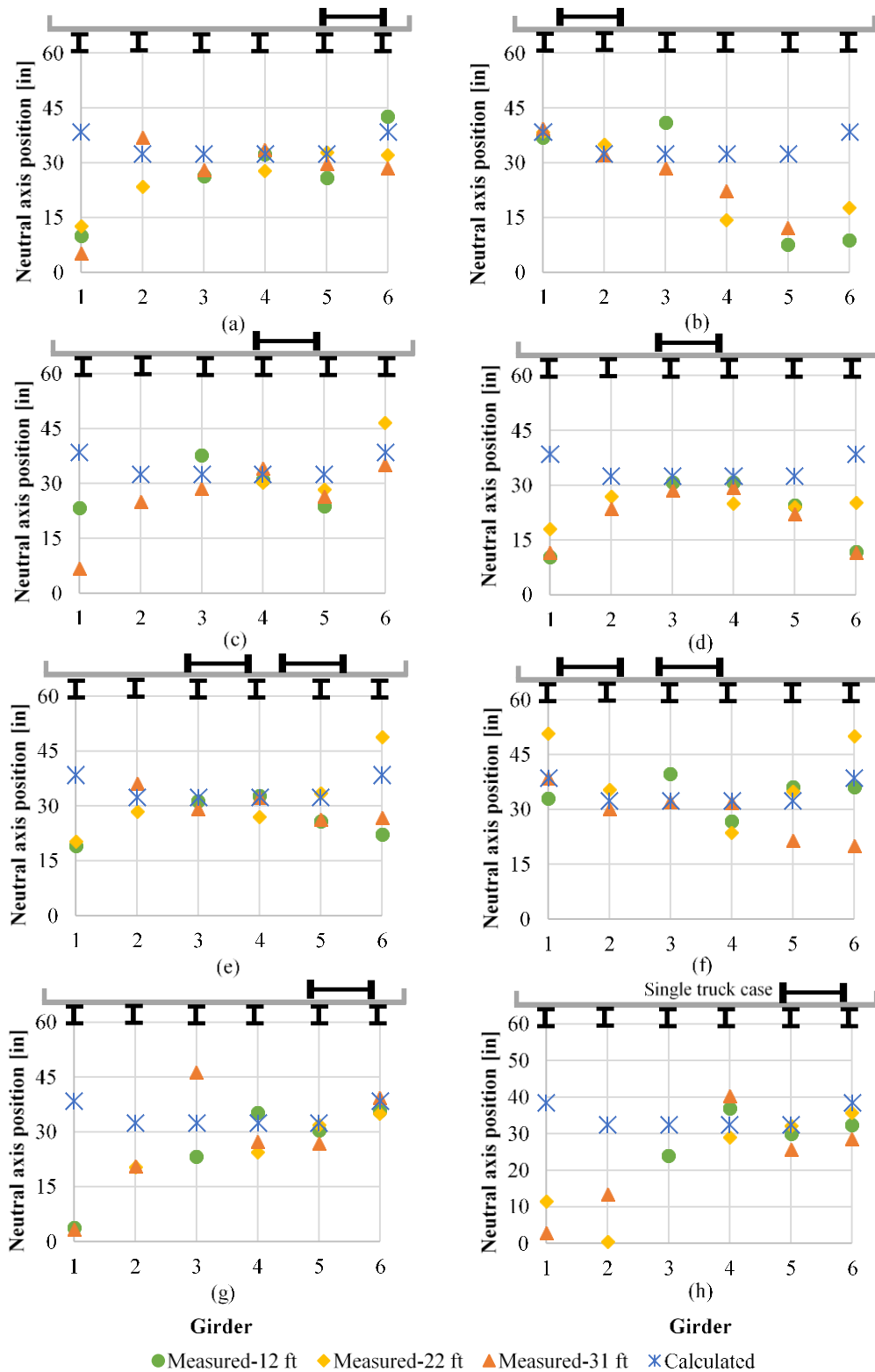


Figure 4.27. Measured and theoretical neutral axis positions for: (a) load configuration 1; (b) load configuration 2; (c) load configuration 3; (d) load configuration 4; (e) load configuration 5; (f) load configuration 6; (g) load configuration 7; (h) load configuration 8.

Live Load Distribution

The distribution of moments and shears on the bridge was evaluated by means of live load distribution factors and is presented in Figure 4.28 and Figure 4.29, respectively. Additionally, live load distribution factors per AASHTO LRFD BDS were calculated and are included in these figures.

Bending moments and shear forces were calculated from the measured strains assuming full composite action. Distribution factors for each girder location were calculated as the ratio of the girder reaction force (moment or shear) and the sum of all girder reaction forces at the corresponding section. Load distribution patterns are shown in Figure 4.28 and Figure 4.29, and were as expected. They clearly displayed that most of the load is carried by girders near loading, and that load distribution is similar at each instrumented location along the span.

Figure 4.28 and Figure 4.29 also compares distribution factors from field test data and AASHTO LRFD BDS. In bending, AASHTO LRFD BDS is conservative in general, but it is on the verge of being conservative for exterior girders. AASHTO LRFD load distribution factors shown in Figure 4.28 and Figure 4.29 include skew reduction factors for bending, which lead to better predictions of actual flexural behavior. However, as many DOT's have opted (see Table 2.1), it seems to be safer not including them in design. On the other hand, in shear, AASHTO is overly conservative for all load configurations and girder types (i.e. interior or exterior).

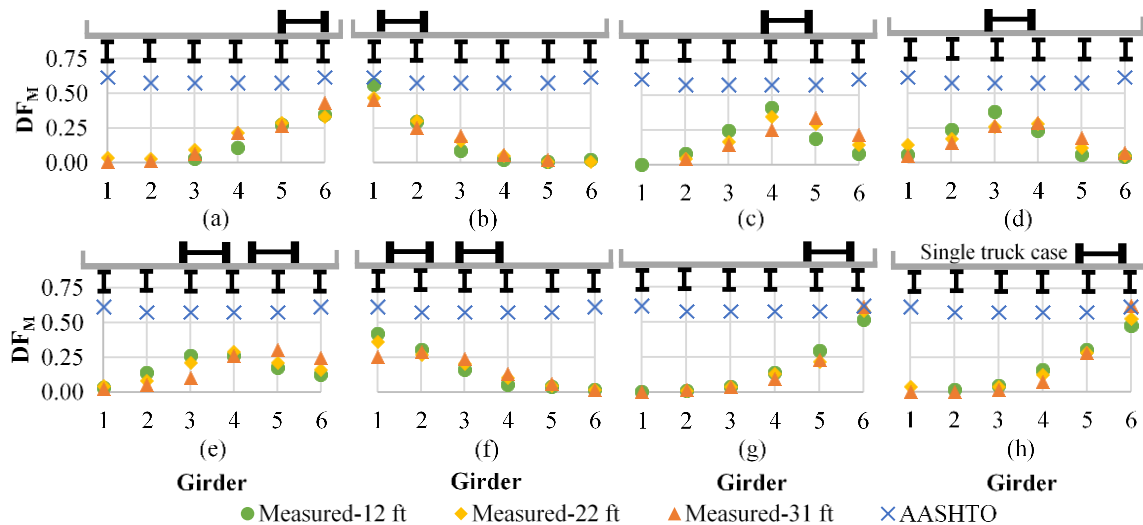


Figure 4.28. Moment distribution factors for: (a) load configuration 1; (b) load configuration 2; (c) load configuration 3; (d) load configuration 4; (e) load configuration 5; (f) load configuration 6; (g) load configuration 7; (h) load configuration 8.

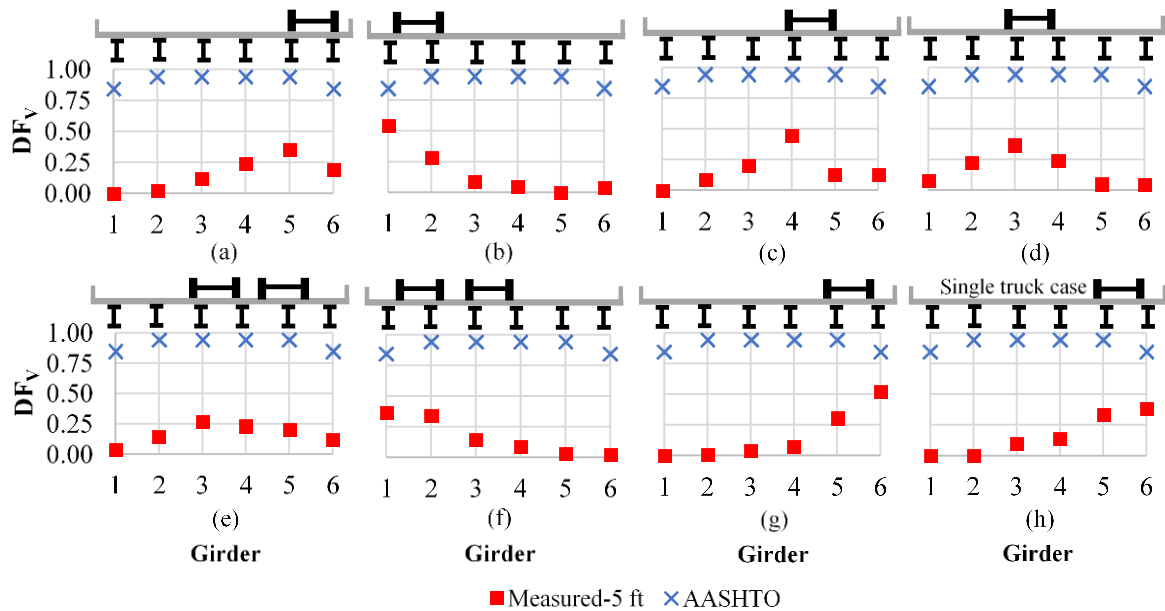


Figure 4.29. Shear distribution factors for: (a) load configuration 1; (b) load configuration 2; (c) load configuration 3; (d) load configuration 4; (e) load configuration 5; (f) load configuration 6; (g) load configuration 7; (h) load configuration 8.

4.3. SUMMARY AND CONCLUSIONS

Short-term load test of the highly skewed prestressed concrete bridge showed that:

- Girder bending and shear strains were small but measurable due to truck loading. Strains in prestressed concrete girders were smaller than the ones of the steel bridge. This is expected due to the higher stiffness of prestressed concrete girders in comparison to steel rolled beams.
- Deck strains and bearing displacements due to truck loading were significantly smaller in comparison to responses generated by long-term loading.

Long-term monitoring of the highly skewed prestressed concrete girder bridge showed that:

1) For bridge displacements:

- Girder end transverse (and therefore, bearing and superstructure) displacements of the prestressed concrete bridge were small and were below 0.28 in during the observation period. Conversely, longitudinal displacements were significant and, on the acute corners, could reach values up to 5 times larger than maximum transverse displacements.
- Longitudinal girder end (bearing) displacements have a strong positive linear correlation with seasonal and daily changes in temperature. This indicates that longitudinal movements are mainly caused by temperature. On the other hand, transverse girder end displacements do not correlate linearly to seasonal changes in temperature, although they have a linear association with temperature on certain days. This is partially due to the small displacements measured, and may also be due to factors in addition to temperature playing a role in these displacements.
- Even though transverse girder end (bearing) displacements were minimized, presumably due to the unique support fixity arrangement employed in design, the maximum parallel-to-joint (racking) displacements were only slightly smaller than maximum longitudinal girder end displacements. This is due to the direct geometric relationship between longitudinal and racking displacement, and the large skew angle. Similarly, the maximum normal-to-joint (expansion) bearing displacements were larger than maximum transverse bearing displacements. Parallel-to-joint displacements were

consistently larger than normal-to-joint displacements. The high skew of the bridge and the small magnitude of transverse displacements explain such results.

- Both parallel-to- and normal-to-expansion joint bearing displacements have strong linear correlations with temperature, with the former having a stronger correlation. This confirms the significant influence of longitudinal movements on these alternative displacement directions.
- Based on the small magnitude of transverse displacements and the evident relationship between significant longitudinal bearing displacements and temperature, movements of the bridge are likely primarily caused by longitudinal thermal contraction and expansion. Any tendency of the bridge to rotate or laterally translate was small.

2) For deck strains:

- When temperatures decreased during the year, the concrete deck accumulated significant compressive strains, which is expected for the superposition of shrinkage and negative temperature changes. Negative changes in strain seemed more pronounced in the deck transverse direction.
- When temperatures increased during the year, strains changed in the tension direction. Larger changes in strain may be found in the deck transverse direction. In general, changes in strain caused by increasing temperatures were not large enough to offset the compression from the cooling period and did not create net tension in the instrumented region. In fact, net strains were beyond 200 μ strain in compression at the end of the observation period at almost all instrumented points.
- Differences between maximum strain measurements from the acute corner of the deck and “stress-free” cylinder gage that only measured temperature and shrinkage effects may indicate deck deformations may not be purely due to unrestrained deformations under uniform thermal changes.
- When residual deck strains were calculated by subtracting strains measured by the “stress-free” cylinder gage, almost all gages had residual compression. Although some differences exist between the shrinkage and temperature strains between deck and “stress-free” gage readings, compression residual strains in the deck show that the deck in this region was not prone to cracking. On the other hand, field inspection results of the HAST bridge presented in Chapter 3 indicated transverse cracking across the span. The conflict between field observations and strain readings can be explained by the fact that cracks may not have crossed gages that were placed in the local acute corner region.
- The deck behavior can be different in locations close to the abutment and closest to the acute corner of the bridge than other locations near the acute corner. This was suggested by the longitudinal gage 1 on line 1 (closer to the abutment) that presented significantly smaller compressive strains at the end of the warming period. This gage also registered a gradual increase of tensile strains, due to what was considered to be external loading and restraining effects, and a subsequent continuous drop in their magnitude towards the end of the observation period, which may be indicative of the presence of deck end diagonal cracking at the gage location.

Short-term load testing of the highly skewed steel girder bridge displayed that:

- After several years in service (i.e., 24 years), the degree of composite action between steel girders and concrete deck could be sustained close to the fully composite behavior. The average difference between the measured and theoretical neutral axis locations assuming a fully composite deck was 12%.
- The instrumentation for shear and bending strains across the entire width of the bridge permitted a complete characterization of the load distribution behavior of the tested bridge. Results showed that in bending, AASHTO LRFD distribution factors predicted the measured flexure distribution to girders with a small safety margin. Therefore, excluding skew reduction factors for bending distribution factors of exterior girders will lead to a more conservative design. In shear, AASHTO

LRFD BDS distribution factors were overly conservative as compared to measured distribution factors. Refinements to skew correction factors for shear may be required.

5. FINITE ELEMENT MODELING METHODS AND VALIDATION

Load testing and long-term monitoring can provide valuable information regarding the structural behavior of the tested structures. However, this information is specific to loading protocols, structural details and geometry of tested bridges. In addition, limited resources typically do not allow instrumenting the entire structure, preventing researchers from directly inferring structural behavior based on experimental results alone. For instance, for the 64° skew prestressed concrete bridge tested, data under live load was only available for three girders out of fifteen. Therefore, additional tools are needed to understand the overall live load distribution.

In order to understand the behavior of bridge regions that were not instrumented, to obtain data on additional bridges under different loading conditions and to be able to perform parametric studies, finite element modeling was used. Finite element modeling can analytically simulate physical phenomena when validated by experimental data. For this project, bridge numerical models were constructed using the commercial finite element software CSiBridge [42] and ABAQUS [43]. CSiBridge was selected due to its extensive use by the bridge industry and ability to simulate moving loads. ABAQUS was used to capture concrete cracking.

5.1. FINITE ELEMENT BRIDGE MODELING TECHNIQUES

Bridges can be modeled in a number of ways, with different levels of complexity, computational cost and accuracy. These methods are the following, listed in the order of simplest to the most complex: 1-D (girder-line) modeling, the grillage method, 2-D modeling, 2.5-D modeling and 3-D modeling. Accuracy of these models as compared to test data are discussed later in Chapter 5.4 on Finite Element Model Validation.

5.1.1. 1-D (Girder-Line) MODELING APPROACH

1-D bridge models can be as simple as a series of interconnected frame elements representing the spans of the bridge. This technique considers the bridge as a one-dimensional system. The models include a single girder and tributary area of the deck. Girder-line modeling is usually employed in simplified bridge design, known as the “Distribution Factor Method”, where AASHTO LRFD BDS live load distribution factors predict girder response. In this project, 1-D modeling was used as a baseline to evaluate AASHTO LRFD BDS distribution factors.

5.1.2. THE GRILLAGE METHOD

A technique that can be more accurate than girder-line modeling is the grillage method. This method is a two dimensional approach, where the continuum superstructure (i.e., deck and girders) is represented by interconnected frame elements in both transverse and longitudinal directions of the bridge. Hambly [2] provides an exhaustive description of this method. The grillage method requires a significant pre-processing effort as several simplifications and assumptions on the transverse frame elements (deck) are needed in order to use this method. For example, deck element stiffness needs to be calculated before modeling, depending on the assumptions of deck element spacing and direction. These assumptions may also have a large impact on the results. This method was popular when efficient computational modeling was essential due to the limited computer power. With modern computational tools and commercial finite element packages available, more refined methods that require the same modeling effort as the grillage method can be readily used and provide more accuracy. Therefore, this project did not consider the grillage method for further investigation.

5.1.3. 2-D BRIDGE MODELING APPROACH

In 2-D modeling, deck was modeled using four-node shell elements. Girders were modeled with 2-node frame elements. The girders were offset from the deck centroid to simulate the eccentricity between deck and girder centroids. Offset nodes of frame and shell elements were connected using “body” constraints [44] which rigidly connect selected nodes, providing full composite action between girders and deck. Secondary structural components such as parapets, partial-depth end diaphragms and steel in-span diaphragms were included in the models as frame elements. Four-node shell elements were used to model full-depth pier diaphragms. Since the deck is modeled with shell elements, deck reinforcement or its stiffness are not discretely modeled using this technique. 2-D models were created using CSiBridge. Figure 5.1 shows the elements of 2-D modeling.

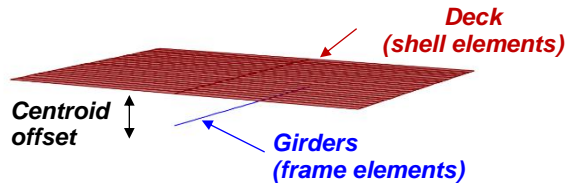


Figure 5.1. Elements of 2-D modeling.

5.1.4. 2.5-D BRIDGE MODELING APPROACH

In 2.5-D modeling, both deck and girders were modeled using four-node shell elements. Girder flanges and web were modeled using separate shell elements at their original locations. Deck and girder top flange were connected using “body” constraints [44] to model composite action. Secondary bridge components were included following the same procedures used in the 2-D modeling approach. 2.5-D models were created using CSiBridge. Figure 5.2 summarizes the details of 2.5-D modeling.

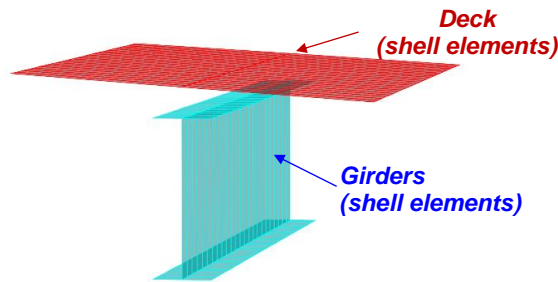


Figure 5.2. Elements of 2.5-D modeling.

5.1.5. 3-D BRIDGE MODELING APPROACH

In the 3-D modeling technique, the bridge is modeled as a three-dimensional system. Deck and girders were modeled using hexahedral solid elements. Fully-composite action between girders and deck was modeled using “tie” constraints [45] which fused together the bottom face of the deck and top face of girders. In regions where non-composite action was detailed (for steel bridges over piers), frictionless contact interaction [45] between deck and girders was implemented. ABAQUS [43] software was used to construct bridge models that use the 3-D modeling technique. Figure 5.3 shows a schematic of 3-D modeling.

The 3D bridge model incorporated all secondary bridge components using hexahedral solid elements with the exception of girder-diaphragm connection plates, which were modeled with four-node shell elements. “Tie” constraints [45] were employed to simulate the interaction between parapets and deck; and diaphragms and connection plates, which join girder webs and steel diaphragms. Connection plates and girders were connected using shell-to-solid coupling [45] that fuses the edges of the shell element (connection plate) to the solid surface (steel girder).

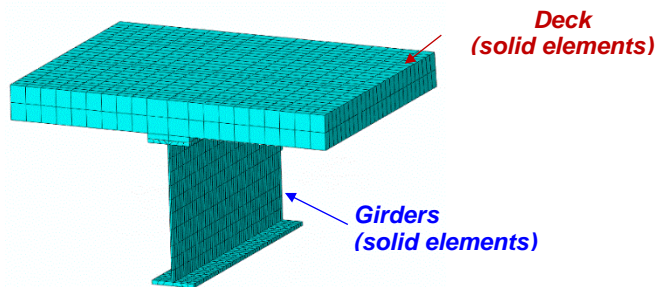


Figure 5.3. Elements of 3-D modeling.

5.1.6. BRIDGE PIERS

Bridge piers were included as frame elements for multi-column and hammerhead pier types. Pile encased piers were modeled using thick shell elements for concrete, and frame elements for piles. In all cases, the pier base was assumed fixed, in other words, restrained from translating and rotating. The exception to this was piers modeled to evaluate pier foundation effects on fixed bearing forces. For these models, footings were modeled using thick shell elements connected to the column base and foundation piles. Piles were simulated using linear springs in the vertical direction, and were laterally restrained. Vertical stiffness per pile was 5,172 k/in. Pier cap expansion joints were only included in the HAST bridge model. All base bridge models had multi-column piers. Only 2-D and 2.5-D models had piers modeled.

5.2. MATERIAL PROPERTIES

5.2.1. CONCRETE MATERIAL PROPERTIES

5.2.1.1. LINEAR CONCRETE PROPERTIES

Concrete and steel unit weights were estimated using AASHTO table 3.5.1-1. Moduli of elasticity for concrete, structural and reinforcing steel were obtained from AASHTO equation 5.4.2.4-1, sections 6.4.1 and 5.4.3.2, respectively. Concrete Poisson's ratio was taken from AASHTO 5.4.2.5. For steel, the Poisson's ratio for steel was 0.3. Coefficients of thermal expansion for concrete and steel were taken from section 28.1.4 of the WisDOT BM [23]. A value of 0.000006 °F-1 was assigned to concrete and prestressed concrete, and 0.0000065 °F-1 was assigned to steel girders and mild reinforcing in the deck when reinforcing was modeled discretely. All bridge secondary elements, steel girders and prestressed girders were modeled using linear elastic elements.

5.2.1.2. NONLINEAR CONCRETE PROPERTIES

Concrete nonlinear behavior was incorporated into the models to capture deck cracking, in select models. The Concrete Damaged Plasticity Model [45] of the ABAQUS software was used as a material model. This material model requires the inclusion of mild reinforcement in nonlinear regions of the deck and concrete stress-deformation laws. These material properties were taken from the FIB Model Code for Concrete Structures 2010 [46]. This technique has proved to be effective simulating cracking during prestress release in pretensioned girders [47-54]. However, it can be computationally expensive. Therefore, nonlinear regions in the deck of modeled bridges were restricted to bridge ends extending approximately one-quarter of the span. These are the regions of the deck where acute corner cracking due to skew is expected. In order to further reduce model analysis times and focus the analysis on the regions of interest, a sub-modeling technique [45] was also implemented. In this technique, only the regions that are not of interest (for this case, area of the deck outside of the nonlinear region) are replaced by boundary conditions obtained from a full analysis.

5.3. LOADING

Two types of loading were included in bridge models: short- and long-term loading. Short-term loading was employed to study load distribution on highly skewed bridges, while long-term loading was implemented to understand bridge horizontal movements and deck cracking on these type of bridges.

5.3.1. SHORT-TERM LOADING

Short-term loading comprised of moving loads used during load testing, or HL-93 AASHTO vehicular loads. Axle weights of load test trucks were given in Chapter 4 for each bridge. In 2-D and 2.5-D models, short-term loading was introduced using the live-load generator of CSiBridge. In 3-D models, short term moving loading (other than self-weight) was only considered for model refinements in section 5.5.2, and was applied as point loads.

When comparing model and load test results, a step-by-step load moving with the actual crawling speeds of load testing trucks was used to achieve a fine loading discretization. When calculating load distribution from models, an influence-based envelope analysis was employed. In envelope analyses, vehicle response is computed by CSiBridge using influence surfaces evaluated for defined truck lanes.

5.3.2. LONG-TERM LOADING

Long-term loading on bridge models consisted of seasonal temperature changes and concrete shrinkage. These two loads are likely responsible for the problems associated with highly skewed girder bridges, i.e., lateral horizontal movements and deck cracking. Details of how these two loads were predicted are given in this section.

5.3.2.1. TEMPERATURE LOADING

Temperature changes used in the models were taken from sections 27.1 and 28.1.4 of the WisDOT BM [23], which provided thermal changes recommended for bearing and expansion joint designs, respectively. Thermal changes used were +/- 55 °F for prestressed concrete bridges and +/- 75 °F for steel bridges. It should be noted, however, that the average maximum thermal changes registered HAST bridge were of +32 °F and -77 °F, with an average temperature right before deck pouring of 72 °F.

5.3.2.2. CONCRETE SHRINKAGE

Shrinkage in concrete, defined as its volume change (contraction) due to loss of moisture, is a complex phenomenon that takes place in both fresh and hardened concretes. Shrinkage introduces time-dependent deformations (strains) in concrete. These deformations, when restrained, may lead to stresses that could exceed the concrete tensile strength, and result in cracking. Several types of shrinkage exist; however, the most detrimental to concrete is drying shrinkage acting on hardened concrete. Variables influencing this type of shrinkage are paste parameters (porosity, age of paste, curing temperature, cement composition, moisture content, admixtures), concrete parameters (aggregate stiffness, aggregate content, cement content, volume-surface ratio, thickness), and environmental parameters (relative humidity, rate of drying, duration of drying) [55].

The number of parameters affecting shrinkage and uncertainties in measuring these parameters impede precision in predicting shrinkage. Several prediction models for shrinkage in hardened concrete have been proposed through the years. The most popular ones are the ACI 209R-92 [56] and the FIB MC 2010 [46] models. The ACI 209R-92 model recommended by the ACI Committee 209 is a crude representation of the phenomenon; however, it leads to adequate estimations for most design applications. The FIB MC 2010 model is more sophisticated than the ACI 209R-92 model, and distinguishes the individual contributions of drying and autogenous shrinkage.

The ACI 209R-92 and FIB MC 2010 predictions of shrinkage in the “stress-free” concrete cylinder used for the HAST bridge (described in Chapter 4.1.2) are compared in Figure 5.4. This cylinder was filled with the same concrete as the deck and was instrumented with a gage that measured shrinkage and temperature strains. Figure 5.4 shows shrinkage strain predictions by the ACI 209R-92 and FIB MC 2010 models for 1 and 70 years after concrete pour, and shrinkage strain measured by the gage installed in the “stress free” concrete cylinder. Shrinkage strain of the “stress-free” cylinder gage is calculated as the total strain measured by the gage in the cylinder minus temperature strains calculated using temperature readings and a coefficient of thermal expansion for concrete of 0.000006 °F-1. “Stress-free” cylinder gage data were only available for a 1 year duration.

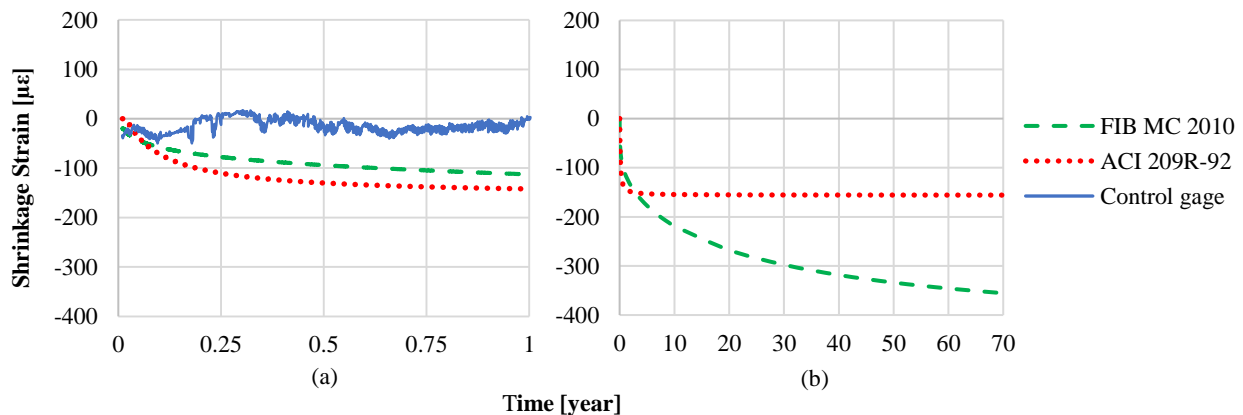


Figure 5.4. Comparison of shrinkage models and gage readings on “stress free” concrete cylinder.

Figure 5.4a shows that ACI 209R-92 and FIB MC 2010 models predict similar shrinkage strain time histories during the first year after concrete pour. On the other hand, shrinkage strains calculated from measured shrinkage and temperature strains in the cylinder were smaller than the ones predicted by analytical models. This difference may have stemmed from the uncertainties in analytical predictions of both ACI 209R-92 and FIB MC 2010 models, or discrepancies between the actual and assumed coefficients of thermal expansion for concrete in the cylinder.

For this project, in finite element models investigating shrinkage, the predictions by the FIB MC 2010 was chosen since it predicts greater ultimate shrinkage strains (Figure 5.4b) leading to a more adverse scenario in the long term.

5.4. FINITE ELEMENT MODEL VALIDATION

Finite element models were validated using girder bending and shear strain measurements from the HAST and Chippewa bridges, detailed in Chapter 4. Analysis models were gradually refined to understand the impact of model refinements such as inclusion of additional bridge elements, and the impact of modeling techniques on the analysis results. At each refinement step, model results were compared to experimental results.

5.4.1. VALIDATION OF PRESTRESSED CONCRETE GIRDER BRIDGE MODELS

In this section, experimental data from the load testing of the HAST bridge with 64° skew and prestressed concrete girders was used for validation. Finite element models were constructed using the 2-D bridge modeling approach. Measurements for live load distribution during load test and girder end (bearing) displacements collected over 1 year at the HAST bridge were used to validate the short-term and long-term load simulation techniques and models.

5.4.1.1. VALIDATION FOR LIVE LOAD DISTRIBUTION

Figure 5.5 compares peak vertical shear and tensile bending strains obtained from testing to finite element model predictions for load cases 1-4 (Figure 4.3), along shear and bending strain gage lines at nominal distances of 5 ft., 15 ft., 40 ft. and 80 ft. from the west girder end (Figure 4.4). In Figure 5.5, for every load case, girder 13 (G13) is on the left, followed by girder 14 (G14) in the middle and girder 15 (G15) on the right.

Figure 5.5 shows that finite element model strain predictions deviate from load test data. However, the transverse distribution of strains are captured in bending and shear for all load cases. To confirm this, the transverse distribution among the three instrumented girders, for shear and bending strains from finite element model predictions and experimental data were compared and plotted in Figure 5.6. This graph clearly shows that 2-D bridge models, in its simplest version (i.e., not featuring any secondary component or any other refinement), are capable of adequately predicting the load distribution behavior of the tested bridge. Based on this finding, this type of 2-D model was employed for all load distribution studies performed through this project. The impact of model refinements on 2-D models is presented later in Chapter 5.5.1.

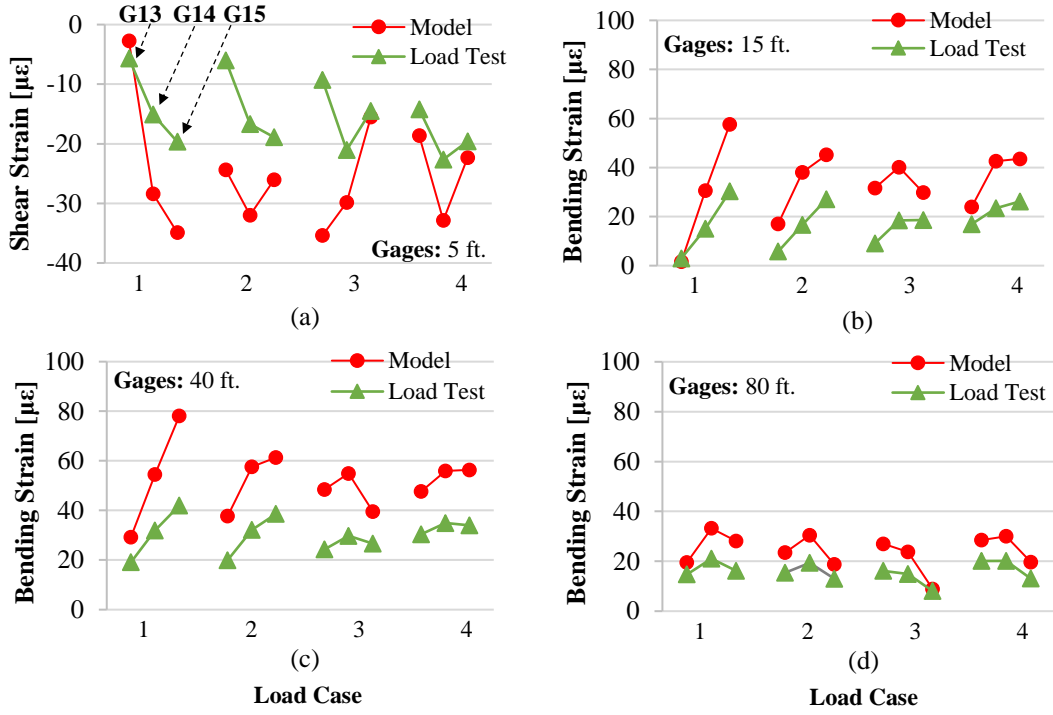


Figure 5.5. Maximum girder tensile bending and vertical shear strains by 2-D model and load test at different instrumentation locations: (a) section at 5 ft. (shear); (b) section at 15 ft.; (c) section at 40 ft.; (d) section at 80 ft. For bending strains, tension: (+); compression: (-).

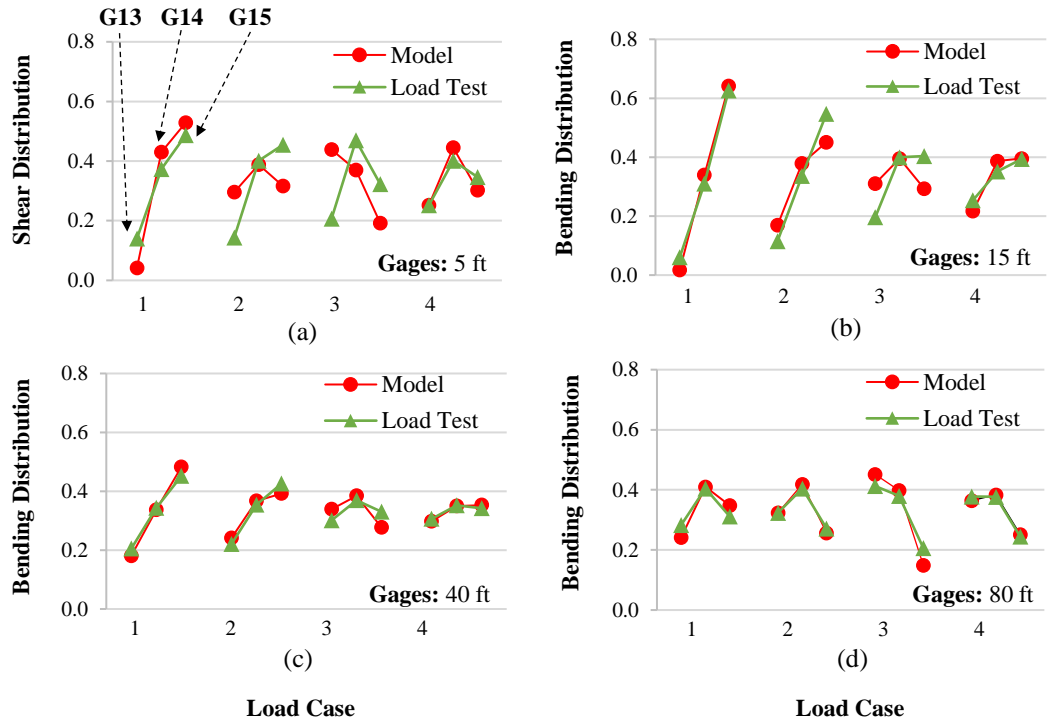


Figure 5.6. Lateral distribution of shear and bending strains by 2-D model and load test data at different instrumentation locations: (a) section at 5 ft. (shear); (b) section at 15 ft.; (c) section at 40 ft.; (d) section at 80 ft. For bending strains, tension: (+); compression: (-).

5.4.1.2. VALIDATION FOR BEARING DISPLACEMENTS

Bearing displacements data of the HAST bridge under long-term loading (Chapter 4.1.3) was used to validate finite element models. Bridge models were constructed using the 2-D modeling approach (Chapter 5.1.3). Bearing flexibility was a variable to determine its effect on displacement response. No secondary bridge components were included in these models.

Three models were constructed: one with an idealized roller only restraining vertical motion, one with the lower-bound stiffness of elastomer and one with the upper-bound stiffness of elastomer pads. Recommendations of WisDOT BM, 27.2.1 was used for shear modulus of elastomer. Expressions to estimate the translational and rotational bearing stiffness were taken from 14.6.3 AASHTO LRFD BDS, as was previously done to study the impact of modeling refinements on bridge response (Chapter 5.5.1).

Following field evidence indicating that bearing displacements were highly correlated with temperature loading (Chapter 4.1.3), and due to uncertainties in analytical models in predicting shrinkage in 1 year, the only load included in finite element models was temperature.

Girder end (bearing) displacements obtained from monitoring and models were compared. Displacement data had gaps due to interruptions to sensors. To exclude these interruptions from the comparison, displacement recordings that corresponded to the minimum and maximum temperatures during the first continuous monitoring period were used for comparisons. When there were differences in temperature recordings between sensors, the average of temperatures measured were used in models. These temperatures are shown in Table 5.1.

Table 5.1. Measured installation (T_o), minimum (T_{min}), and maximum (T_{max}) temperatures and temperatures used in the models.

Temperature	S-E Corner	N-W Corner	FEA Models
T_o [°F]	45	48	46.5
T_{min} [°F]	4	6.5	5.25
T_{max} [°F]	65	60	62.5

The comparison between model predictions and test data for bearing displacements is presented in Table 5.2. Sign conventions are shown in Figure 4.14. Results showed that finite element models predict longitudinal bearing displacements well. This indirectly supports the conclusion that bridge movements are mainly caused by thermal loading. On the other hand, transverse displacement predictions of models were higher than measured displacements. The difference may be explained by the very small magnitude of transverse displacements measured, which are prone to measurement errors. It was also seen in Chapter 4.1.3 that transverse bearing displacements do not correlate well with temperature.

Table 5.2 also shows that the support horizontal flexibility does not have a strong impact on the results, and can be conservatively neglected. Therefore, finite element models used to study bearing displacement response had expansion bearings modeled as roller supports.

Table 5.2. Comparison of bearing displacement measurements and predictions by finite element models.

Location	Temperature [°F]		Transverse direction [in]				Longitudinal direction [in]			
			Test	FEA model with			Test	FEA model with		
				Idealized roller	Flexible bearing, E _{lower bound}	Flexible bearing, E _{upper bound}		Idealized roller	Flexible bearing, E _{lower bound}	Flexible bearing, E _{upper bound}
S-E corner	T _{min}	4	-0.033	-0.13	-0.11	-0.10	-0.81	-0.81	-0.81	-0.80
	T _{max}	65	-0.024	0.052	0.04	0.04	0.20	0.31	0.31	0.31
N-W corner	T _{min}	6.5	-0.048	-0.15	-0.13	-0.13	-0.62	-0.73	-0.74	-0.74
	T _{max}	60	0.005	0.060	0.05	0.05	0.23	0.28	0.29	0.29

5.4.2. VALIDATION OF STEEL GIRDER BRIDGE MODELS

For the validation of steel girder bridge models, the Chippewa Bridge with 47° skew angle and steel girders was used. The details of this bridge are given in Chapter 4.2. The finite element models were constructed using the 2-D bridge modeling approach. Steel girders were modeled as fully-composite with concrete deck where shear studs were detailed. Expansion bearings only restrained vertical motion, while fixed bearings restrained only translation in the vertical and bridge principal directions. Expansion bearings were idealized as rollers, instead of flexible supports. The model included principal structural components only, as for the case of the model used for prestressed concrete bridges, was also employed for steel girder bridges. Finite element model assumed linear elastic material behavior for all components.

Finite element model and field test results were compared at truck stops for all eight load configurations (Figure 4.22) generated during load testing. The comparison is presented in Figure 5.7. In this figure, girder 1 (G1) is located on the left most and girder 6 (G6) is located on the right most of each graph. In general, results from truck loading and 2-D bridge finite element model were in good agreement, which is why this approach was also used for load distribution studies on steel girder bridges. The impact of refined techniques (i.e., 2.5-D and 3-D bridge modeling) on the prediction of girder strain response is presented in Chapter 5.5.2.

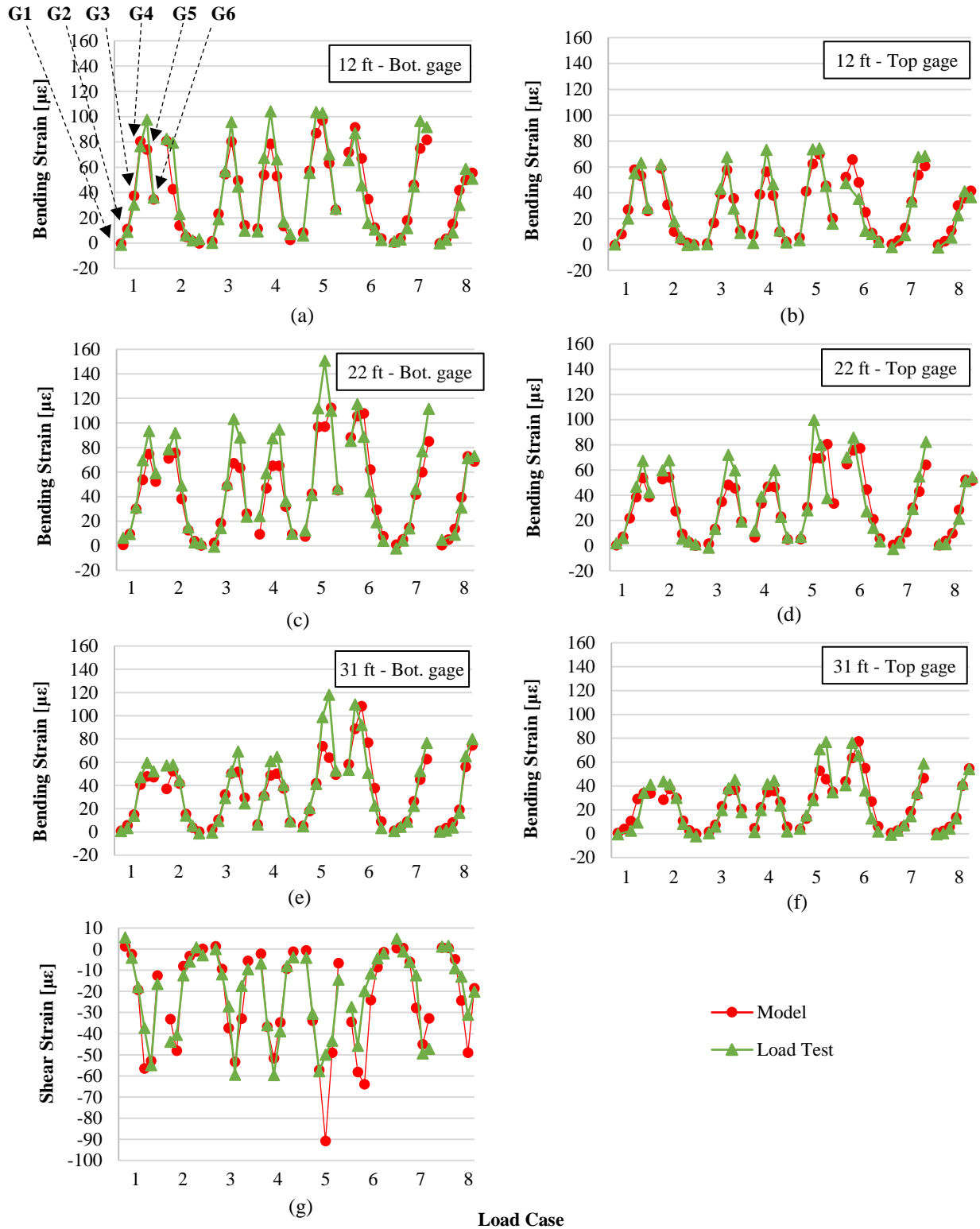


Figure 5.7. Girder bending and shear strains by 2-D finite element model and load test at (a) top and (b) bottom gage bending strains at 12 ft; (c) top and (d) bottom gage bending strains at 22 ft; (e) top and (f) bottom gage bending strains at 31 ft; (g) shear strains at 5ft. For bending strains, tension: (+); compression: (-).

5.5. IMPACT OF MODEL REFINEMENTS ON ANALYSIS RESULTS

Analytical models, results of which were presented above, can be refined to improve accuracy. The desired accuracy level determines the level of refinement required in modeling. Some refinements such as addition of secondary bridge elements are simple to incorporate and do not add considerably to computation time. Other types of refinements, such as using 3D solid elements for deck and girders, may significantly increase computation efficiency. This section discusses the impact of several refinements on finite element modeling results as evaluated by comparisons to test data.

5.5.1. REFINEMENTS BY SECONDARY BRIDGE MEMBERS AND MATERIAL PROPERTIES

The impact of including secondary bridge members (parapets, end, pier and intermediate diaphragms), elastomeric bearings as flexible supports, measured material properties and time adjusted material properties on analysis results was studied using the models of the HAST bridge. Table 5.3 summarizes refinements added to the initial, simplest model (model v1). The most refined, final model (model v7) includes all secondary members, flexible supports and actual material properties. The model shown in Chapter 5.4.1 for validation of finite element model corresponds to model v1 in Table 5.3.

The HAST bridge had concrete parapets, end diaphragms, pier diaphragms, and steel intermediate diaphragms. These secondary elements were added to the basic model (model v1) one by one. Parapets, partial-depth end diaphragms and steel intermediate diaphragms were included as frame elements. Four-node shell elements were used to model full-depth pier diaphragms.

The prestressed concrete girders were supported on elastomeric bearings. Although these bearings are idealized in design as pinned or roller supports that can accommodate free rotations and horizontal movement, they have a small but non-zero translational and rotational stiffness. Translational and rotational stiffness of bearings were calculated using expressions on section 14.6.3 of AASHTO LRFD Bridge Design Specifications (BDS) [22] and the upper-bound of elastomer shear modulus from section 27.2.1 of the WisDOT BM [23]. These stiffness values were included in the final model to understand the impact of modeling bearings as flexible supports.

28-day cylinder tests revealed that the concrete used in the deck and diaphragms had an average compressive strength of 5.31 ksi, while for parapets, it was 4.07 ksi. The design compressive strength for the same concrete was 4.0 ksi. Similarly, 28-day cylinder tests for concrete used in prestressed girders resulted in an average compressive strength of 10.63 ksi. The design 28-day compressive strength for prestressed girders was 8.0 ksi. To refine the material properties used in the simple model (v1), a new model (model v7) was created with the concrete modulus of elasticity estimated using measured 28-day compressive strengths for concrete components. The load test was performed within 24 hours after the 28-day cylinder break for the deck, and on average 203 days after the 28-day cylinder break for prestressed girders. Therefore, the modulus of elasticity of each prestressed girder was evaluated recognizing the concrete's strength gain with age. Projected compressive strengths were calculated using expressions proposed by the ACI Committee 209 [56] and varied between 9.87 ksi and 13.96 ksi for girders 1-15. It should be noted that at the analysis stage, most bridges will not have compression strength data available.

Table 5.3. Refinement steps of the finite element models.

Improvements	Models for validation						
	<i>The simplest</i> ← → <i>The most complex</i>						
	v1	v2	v3	v4	v5	v6	v7 (final)
Parapets	X	✓	✓	✓	✓	✓	✓
End diaphragms	X	X	✓	✓	✓	✓	✓
Pier diaphragms	X	X	X	✓	✓	✓	✓
Intermediate diaphragms	X	X	X	X	✓	✓	✓
Bearing stiffnesses	X	X	X	X	X	✓	✓
Refined material properties	X	X	X	X	X	X	✓

The impact of model refinements on analysis results is presented in Figure 5.8 as error normalized with respect to the error of the initial and the simplest model (model v1). Error in analysis results is defined as the sum of strain deviations (in absolute value) from load test results at all sensor locations and for all load cases. Figure 5.8a shows that better estimates of material properties, and inclusion of secondary members such as parapets and end diaphragms play a significant role in bending behavior, and that including estimated bearing stiffnesses had a small contribution to the accuracy of results. In relation to shear behavior, Figure 5.8b shows a major impact of end diaphragms on model accuracy, followed in importance by bearing stiffnesses.

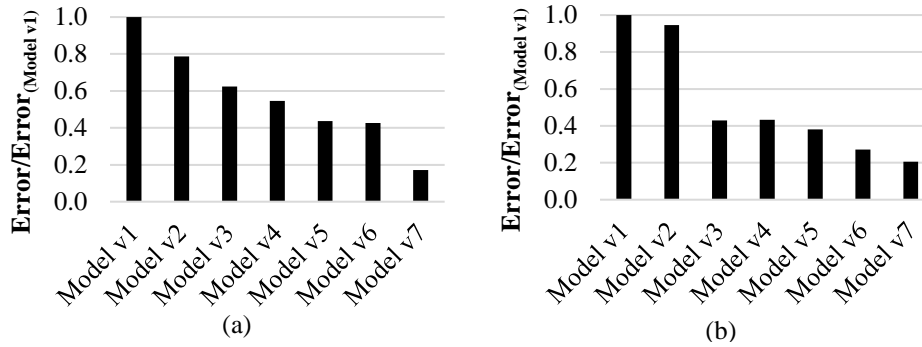


Figure 5.8. Error from refined models normalized with respect to the initial model: (a) bending; (b) shear.

In general, results from truck loading and the most refined bridge finite element model (model v7) were in good agreement. Figure 5.9 compares peak vertical shear and tensile bending strains obtained from testing to finite element model predictions for load cases 1-4, along shear and bending strain gage lines at nominal distances of 5 ft., 15 ft., 40 ft. and 80 ft. from the west girder end. In this figure, for every load case, girder 13 is located on the left.

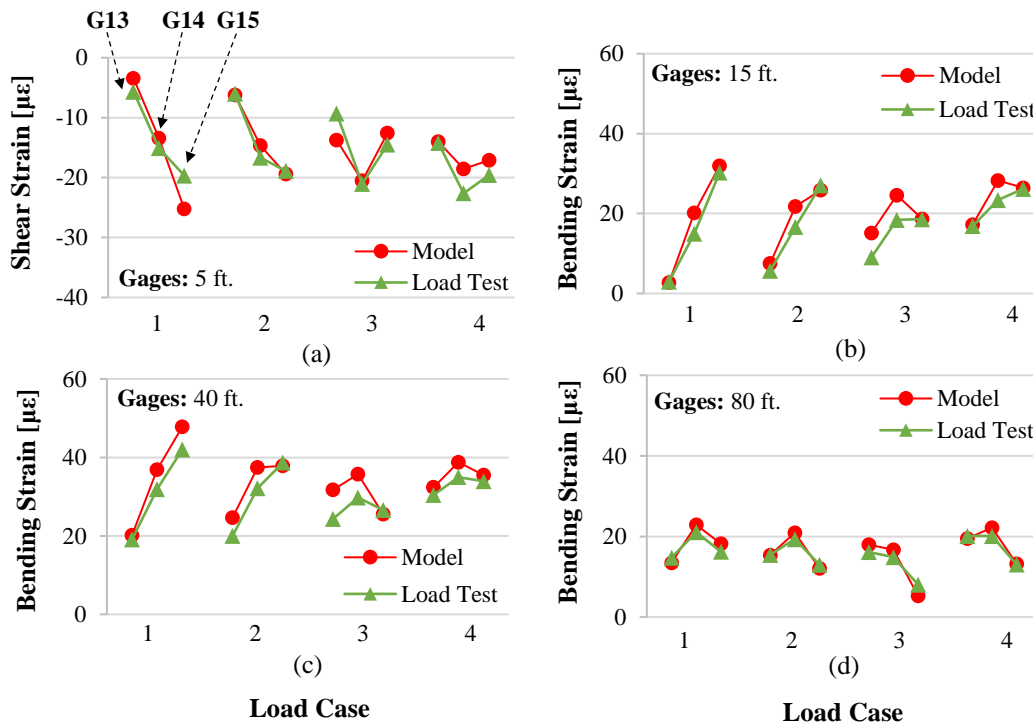


Figure 5.9. Maximum girder tensile bending and vertical shear strains by finite element model and load test at different instrumentation locations: (a) section at 5 ft. (shear); (b) section at 15 ft.; (c) section at 40 ft.; (d) section at 80 ft. For bending strain, tension: (+); compression: (-).

5.5.2. REFINEMENTS THROUGH MODELING TECHNIQUES

The impact of different modeling techniques on analysis results was studied using the models for the Chippewa bridge. Three modeling approaches were considered: 2-D bridge modeling, 2.5-D bridge modeling, and 3-D bridge modeling as described in more detail in sections 5.1.3, 5.1.4 and 5.1.5.

Models that used the 2-D and 2.5-D approaches included secondary members such as parapets, intermediate and end diaphragms using frame elements offset to simulate their actual locations. Diaphragms were assumed capable of transferring moments to steel girders. The 3D bridge model incorporated all bridge components using hexahedral solid elements with the exception of girder-diaphragm connection plates, which were modeled with four-node shell elements.

Results of finite element analysis and field load test were compared at truck stops for the eight load configurations. The comparison is presented in Figure 5.10. In this figure, for every load case, girder 1 is on the left.

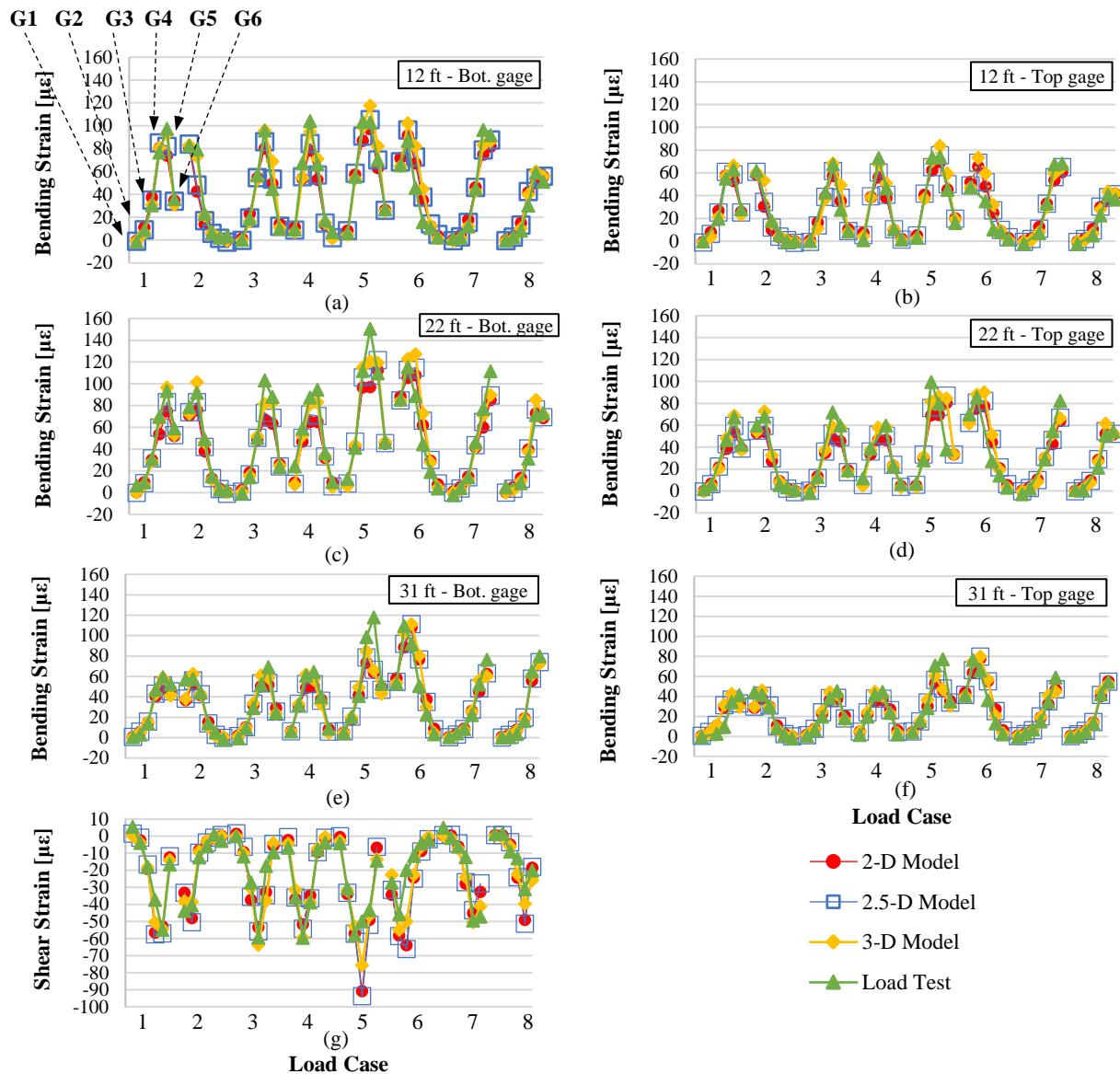


Figure 5.10. Girder strains by models and load test (a) 12 ft – top bending and (b) 12 ft - bottom bending; (c) 22 ft - top bending and (d) 22 ft - bottom bending; (e) 31 ft - top bending and (f) 31 ft - bottom bending (g) 5 ft - shear. For bending, tension: (+); compression: (-).

Results in Figure 5.10 display a reasonable agreement between models and field results. The maximum error, calculated at peak strain per load case, between test and analytical model results in bending was 46%, 43% and 44% for 2-D, 2.5-D and 3-D models, respectively. In shear, it was 58%, 65% and 27% for 2-D, 2.5-D and 3-D models, respectively. The average error, calculated at peak response per load case, between test and analytical model results in bending was 19%, 14% and 10% for 2-D, 2.5-D and 3-D models, respectively. On the other hand, in shear it resulted as 18%, 19% and 10% for 2-D, 2.5-D and 3-D models, respectively.

To visualize the differences between models better, the impact of different modeling techniques is presented in Figure 5.11 as normalized error with respect to the error of the 2-D bridge model. The error is defined as the sum of strain deviations (in absolute value) from load test results at all sensor locations and for all load configurations.

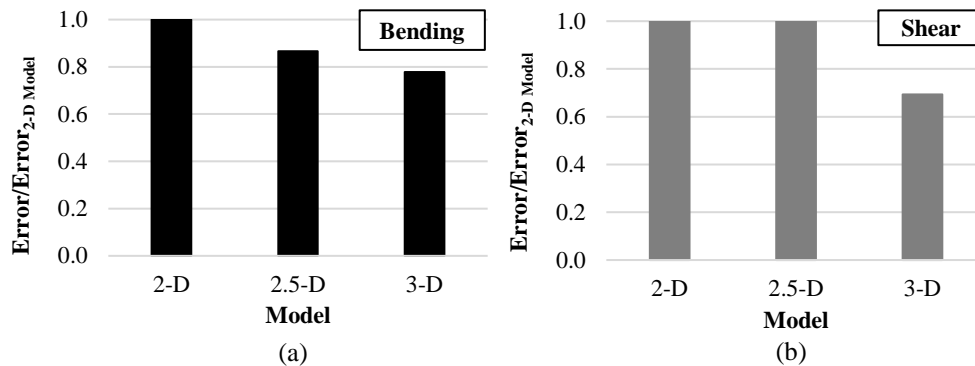


Figure 5.11. Error from different modeling techniques normalized with respect to the error of the 2-D model in: (a) bending; (b) shear.

Figure 5.11a shows that in bending, the 2.5-D model is only slightly better (i.e., 13% reduction in relative error) than the counterpart using frame elements (2-D model) and that the 3-D model could further reduce the error by more than 20% compared to the 2-D model. Figure 5.11b displays the same error comparison for end shear. For end shear, using 2-D or 2.5-D models makes essentially no difference. Similar to what was seen for bending, 3-D models may allow an error reduction of 30% as compared to a 2-D model. In general, it is clear that 3-D modeling provides better results than both 2-D and 2.5-D modeling techniques; however, constructing and running a 3-D model is considerably more time consuming. In addition, results in Figure 5.10 indicate that the level of error of 2-D and 2.5-D models is likely within acceptable limits. For these reasons, for the rest of this project, the 2-D modeling technique was used.

5.6. CONCLUSIONS AND SUMMARY

This section summarized the details, such as modeling techniques and loading, of the finite element models employed in this study. Modeling methods reviewed included 1-D, grillage, 2-D, 2.5-D and 3-D finite element modeling. Grillage models were not considered for further study since they require multiple analysis assumptions, and the computational simplification they provide in modeling is not needed with modern computers. Short term loading included load test trucks or AASHTO HL93 loading. Long term loading included seasonal temperature changes and concrete shrinkage.

Finite element models were validated using test data available on a prestressed concrete girder and a steel girder bridge, called the HAST and Chippewa bridges, respectively. In general, finite element models were in good agreement with test data. Maximum error measured for the HAST and Chippewa bridges between any peak strain result was 90% and 46%, respectively, in bending. In shear, it was 78% and 58%, respectively. The average error in bending measured for the HAST and Chippewa bridges between peak strain results was 66% and 19%, respectively. In shear, the average error was 51% and 18% for HAST and Chippewa bridges, respectively. It should be noted that these errors are in strain values, which are inherently small for bridges tested under service loads, particularly for stiffer prestressed concrete girders. When load distribution to each girder is calculated from the measured strain values and from finite element models, correlation between model and test data was much closer. Since one goal of this project is to understand load distribution in skewed bridges, finite element models were deemed acceptable.

Once finite element models were validated, the impact of model refinements on analysis results were investigated. The refinements were the inclusion of secondary bridge elements, flexible supports, measured and concrete aged material properties for the prestressed concrete girder bridge; and evaluation of 2-D, 2.5-D and 3-D modeling for the steel girder bridge.

In general, refinement requirements depend on the level of accuracy deemed acceptable and whether a correlation between strain or load distribution is desired. The results show that an acceptable representation of the strain behavior of concrete bridges may require more than the inclusion of only principal structural components. For a prestressed concrete bridge, parapets, end and intermediate diaphragms, and enhanced estimates of material properties (typically not available at analysis stage) are important for predicting girder bending strains. Shear strain was highly influenced by end diaphragms, and to some extent by bearing stiffnesses. Similarly, 3-D models were capable of producing a better representation of the actual bridge behavior; however, they require significantly more computational resources and effort to yield practical results. 2-D and 2.5-D models also provided acceptable results. On the other hand, girder load distribution was accurately captured by 2-D models without additional members. These analyses are computationally efficient and can be performed with most commercially available analysis software. Due to their accurate representation of load distribution and simplicity, 2-D models were selected for use in the parametric studies related to load distribution.

6. EVALUATION OF GIRDER LINE ANALYSIS METHODS

This section deals with the effect of skew angle, secondary bridge elements and bridge geometry on load distribution of highly skewed girder bridges. Parametric studies were conducted using validated finite element models. Results of finite element models were used to evaluate the level of conservatism of AASHTO LRFD BDS live load distribution factors. These parameters were studied for prestressed concrete and steel girder bridges. The effects of bridge details on load distribution in the HAST bridge may be found elsewhere [57].

6.1. PARAMETRIC STUDIES ON PRESTRESSED CONCRETE BRIDGES

The base bridge used for the parametric study on prestressed concrete bridges was the visually inspected, two span, 52° skew, prestressed concrete bridge. Details of this bridge are given in Table 3.1. Parameters considered as variables were the skew angle, existence of secondary bridge elements, and bridge geometry. Moment and shear distribution of live load with varying parameters was obtained from finite element models and was used to evaluate AASHTO LRFD live load distribution factors with WisDOT BM exceptions.

6.1.1. EFFECT OF SKEW ANGLE AND SECONDARY BRIDGE ELEMENTS

Skew angles considered in the parametric study were 0°, 15°, 30°, 45° and 60°. In addition, bridges with each skew angle were modeled with and without secondary components to understand the contribution of secondary members to load distribution. These results are labeled as “End Diaph.” (for bridges with end diaphragms but no intermediate diaphragms) and “End and Int. Diaph.” (for bridges with both end and intermediate diaphragms), respectively in Figure 6.1 and Figure 6.2.

HL93 loading was applied to obtain envelope shear and moment reactions. Figure 6.1 and Figure 6.2 show maximum bending moments and shear forces, respectively, at different skew angles and with different secondary bridge elements, predicted by finite element models and AASHTO LRFD BDS live load distribution factor method. AASHTO LRFD BDS live load distribution factors were modified by WisDOT BM exceptions, where applicable.

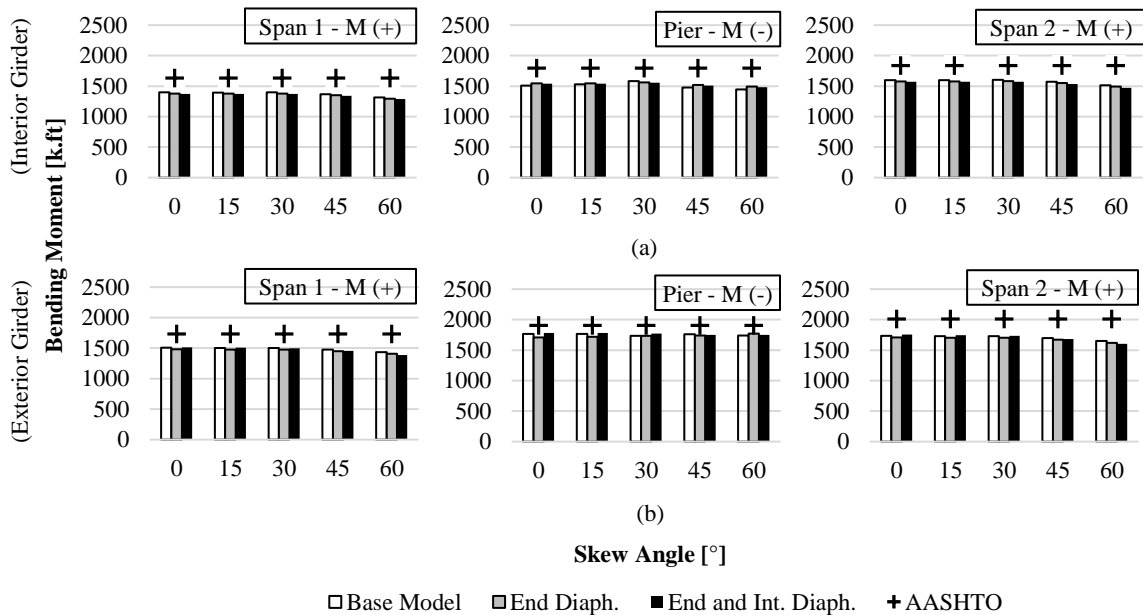


Figure 6.1. Maximum bending moments from AASHTO LRFD BDS and from finite element models of prestressed concrete bridges for: (a) interior girder; (b) exterior girder.

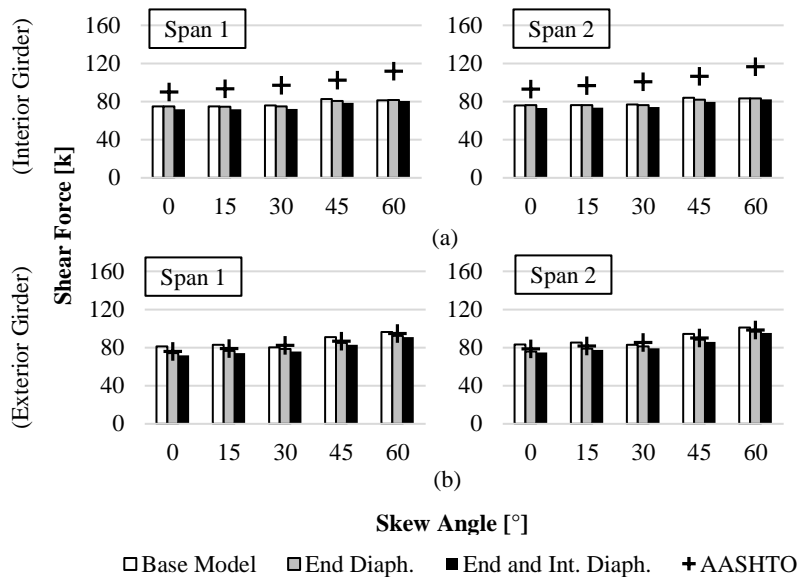


Figure 6.2. Maximum shear forces from AASHTO LRFD BDS and from finite element models of prestressed concrete bridges for: (a) interior girder; (b) exterior girder.

Figure 6.1 shows that for interior and exterior girders, the reduction in maximum bending moments is small with increasing skew angles. Reductions in moment become more noticeable for skew angles larger than or equal to skew angle of 45°. The maximum reduction, at 60° skew, with respect to non-skewed bridge response is of 6% and 9% for interior and exterior girders, respectively. In shear, prestressed concrete bridges (Figure 6.2) exhibit a gradual increase in maximum shear forces as the skew angle increases. The increase in shear with skew is more pronounced for exterior girders (Figure 6.2b). At 60° skew, exterior girders could carry a maximum shear force that is 28% higher than the magnitude supported by exterior girders in the non-skewed counterpart. For interior girders, this increase is only 12%.

When AASHTO and analysis results are compared, it is seen that AASHTO is always conservative for moment (Figure 6.1). For shear of bridges without secondary components, AASHTO leads to slightly unconservative results on exterior girders, on average 4% below the shear from analyses (Figure 6.2b). On average, AASHTO predictions of shear forces for bridges with secondary components were 4% above the analysis results. For shear on interior girders, AASHTO was conservative with skew.

Figure 6.1 and Figure 6.2 also show that the inclusion of end and intermediate diaphragms does not have a significant impact on moment and shear girder response. However, in general they provide a slightly improved load distribution behavior leading to smaller shear and moment predictions. This may explain reactions from models without secondary members marginally exceeding AASHTO predictions.

Limited conservatism of AASHTO for shear on exterior can be improved considering the following. Live load continuity is not considered by approximate AASHTO distribution factors. AASHTO C4.6.2.2.1 indicates that correction factors for superstructure continuity have been deleted in newer editions mainly because they seem to introduce a false sense of accuracy to an approximate analysis method, and because it appears that mentioned increases could be cancelled or compensated by the spreading of reactions near supports. According to NCHRP Project 12-26 [6], when the superstructure is continuous over piers, positive and negative moments must be increased by correction factors varying between 5% and 10%, respectively, and by 5% for support shears.

6.1.2. EFFECT OF BRIDGE GEOMETRY

This section investigates the effect of bridge geometry on live load distribution of highly skewed prestressed concrete girder bridges. For these analyses, the skew angle of the base bridge was modified to 60°, the upper limit of AASHTO skew correction factors, and led to case 0 displayed in Table 6.1. Variables studied by creating separate models for each case are summarized in Table 6.1.

Table 6.1. Matrix for parametric studies on highly skewed prestressed concrete bridges.

Feature	Case 0	Case 1	Case 2	Case 3	Case 4	Case 5	Case 6	Case 7	Case 8
Skew [°]	60	60	60	60	60	60	60	60	60
No. Spans (lengths [ft])	2 (130-147)	1 (139)	3 (104-139-104)	2 (130-147)	2 (130-147)	2 (130-147)	2 (130-147)	2 (130-147)	2 (130-147)
Bridge Width [ft]	43	43	43	101	32	43	43	43	43
(L/W) _{max}	3.5	3.3	3.3	1.5	4.6	3.5	3.5	3.5	3.5
Girder Depth [ft-in]	5-10	5-10	5-10	5-10	5-10	4-6	6-10	5-10	5-10
Girder Spacing [ft-in]	5-4	5-4	5-4	5-4	5-4	5-4	5-4	9-3	5-4
Deck Thickness [in]	8	8	8	8	8	8	8	8.5	11

AASHTO LRFD BDS live load distribution factors for moment and shear, modified per WisDOT BM exceptions, were compared to distribution factors obtained from bridge finite element models. The goal was to determine how bridge geometry affects load distribution on highly skewed prestressed concrete bridges, and to evaluate AASHTO factors for various bridge geometries. Results are presented in Figure 6.3 as the ratio of AASHTO and finite element model distribution factors. Ratios larger than 1.0 indicate that AASHTO is conservative.

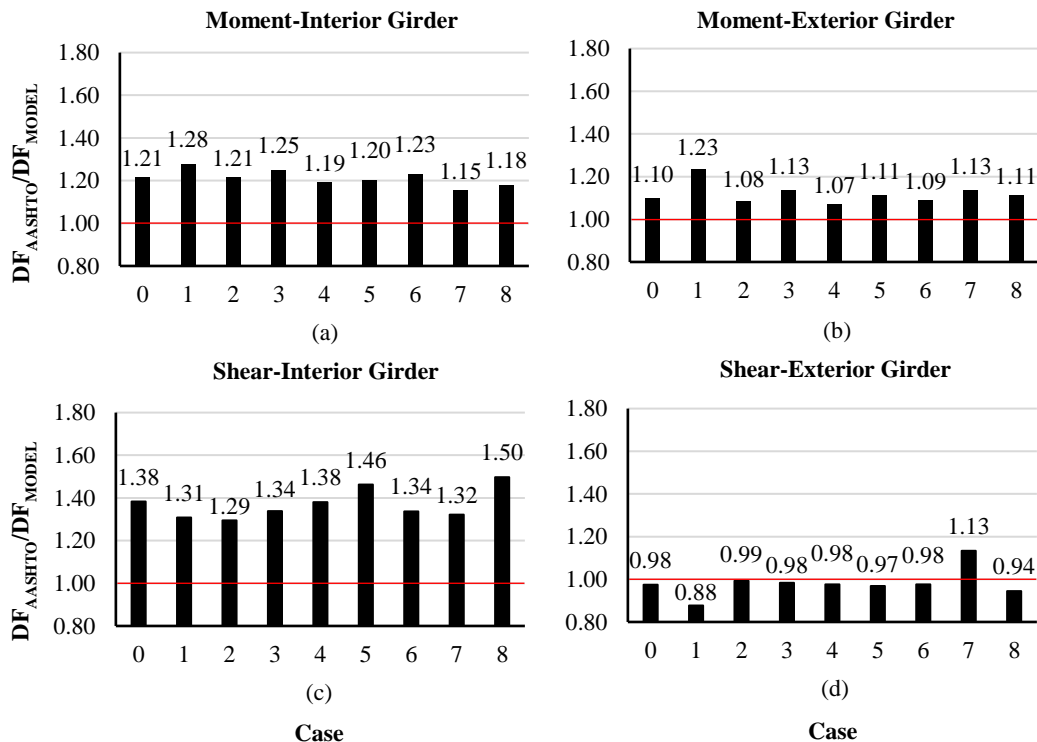


Figure 6.3. Comparisons of live load distribution factors from AASHTO LRFD BDS and from finite element models of prestressed concrete bridges for: (a) moment-interior girder; (b) moment-exterior girder; (c) shear-interior girder; (d) shear-exterior girder.

Figure 6.3a and Figure 6.3b show that AASHTO distribution factors are conservative for moment, for both interior and exterior girders. Figure 6.3c and Figure 6.3d indicate that the accuracy of AASHTO distribution

factors depends on girder location (interior or exterior). For instance, Figure 6.3c displays that for shear in interior girders, AASHTO is overly conservative in all cases. Conversely, for shear in exterior girders (Figure 6.3d), AASHTO is slightly unconservative for all cases, except for the bridge with increased girder spacing (case 7, Table 6.1). Based on results of Chapter 6.1.1, including end and intermediate diaphragms to finite element models could possibly result in slightly conservative AASHTO distribution factors for shear on exterior girders. Results of this section show the importance of more refined analysis on highly skewed bridges, both for economy and safety, even though AASHTO Load Distribution Factor Method is theoretically valid.

6.2. PARAMETRIC STUDIES ON STEEL GIRDER BRIDGES

The base bridge considered for the steel girder parametric studies was the Chippewa bridge. Additional details of this bridge can be found in Table 4.6. Parameters considered were also skew angle, secondary components and bridge geometry. Similar to prestressed concrete bridges, live load distribution with varying parameters was obtained from finite element models and was used to assess AASHTO LRFD live load distribution factors with WisDOT BM [23] exceptions.

6.2.1. EFFECT OF SKEW ANGLE AND SECONDARY BRIDGE ELEMENTS

In the parametric study, the skew angle was varied as 0°, 15°, 30°, 45°, and 60°. Secondary bridge elements were treated as variables and were added to base models in separate models. These models were named as “End Diaph.” and “End and Int. Diaph.” in Figure 6.4 and Figure 6.5 for models with only end diaphragms, and for models with all diaphragms, respectively.

Figure 6.4 and Figure 6.5 show maximum bending moments and shear forces, respectively, at different skew angles and with different secondary bridge elements. The distribution factors were obtained from the envelope reactions of the bridge to a moving load with HL93 loading in finite element analyses. Analysis results were compared to load distribution obtained from AASHTO LRFD BDS.

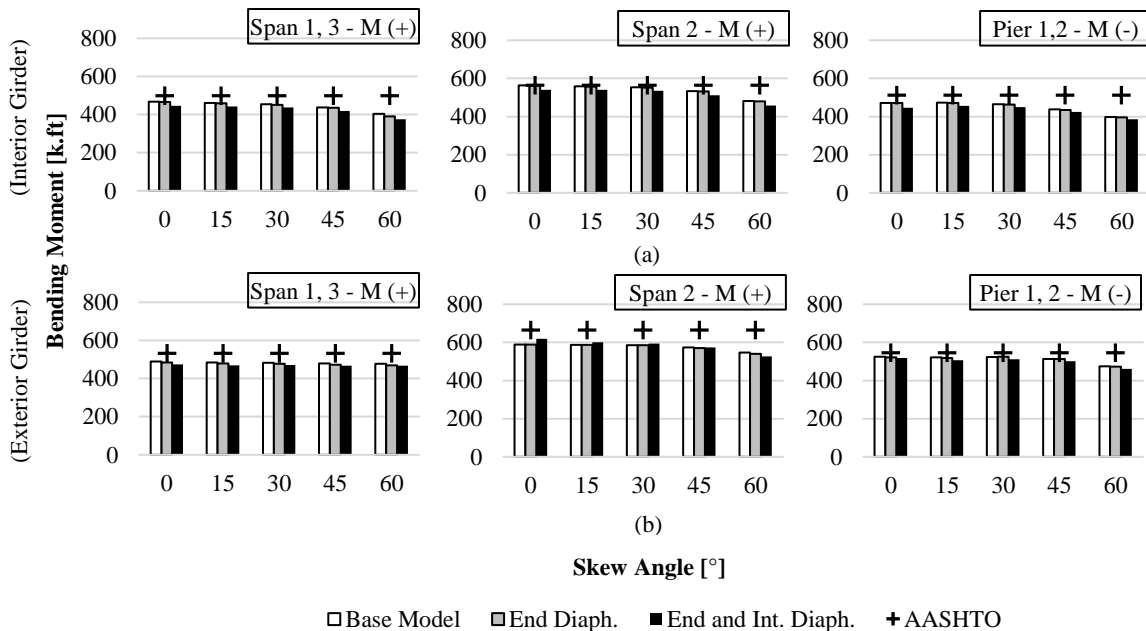


Figure 6.4. Maximum bending moments from AASHTO LRFD BDS and from finite element models of steel bridges for: (a) interior girder; (b) exterior girder.

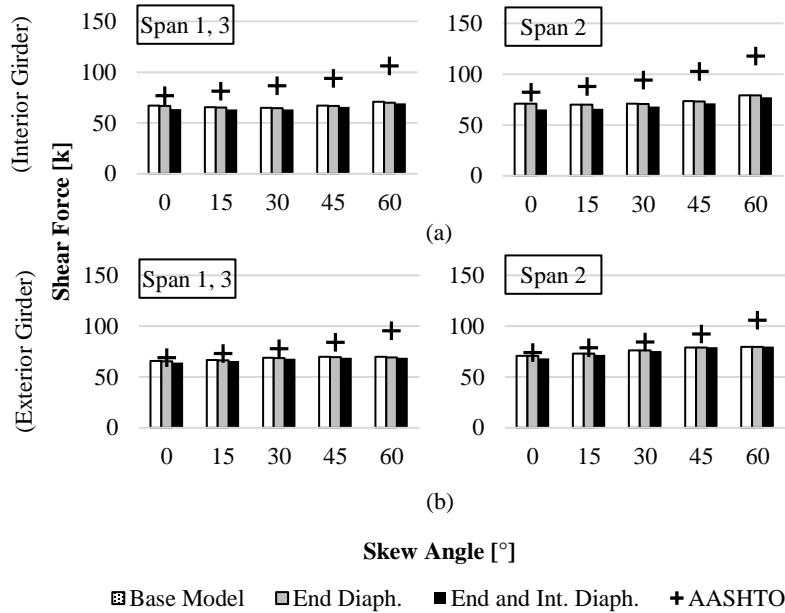


Figure 6.5. Maximum shear forces from AASHTO LRFD BDS and from finite element models of steel bridges for: (a) interior girder; (b) exterior girder.

Similar to prestressed concrete bridges, Figure 6.4 shows that for interior and exterior girders, the reduction in maximum bending moments is not significant with increasing skew angles, particularly for angles smaller than 45°. However, the reduction at 60° skew with respect to the non-skewed case is greater for steel bridges, and approximately 16% for interior and exterior girders. On the other hand, in shear, maximum shear forces moderately increase with skew angle. The increase is on average approximately 18% for interior and exterior girders (Figure 6.5) at a skew angle of 60°, with respect to the non-skewed bridge. The difference in shear behavior between interior and exterior girders of prestressed concrete bridges is not observed in steel bridges.

When AASHTO and 2-D model results are compared, AASHTO predicts bending moments and shear forces conservatively for all skew angles (Figure 6.4 and Figure 6.5). The level of conservatism for moments on interior (Figure 6.4a) and exterior (Figure 6.4b) girders is of similar magnitude. In shear, AASHTO is more conservative on interior girders (Figure 6.5). In addition, unlike in the case of exterior girders of prestressed concrete bridges, AASHTO remains conservative even when compared to analysis results from base models of steel bridges.

Figure 6.4 and Figure 6.5 show that the inclusion of end and intermediate diaphragms does not have a significant impact on moment and shear girder response. In general, excluding diaphragms from bridge models seems to be slightly conservative for moment and shear in interior and exterior girders.

Live load continuity correction factors may also improve the limited safety margin observed at certain skew angles for bending moments on interior and exterior girders (Figure 6.4). A discussion on the live load continuity effects is included in Chapter 6.1.2.

6.2.2. EFFECTS OF BRIDGE GEOMETRY

For parametric studies on the effects of bridge geometry on live load distribution, the skew angle of the base bridge was modified to 60° to create case 0 shown in Table 6.2. Geometric parameters considered for steel bridges are also presented in Table 6.2.

Table 6.2. Matrix for parametric studies on highly skewed steel bridges.

Feature	Case 0	Case 1	Case 2	Case 3	Case 4	Case 5	Case 6	Case 7	Case 8	Case 9
Skew [°]	60	60	60	60	60	60	60	60	60	60
No. Spans (lengths [ft])	3 (47-69.5-47)	1 (54.5)	2 (54.5-54.5)	3 (47-69.5-47)	3 (47-69.5-47)	3 (47-69.5-47)	3 (47-69.5-47)	3 (47-69.5-47)	3 (47-69.5-47)	3 (47-69.5-47)
Bridge Width [ft]	43	43	43	101	29	43	43	43	43	43
(L/W) _{max}	1.62	1.28	1.28	0.69	2.40	1.62	1.62	1.62	1.62	1.62
Girder Depth [in]	33.1 (W33 x130)	33.1	33.1	33.1	33.1	18.6 (W18 x 97)	38.2 (W40 x 149)	33.1	33.1	33.1
Girder Spacing [ft-in]	7-3	7-3	7-3	7-3	7-3	7-3	7-3	12-0	7-3	7-3
Deck Thickness [in]	8	8	8	8	8	8	8	10	11	8
Girder-Deck Connection	Not comp. over piers	Fully composite								

The effect of bridge geometry on load distribution was evaluated by comparing distribution factors for moment and shear as per AASHTO LRFD BDS, with WisDOT BM exceptions, and the ones obtained from bridge finite element models. Results are summarized in Figure 6.6 as the ratio of AASHTO and finite element model distribution factors. Ratios larger than 1.0 show that AASHTO is conservative.

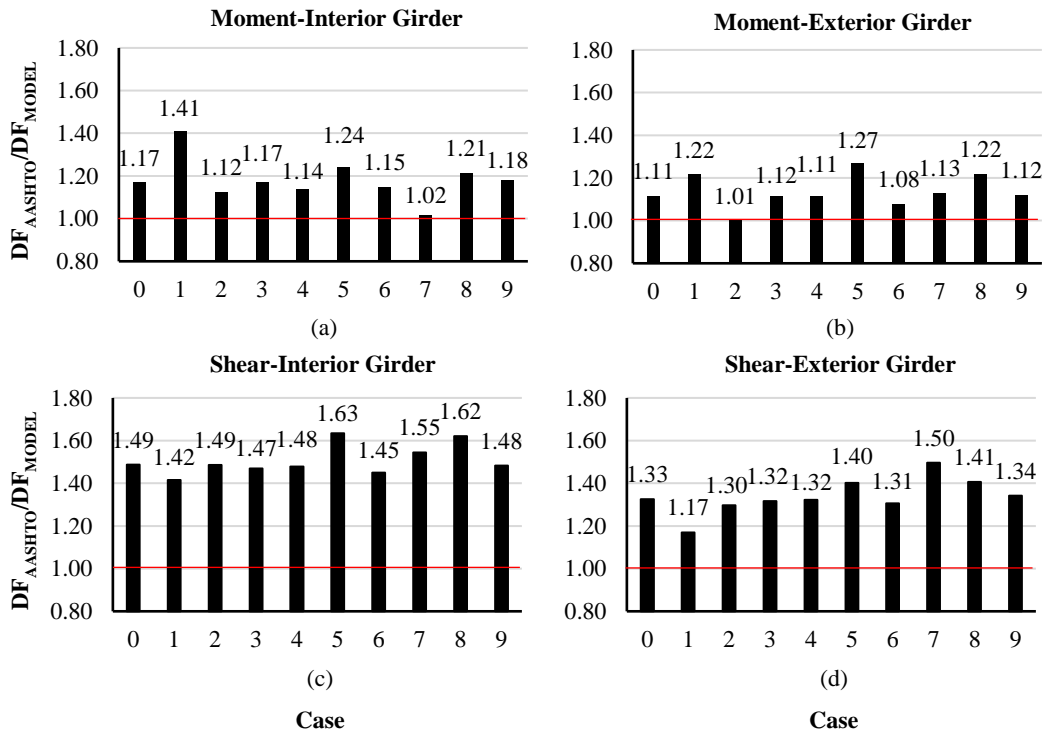


Figure 6.6. Comparisons of live load distribution factors from AASHTO LRFD BDS and from finite element models of steel bridges for: (a) moment-interior girder; (b) moment-exterior girder; (c) shear-interior girder; (d) shear-exterior girder.

Results for moment response in Figure 6.6a and Figure 6.6b indicate that AASHTO distribution factors are conservative in all cases. However, AASHTO factors are only slightly conservative for moment on interior

girders of the bridge with greater girder spacing (case 7, Figure 6.6a), and for moment on exterior girders of the two-span bridge (case 2, Figure 6.6b). For shear, AASHTO is substantially conservative in almost all cases (Figure 6.6c and Figure 6.6d). Situations where AASHTO and analysis predictions are very close, or where AASHTO predictions are excessively conservative, are a reminder of the significance of refined analysis on the design of highly skewed bridges.

Fully-composite action between girders and deck over piers had a negligible effect on moment and shear distribution. This can be seen in Figure 6.6 when distribution factor ratios from the bridge with this detail (case 9, Table 6.2) are compared with the ones from the corresponding bridge featuring non-composite action over piers (case 0, Table 6.2).

6.3. SUMMARY AND CONCLUSIONS

The investigation on skew angle effects showed that:

- The reduction in bending moments with increasing skew angles was not significant.
- Moment reduction amounts in interior and exterior girders due to skew were similar. Steel bridges had greater moment reductions than prestressed concrete bridges.
- Greater skew angles magnify shear forces. The increase amount depended on the type of bridge and girder.
- The increase in shear due to skew was more significant for exterior girders of the prestressed concrete bridge than it was for the steel bridge. For interior girders, the increase was more pronounced for steel bridges.
- The inclusion of continuity correction factors may add a moderate amount of conservatism to AASHTO distribution factors.

The investigation on secondary bridge elements showed that:

- End and intermediate diaphragms do not affect load distribution to girders significantly.
- Modeling girder bridges excluding end and intermediate diaphragms leads to slightly conservative load distribution representations.

The investigation on effects of bridge geometry showed that:

- Distribution factors obtained from AASHTO for bending moment and shear force can be slightly above or below values obtained from models. This shows that underprediction of load effects is possible and that refined analysis of highly skewed bridges should be considered in design to complement 1-D analyses.
- AASTHO distribution factors for bending moment and shear force may also be overly conservative. This presents another reason to consider more refined analysis methods that could lead to more economical designs of highly skewed bridges.
- Non-composite action over piers for steel girders did not cause measurable changes in moment and shear distribution.

7. BEARING DISPLACEMENTS UNDER LONG-TERM LOADING

This section is devoted to explore the effects of skew angle, bridge geometry and bearing fixity arrangements on the bearing (girder end) displacement response for highly skewed prestressed concrete and steel girder bridges under long-term loading. For this purpose, validated 2-D bridge finite element models subjected to temperature loading were employed. As shown in Chapter 4.1.3 on long-term monitoring and Chapter 5.4.1, bearing movements are highly correlated to temperature changes, which is why no other long-term loading was considered. Temperature loading was applied to the superstructure only, and not to substructure, unless otherwise stated.

7.1. BRIDGE SKEW ANGLE

Rotations in the horizontal plane of the bridge superstructure are usually associated with long-term loading and skewed geometry (Chapter 2.1.2). This section concentrates on evaluating the role of bridge skew angle on superstructure horizontal displacements at girder bearings under thermal loading for prestressed concrete and steel girder bridges.

7.1.1. PRESTRESSED CONCRETE BRIDGES WITH VARYING SKEW ANGLES

The visually inspected, two span, 52° skew prestressed concrete bridge (Table 3.1.) was used as base bridge to study the effect of varying skew angles on bearing displacement response under thermal loading at bridge ends. Skew angles considered were 0°, 15°, 30°, 45°, and 60°. The thermal loading was $\Delta T = -55$ °F (thermal contraction).

Bearing displacements in longitudinal direction of the bridge at each girder across the width of the bridge were similar to one another. This was the case for bridges of all skew angles. For 60° skew, there was a gradual but small increase in longitudinal bearing displacements from the obtuse to the acute corner of bridge ends. The greatest difference between bearing displacements of two girders was 15%.

When longitudinal displacements of bridges with different skew angles were compared, small changes were observed. At 60° skew, the maximum acute corner longitudinal bearing displacements were only 5% higher than ones of a non-skewed bridge. Similarly, the maximum obtuse corner longitudinal bearing displacement reduction was 8% between no-skew and 60° skew. The average of longitudinal displacements of all bearings were the same at all skew angles, and perfectly matched calculated displacements using closed form equations.

Transverse bearing displacement trends were investigated by monitoring bridge ends corners, as shown in Figure 7.1, where transverse bearing displacements at bridge corners are plotted as a function of skew. Figure 7.1 shows that there seems to exist a nonlinear relationship between transverse displacements and skew, and that acute corner displacements are always greater than obtuse corner ones, with growing differences between the two with greater skew angles. More importantly, this figure shows that with increasing skew angles, transverse bearing displacements substantially increase with respect to transverse displacements in the non-skewed bridge. In fact, transverse displacements in the acute corners at 60° skew increased by 1157% and 1300% for the shorter span (adjacent to red marks) and longer span (adjacent to green marks), respectively, relative to non-skewed bridge displacements. In addition, transverse displacements varied between girders over the same support linearly.

Another distinguishable trait from Figure 7.1 is the direction of bridge rotation, which for a negative change in temperature seemed directed towards obtuse corners (counterclockwise in Figure 7.1). The opposite is expected for a positive thermal change.

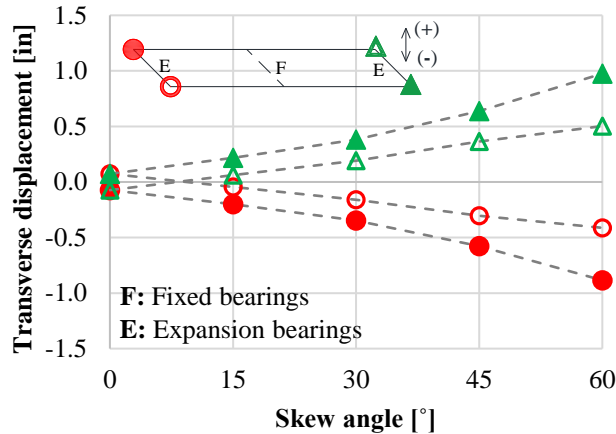


Figure 7.1. Transverse corner bearing displacements under thermal loading from bridge finite element models with different skew angles for prestressed concrete bridges.

7.1.2. STEEL BRIDGES WITH VARYING SKEW ANGLE

The Chippewa bridge (Table 4.6) was considered as the base bridge to evaluate the impact of varying skew angles on bridge ends bearing displacements under thermal loading. Skew angle was varied from 0° to 60°, in 15° increments. Temperature loading considered was $\Delta T = -75$ °F (thermal contraction).

Longitudinal bearing displacements did not change across the bridge width for different girders. They also did not change between bridges of different skew angles for steel bridges. Analytical estimates of displacements using mechanics equations were 5% higher than the ones from finite element model results for the longer, free span length (adjacent to red marks) This may be because equations neglect the deck restraining effect on girders due to the difference in thermal expansion coefficients.

Figure 7.2 displays transverse bearing displacements for different skew angles at each bridge corner. The figure reveals a nonlinear relationship between transverse displacements and bridge skew angle, and that obtuse corner displacements are consistently smaller than acute corner displacements. For greater skew angles, the differences between acute and obtuse corner displacements increases. Figure 7.2 also shows that transverse bearing displacements significantly increase with increasing skew angles relative to the ones of the non-skewed counterpart. At 60° skew, transverse displacement magnification at acute corners was 1390% and 730% for the longer span (adjacent to red marks) and shorter span (adjacent to green marks), respectively, with respect to transverse displacements in the non-skewed bridge. Bearing displacements between different girders over the same support varied linearly across the bridge width.

Bridge rotation tendencies can also be inferred from Figure 7.2. For a negative change in temperature, bridge rotation appears to be towards obtuse corners (clockwise in Figure 7.2). For a positive temperature change, the opposite would be observed.

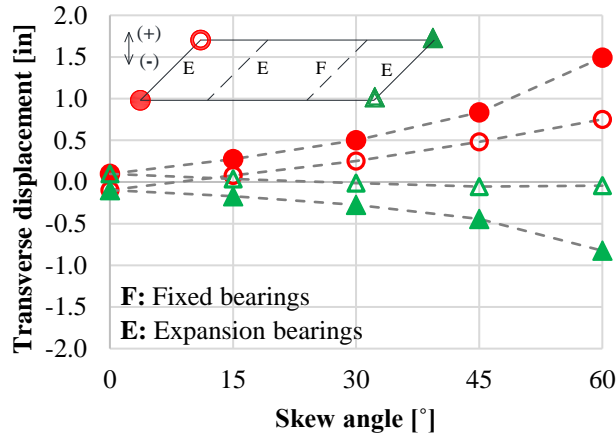


Figure 7.2. Transverse corner bearing displacements under thermal loading from bridge finite element models with different skew angles for steel bridges.

7.2. BRIDGE DETAILS AND GEOMETRY

In this section, the impact of selected bridge details and geometry on the bearing displacement response under thermal loading of prestressed concrete and steel girder bridges is investigated. Bridge models (cases) and corresponding details are described in Table 6.1 and Table 6.2 for concrete and steel, respectively. These bridges were also analyzed under short-term live loading in Chapter 6.

7.2.1. PRESTRESSED CONCRETE BRIDGES WITH VARYING BRIDGE DETAILS AND GEOMETRY

The concrete bridge inspected with 60° skew (case 0 in Table 6.1) and with varying details was subject to thermal loading ($\Delta T = -55$ °F). Figure 7.3 shows maximum bearing displacement components and deformed shapes on a full plan view for this loading condition.

As the number of spans increased (cases 0, 1, and 2), maximum longitudinal bearing displacements increased by 77% for the three-span bridge (case 2), which had the greatest free span length on one side of fixed bearings, with respect to the single-span bridge (case 1). The smallest maximum longitudinal displacement corresponded to the single-span bridge (case 1). This displacement was 92% of the one corresponding to the bridge with 2 spans (case 0), which had a comparable free span length. Maximum transverse, parallel-to-(racking), and normal-to-joint bearing displacements were the greatest for the bridge with three spans (case 2), and were 50%, 56%, and 44% greater, respectively, than the corresponding displacements in the two-span bridge (case 0). No clear trend was identified for these displacement components.

Increasing the deck width (cases 0, 3, 4) or decreasing length-to-width ratio increased maximum longitudinal and racking displacements by 23% and 9%, respectively, for the bridge with the widest deck (case 3) with respect to the bridge with the narrowest deck (case 4). On the other hand, maximum transverse and normal-to-joint displacements decreased with increasing deck widths, with values 8% and 24% smaller, respectively, relative to the narrowest bridge (case 4).

As the girder depth increased (cases 0, 5, and 6), maximum longitudinal bearing displacements did not have any measurable changes. However, transverse displacements changed by 11% between cases with the extreme girder depths (cases 5 and 6). Maximum racking and normal-to-joint displacements exhibited similar increasing trends with greater girder depths, with values of 5% and 21% greater, respectively, with respect to the bridge with shallower girders (case 5).

Changes in girder spacing (cases 0 and 7) had no effects on the longitudinal displacement component. Small increments in the maximum transverse, racking and normal-to-joint displacements of 5%, 2%, and 9%, respectively, were detected for the bridge with the wider girder spacing (case 7).

Similarly, modifications to the deck thickness (cases 0 and 8) did not change maximum longitudinal bearing displacements. However, reductions in the maximum transverse, racking and normal-to-joint displacements of 13%, 5%, and 20%, respectively, were found for the bridge with the thicker deck (case 8).

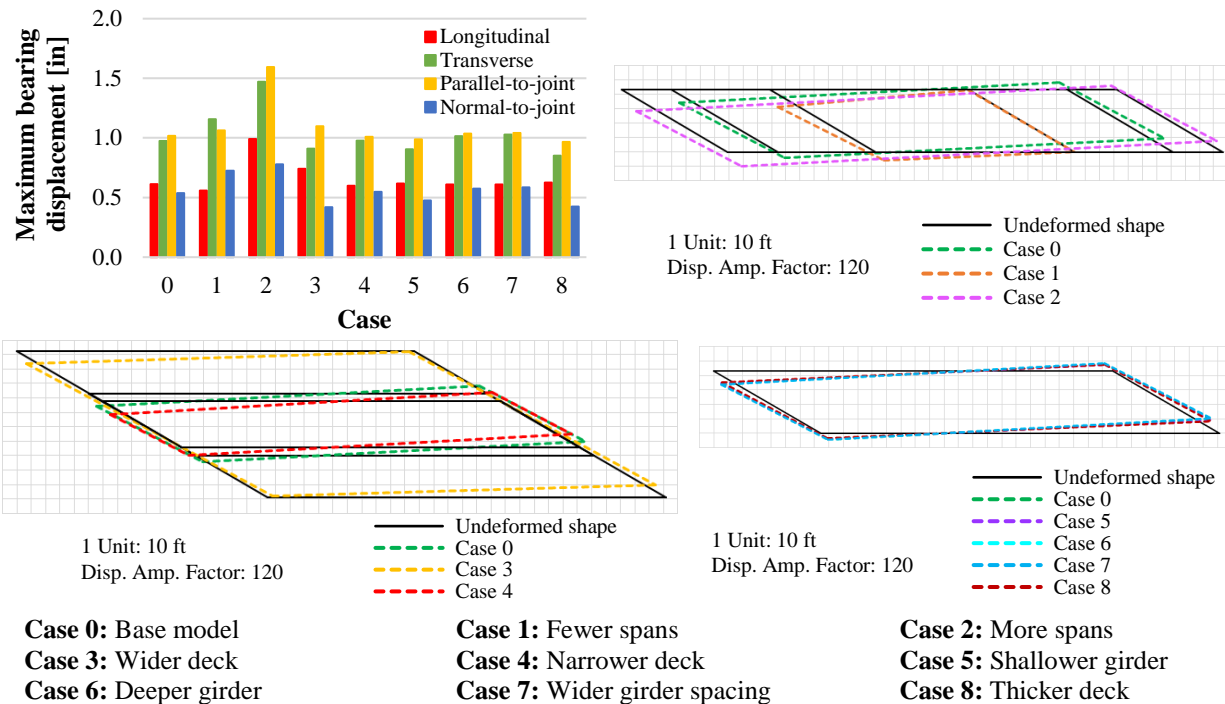


Figure 7.3. Maximum bearing displacements (absolute values) under thermal loading, and deformed shape from bridge finite element models with different design details for prestressed concrete bridges.

7.2.2. STEEL BRIDGES WITH VARYING DETAILS AND GEOMETRY

The Chippewa bridge with 60° skew (case 0 in Table 6.2) and with varying details was subject to thermal loading ($\Delta T = -75$ °F). Figure 7.4 presents maximum bearing displacement components under temperature changes for different 60° skew steel bridges, and deformed shapes on a full plan view for this loading scenario.

In general, increasing the number of spans (cases 0, 1, 2) resulted in greater maximum displacement components, with increases, for the three-span bridge (case 0) with respect to the single-span bridge (case 1), of 86%, 113%, 102% and 126% for longitudinal, transverse, racking and normal-to-joint maximum bearing displacements, respectively. Changes in bearing displacements were smaller between the single- and two-span bridges, and a slight reduction of 11% was observed in the maximum longitudinal bearing displacement for the two-span bridge (case 2) relative to the single-span bridge (case 1).

Increasing the deck width (cases 0, 3, 4) led to negligible changes in maximum longitudinal bearing displacements. It also led to greater maximum transverse, racking and normal-to-joint bearing displacements, with magnitudes 57%, 32%, and 80% larger, respectively, for the bridge with the maximum deck width (case 3) with respect to the bridge with minimum deck width (case 4).

When the girder depth is increased, no displacement components seemed affected (cases 0, 5, 6). Increases were small, and below 3% for the bridge with the deeper girder (case 6) in relation to the bridge with the shallower girder (case 5).

Changes in girder spacing (cases 7, 8), and deck thickness (cases 0, 8) seemed to have no measurable effects on all displacement components.

Results also showed that in the fully composite bridge (case 9), maximum transverse, racking and normal-to-joint bearing displacements may be reduced by 36%, 17%, and 52%, respectively, with respect to the equivalent bridge non-composite over piers (case 0). Maximum longitudinal bearing displacements showed a small increase of only 9% with respect to the same bridge (case 0).

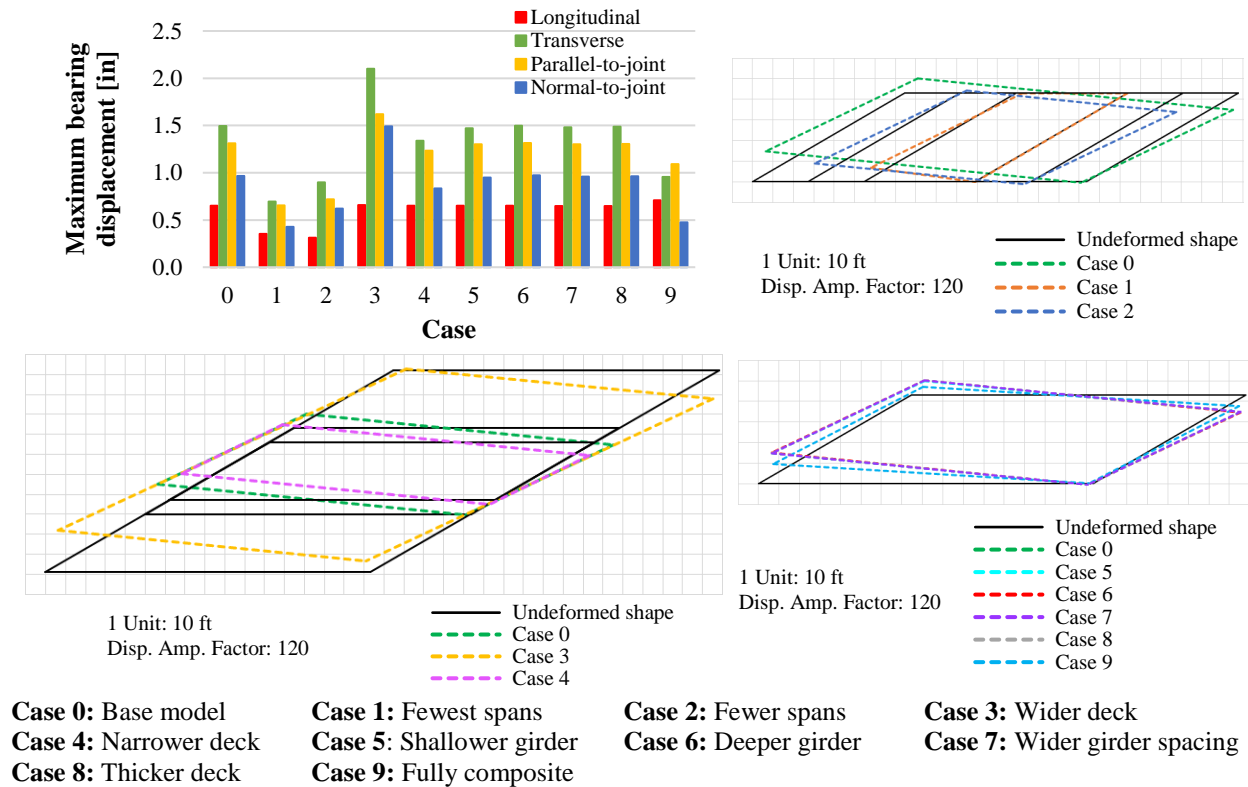


Figure 7.4. Maximum bearing displacements (absolute values) under thermal loading, and deformed shape from bridge finite element models with different design details for steel bridges.

The effects of temperature that were common for the concrete and steel bridges were: 1) longitudinal displacements increased with increasing number of spans, 2) longitudinal displacements were minimally affected by changes in girder depth, girder spacing and deck thickness, and 3) racking displacements increased with increase in deck width.

7.3. BEARING FIXITY ARRANGEMENTS

The HAST bridge featured a special mixed bearing fixity arrangement over piers, with the main goal of limiting transverse horizontal superstructure movements. Long-term monitoring of selected exterior girder end displacements of the HAST bridge showed that transverse displacements were small and did not exceed 0.28 in. during the observation period (Chapter 4.1.3). This section used finite element modeling to recreate girder end displacements with different pier bearing arrangements. Pier fixity arrangements considered are shown in Figure 7.5. HAST bridge was designed and constructed with configuration 6. This investigation was run for the HAST bridge, and for the Chippewa bridge with a modified skew angle of 60° (case 0, in other parametric studies).

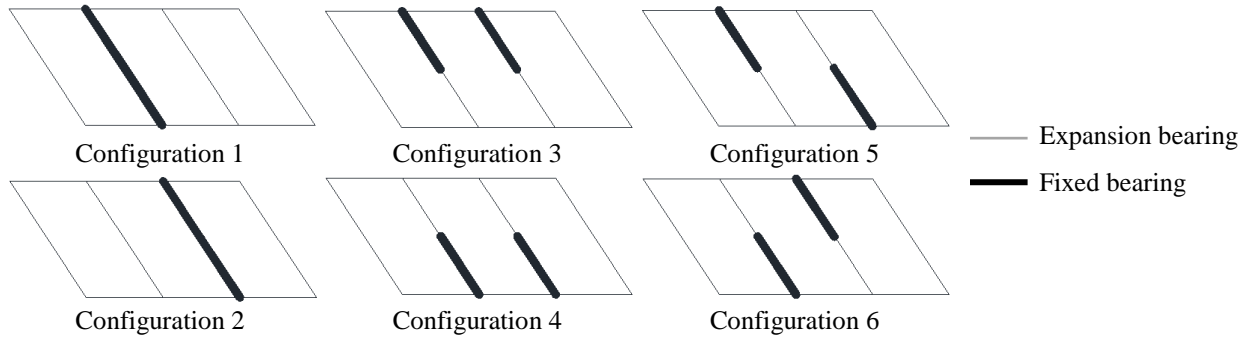


Figure 7.5. Bearing fixity arrangements shown on plan view.

7.3.1. PRESTRESSED CONCRETE BRIDGES WITH VARYING BEARING FIXITY ARRANGEMENTS

In this study, the actual HAST bridge was used. Thermal load of $\Delta T = -55$ °F was applied to the HAST bridge model to obtain girder end or bearing displacements. Figure 7.6a shows, under thermal loading and for fixity configurations 1-6, maximum bearing displacements in the bridge principal directions (i.e., longitudinal and transverse), and parallel-to-joint (racking) and normal-to-joint directions. This figure shows that transverse displacement greatly reduced using the proposed configuration (configuration 6, Figure 7.5), which led to the smallest peak transverse displacement of all studied configurations. The reduction in transverse displacement with configuration 6 was in the order of 71% with respect to a typical bearing fixity arrangement such as configuration 1. Concerning longitudinal displacements, a decrease of 9% was observed.

The displacement components in the alternative directions, racking and normal-to-joint, showed some changes with configuration 6. The maximum racking and normal-to-joint displacements reduced in 26% and increased in 8%, respectively, relative to the corresponding displacements with configuration 1. It should also be noted that with configuration 6, the maximum racking displacement was comparable to the maximum longitudinal displacement. This behavior was expected and attributed to the high skew angle of the bridge, as mentioned in Chapter 4.1.3.

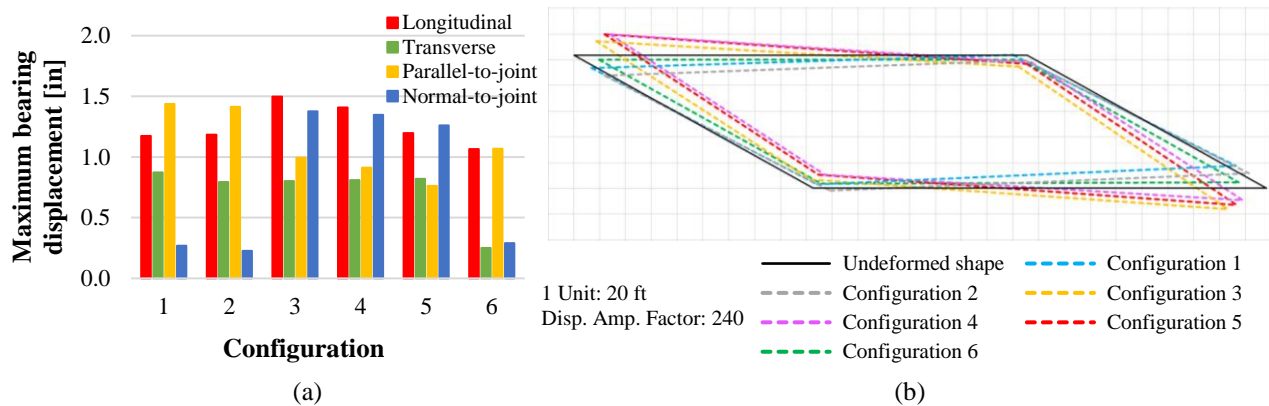


Figure 7.6. Maximum girder end displacements (absolute values) at bearings under thermal loading, and deformed shape from bridge finite element models with different bearing fixity arrangements over piers for the HAST bridge.

Figure 7.6b presents deformed shapes of bridge models on plan view including all spans under thermal loading for all bearing fixity configurations. Deformations are scaled up for presentation. The figure makes evident that skewed bridges tend to rotate under thermal loading, and that the magnitude and direction of this rotation is directly related to the fixity arrangement, and consequently, pier stiffness of the bridge. It also shows that greater deformations seem to be observed on the acute corners of the bridge. Effects of varying skew angle on bridge rotations under thermal loading was discussed in Chapter 7.1. Finally, one may clearly identify in Figure 7.6b that the proposed configuration (configuration 6) leads to an essentially uniform deformed shape.

7.3.2. STEEL BRIDGES WITH VARYING FIXITY ARRANGEMENTS

A similar investigation was performed on the Chippewa bridge, with the skew increased to 60° for the bearing configurations shown in Figure 7.5. The bridge used for this study is the same as case 0 studied in Chapter 6 (Table 6.2). The original Chippewa bridge had a regular fixity arrangement shown as Configuration 2 in Figure 7.5. Thermal loads of $\Delta T = -75$ °F were applied to obtain displacement results.

Figure 7.7a displays maximum bearing displacement components under thermal loading for configurations 1-6 (Figure 7.5). As expected, mixed bearing arrangements over piers greatly improved the lateral bearing displacement response of the bridge. However, in this case configuration 5 led to the smallest maximum transverse bearing displacements since this bridge has the opposite orientation of the skew compared to the HAST bridge. In comparison to its actual configuration (configuration 2), Figure 7.7a shows that the reduction on this displacement component was as high as 86%. The maximum longitudinal displacement reduced, but this reduction was only about 6%. The maximum parallel-to-joint (racking) displacement was reduced by a significant percentage of 52%. The maximum normal-to-joint displacement was also importantly reduced and was only 20% of the value from the original configuration.

In terms of the global deformation behavior under thermal changes, Figure 7.7b, showing plan view of all spans of bridges, indicates that steel girder bridges exhibit a response similar to concrete bridges. That is, rotations in the plane of the superstructure with greater displacements concentrated in the acute corners. Figure 7.7a and Figure 7.7b show that the original bearing configuration (configuration 2) led to one of the largest transverse displacements of all configurations, and the proper mixed bearing fixity arrangement (configuration 5) resulted in an almost uniform deformation, as would be the case for a non-skewed bridge.

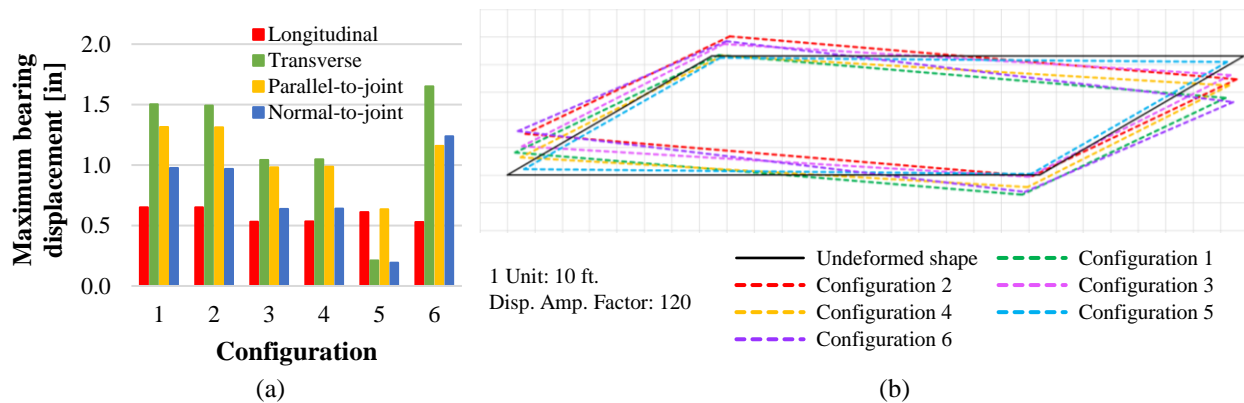


Figure 7.7. Maximum bearing displacements (absolute values) under thermal loading, and deformed shape from bridge finite element models with different bearing fixity arrangements over piers for the Chippewa bridge with 60° skew.

Responses in concrete and steel girder bridges, under the proper mixed bearing arrangement, showed similar traits when comparing bearing displacement responses, and made evident the advantages of this support configuration on limiting transverse displacements. However, some differences were noted between concrete and steel girder bridge behavior considering all support configurations. First, models of the concrete bridges showed slight changes in the magnitude of maximum transverse bearing displacements for different bearing arrangements (Figure 7.6a), and only noticeable for the mixed configuration 6, while for models of the steel bridges the variability was evident (Figure 7.7a). As a matter of fact, the maximum transverse bearing displacement was clearly the greatest for the improper mixed configuration 6, followed by the traditional configurations 1 and 2 (Figure 7.7a). In addition, maximum normal-to-joint bearing displacements were the greatest for configurations 3, 4 and 5 for concrete bridges (Figure 7.6a); however, for steel bridges those arrangements led to the smallest values (Figure 7.7a).

7.3.3. FACTORS AFFECTING MIXED BEARING FIXITY ARRANGEMENT PERFORMANCE

It was seen in the previous two sections (Chapter 7.3.1 and Chapter 7.3.2) that the mixed bearing fixity arrangement over piers is capable of controlling lateral displacements in highly skewed prestressed concrete and steel girder bridges. However, these results corresponded to specific bridges that may not necessarily be representative of all bridge geometries and details. This section explores the effect of bridge

skew angle, pier type and length-to-width ratio on the performance of the mixed bearing fixity arrangement in controlling displacements. Such variables were selected based on input from the project oversight committee indicating their potential influence on the displacement response.

The base bridge for this parametric study was the Chippewa bridge. Bridge end displacement results were obtained under a thermal loading of $\Delta T = -75$ °F. The effectiveness of the mixed support configuration was evaluated for different skew angles, substructure conditions and bridge geometry. With these variables, the comparison of maximum transverse bearing displacements was made between bridges with the mixed bearing configuration (configuration 5 in Figure 7.5) and a traditional bearing configuration as originally used in the Chippewa bridge (configuration 2 in Figure 7.5).

7.3.3.1. BRIDGE SKEW ANGLE EFFECTS

Effects of bridge skew angle were studied considering skews in increments of 15°, from 0° to 60°. Figure 7.8 presents maximum longitudinal and transverse bearing displacements under thermal loading for increasing bridge skew angles. It is clearly seen that as the skew angle increased, the effectiveness of the mixed bearing arrangement greatly improved over a traditional (regular) bearing arrangement. At a skew angle of 15°, the reduction in transverse displacement magnitude was only 8% due to a mixed bearing arrangement. At a skew of 60°, the mixed configuration led to a significant reduction of 86% in transverse bearing displacements.

It should be noted that mixed bearing arrangements are not justified for bridges with no skew. Figure 7.8 shows that for a non-skewed bridge, the regular arrangement had 30% smaller transverse displacements than one with a mixed arrangement. In fact, the regular arrangement in the non-skewed version of the Chippewa bridge induced a uniform deformation along bridge principal directions, while the mixed bearing arrangement caused a horizontal rotation.

Smaller longitudinal bearing displacements were observed under the mixed bearing arrangement, at all skew angles. The difference between longitudinal bearing displacements of bridges with mixed and regular bearing arrangements decreased with increasing skew angles.

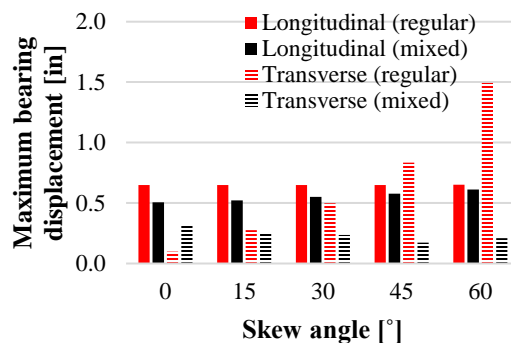


Figure 7.8. Maximum bearing displacements (absolute values) under thermal loading from bridge finite element models with different skew angles for steel bridges with regular and mixed bearing arrangements over piers.

7.3.3.2. PIER TYPE EFFECTS

Piers considered in this section were an infinitely rigid fictitious pier, a pile encased pier, a multi-column pier and a hammerhead pier. Pier dimensions and details were mostly based on standard drawings of the WisDOT. All bridge models had a constant skew angle of 60°. Figure 7.9 displays maximum longitudinal and transverse bearing displacements under thermal loading for the considered pier types, ordered from the stiffest (rigid) to the least stiff (hammerhead) in torsion.

The figure shows that under any pier type, the mixed bearing fixity arrangement was quite effective in reducing transverse bearing displacement with respect to displacements in bridges with a regular bearing configuration. It is also evident that pier stiffness had a role in the magnitude of this displacement component. The smallest reduction in transverse displacement was of 50%, and corresponded to the bridge with the most flexible pier (hammerhead) in torsion. On the other hand, greater reductions of 79%, 84% and 86% were found for bridge models with the rigid, pile encased and multi-column piers, respectively. These piers are stiffer in torsion than a hammerhead pier.

Figure 7.9 suggests that as the pier torsional stiffness decreased, the transverse bearing displacement decreased for bridges with the mixed bearing arrangements. This was not the case for the hammerhead pier, which had larger transverse displacements than bridges with other pier types with mixed bearings. This contradiction may be explained by the difference in pier structural response under thermal loading. It was found that induced forces under this loading condition caused the pile encased and multi-column piers to respond in flexure along the height and width, with the greatest demands observed near the center of the pier top. In the case of the hammerhead pier, displacement demand was higher on one side of the pier cap, leading mainly to out-of-plane flexure. This may indicate that trying to characterize bridge displacement behavior only with the pier torsional stiffness may not be possible.

Figure 7.9 also shows that for all pier types, longitudinal bearing displacements were similar for bridges with mixed and regular bearing arrangements. The largest longitudinal displacement was 16% larger than others were, and corresponded to the bridge with hammerhead piers with a mixed bearing arrangement.

Finally, pier type affected displacements only when bridges had mixed bearing arrangements. For bridges with a regular bearing configuration, changes in predicted displacement components were negligible.

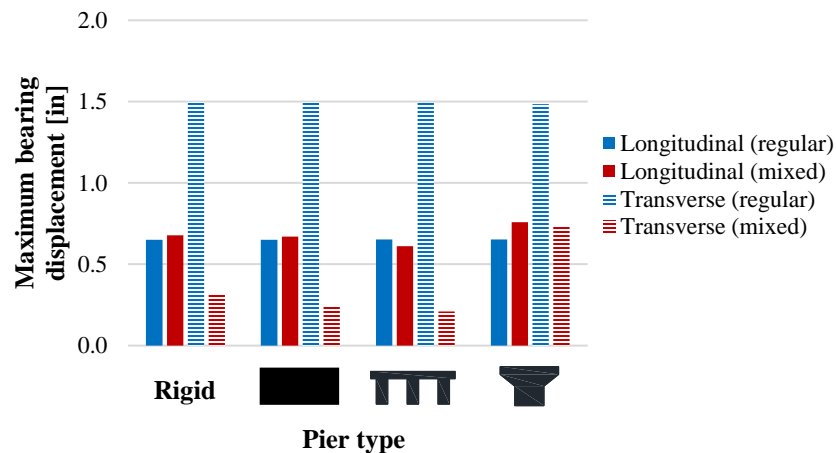


Figure 7.9. Maximum bearing displacements (absolute values) under thermal loading from bridge finite element models with different pier types for steel bridges with regular and mixed bearing arrangements over piers.

7.3.3.3. LENGTH-TO-WIDTH RATIO EFFECTS

Superstructure length-to-width ratio effects were studied by considering two scenarios leading to varying ratios: 1) one where only the bridge width was modified, and 2) one where the bridge length was changed. The first group of bridge models with length-to-width ratios of 0.69, 1.62 and 2.40 corresponded to cases 3, 0 and 4, respectively, in Table 6.2. For the other group, the first model with a length-to-width ratio of 1.62 was case 0 in Table 6.2. The additional two models for this group were built by multiplying the span lengths of case 0 by of 1.5 and 2.25, which led to length-to-width ratios of 2.43 and 3.64, respectively. All bridge models had a skew angle of 60°. Figure 7.10 shows maximum longitudinal and transverse bearing displacements under thermal loading for these length-to-width ratios. Bearing displacement results that

correspond to bridge models with decreasing widths and increasing lengths are shown in Figure 7.10a and Figure 7.10b, respectively.

Figure 7.10 displays that under varying length-to-width ratios, the mixed bearing arrangement remained efficacious in reducing transverse displacements. However, trends seemed to depend on the actual variable (length or width) modifying the length-to-width ratios. For instance, Figure 7.10a indicates that with decreasing widths (increasing length-to-width ratios), mixed bearing arrangements lead to greater reductions in transverse displacements of 51%, 86% and 91% for ratios of 0.69, 1.62 and 2.40, respectively, compared to bridges with regular bearing arrangements. Figure 7.10b shows that with increasing lengths (also increasing length-to-width ratios), mixed bearing arrangements were still effective but lead to smaller reductions in transverse displacements of 86%, 82%, and 50% for ratios of 1.62, 2.43 and 3.64, respectively, with respect to bridges with regular support configurations.

Longitudinal bearing displacements on bridges with the mixed configuration did not significantly differ from displacements on counterpart bridges with regular bearing arrangements. The greatest differences were found for bridges with the greatest length-to-width ratios, and were of 12% and 9% for bridges with ratios of 2.40 and 3.64, respectively.

Another important feature observed in Figure 7.10 was that the bearing transverse displacement response on bridges with regular or mixed arrangements seemed to be better explained by the individual variables, bridge width and length, rather than by their ratio. For example, in Figure 7.10a, it is clear that with decreased bridge widths, transverse bearing displacements also decreased, regardless of the type of bearing configuration. Conversely, in Figure 7.10b, it is seen that with increased bridge lengths, transverse displacements increased for bridges with regular or mixed bearing arrangements.

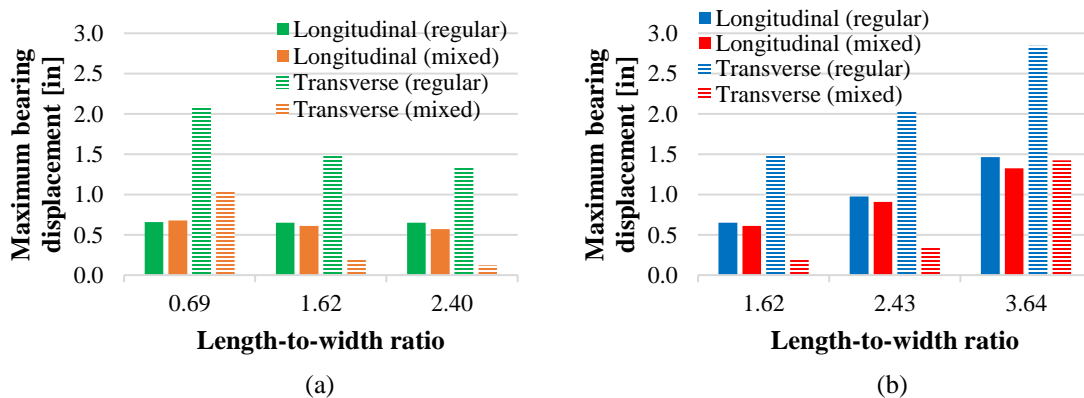


Figure 7.10. Maximum bearing displacements (absolute values) under thermal loading from bridge finite element models with different length-to-width ratios under: (a) decreasing widths and (b) increasing lengths, for steel bridges with regular and mixed bearing arrangements over piers.

7.4. SUMMARY AND CONCLUSIONS

This section analyzed prestressed concrete and steel girder bridges with varying skew angles, geometries and parameters under temperature loading to understand superstructure displacements. Displacements were reported at girder bearings.

In general, it was seen that the bridge skew angle plays a major role in bridge horizontal transverse movements, and consequent bridge rotation. Results showed that increasing skew angles may lead to significantly greater bearing transverse displacements, and that acute corner bearing lateral displacements exceed those of obtuse corner bearings at the same bridge end. The importance of refined modeling in predicting transverse bearing displacement magnification was evident. Bridge rotation tendencies were found to move bridges towards obtuse corners for negative changes in temperature. These tendencies were similar for both prestressed concrete and steel bridges with regular support configurations over piers.

The limited number of bridge models was not sufficient to draw conclusions on the relationship between bridge geometry and bearing displacement response. However, it was evident for all cases that increasing number of spans led to increasing longitudinal displacements; that changes in girder depth, girder spacing and deck thickness did not affect longitudinal deformations; and that increasing deck width resulted in greater racking deformations. Moreover, steel bridges that were non-composite over piers, could experience greater bearing transverse, racking and normal-to-joint displacements at bridge ends than those on fully composite steel bridges. Bearing longitudinal displacements were similar.

The effect of mixed bearing arrangements over the same piers (based on the HAST bridge bearing assignment) was studied using finite element models. This arrangement significantly reduced transverse bearing displacements, and improved displacements in other directions compared to bridges with typical bearing fixity configurations. A uniform global deformation pattern of the superstructure was achieved.

Parametric studies demonstrated that bridge geometry and details may affect the performance of mixed bearing arrangement over piers. Compared to transverse bearing displacements on bridges with regular fixity arrangement, it was seen that this configuration could greatly reduce peak transverse displacements at high skew angles, and that as the bridge skew angle decreases the effectiveness also decreases. In fact, this special configuration should not be used in non-skewed bridges, and benefits should be reviewed for low skew angles based on the results presented in this report.

The mixed configuration has similarly remarkable performance in bridges with piled encased and multi-column piers. On bridges with hammerhead piers, the mixed configuration still reduces transverse displacements but is less effective.

Under all bridge length-to-width ratios studied in this report, the mixed fixity configuration reduced transverse displacements. Some attention should be given to bridges significantly wide or long where the mixed configuration had the lowest reductions in transverse bearing displacements. Smaller deck widths and shorter spans also led to smaller transverse displacements for regular bearing configurations.

8. BEARING FORCES UNDER LONG-TERM LOADING

This chapter reports horizontal (lateral) forces acting on fixed bearings of highly skewed prestressed concrete bridges under temperature loading. Achieving a reasonable estimate of these forces is of primary importance for the performance and integrity of fixed bearings and bridge piers. The chapter initially evaluates factors affecting bearing force predictions. It continues with parametric studies aimed at further exploring the role of bridge skew angle, varying details and geometry, and mixed bearing arrangement on the magnitude of horizontal forces on fixed bearings. Validated 2-D bridge finite element models subject to thermal loading were used. Shrinkage-related forces were not explored. However, since shrinkage is typically modeled by applying temperature changes in finite element modeling, the models that considered temperature can be used to infer loads due to shrinkage. Fixed bearing horizontal shear forces were reported along bridge principal directions (i.e., longitudinal and transverse directions).

8.1. MODELING TECHNIQUES AFFECTING FIXED BEARING FORCE PREDICTIONS

Several factors affecting the magnitude of bearing force estimates were investigated in this section. The base model corresponded to the HAST bridge subject to a change in temperature of $\Delta T = -55$ °F. Temperature was applied to the superstructure only, unless otherwise stated. The HAST bridge was chosen due to its mixed bearing arrangement that may lead to high fixed bearing forces, since the intermediate span of the HAST bridge is not free to deform under thermal loading (or shrinkage) between fixed bearing segments over piers. The base model included the superstructure and the piers of the HAST bridge, but not the flexible foundation.

8.1.1. SUPPORT RIGIDITY

Two-dimensional models that do not include piers have been widely used for bridge design. This approach assumes that piers are infinitely rigid. The impact of this assumption was evaluated by comparing the base model that had piers to a model that excludes piers. Results are shown in Figure 8.1, where longitudinal and transverse horizontal fixed bearing forces were presented along the bridge width.

Figure 8.1 shows that bearing force trends along the width were similar; however, peak force predictions were significantly different. For both models, bearing forces in both longitudinal and transverse directions were the highest in the bearings around the centerline of the bridge (Girder 7 and Girder 8). The model without piers estimated a peak longitudinal bearing force that was 454% greater than the one given by the base model (Figure 8.1a). The difference between a model with and without piers was not as significant in the transverse direction. The peak bearing force from the model without piers (rigid supports) was 50% greater than the one with piers.

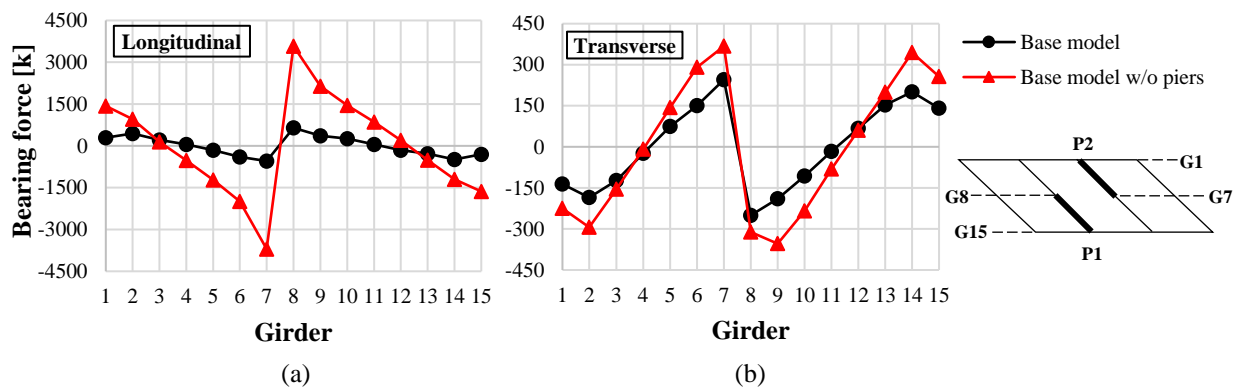


Figure 8.1. Bearing horizontal forces considering pier effects in the (a) longitudinal and (b) transverse bridge directions under thermal loading from finite element models for the HAST bridge.

8.1.2. PIER FOUNDATION EFFECTS

More refined models that include piers are at times built to simulate soil-foundation-structure interaction in order to have more accurate representations of the structural response. However, depending on the target response, such refinements may or may not have a measurable impact on analysis results. In this section, the base model was compared to a model that featured the foundation of pier columns to evaluate its importance on fixed bearing force estimates. The foundation of pier columns consisted on concrete footings and HP 14x73 steel piling, as indicated on construction drawings. Average footing dimensions (plan: 9 ft x 11 ft, height: 4 ft) were used. Details on how this bridge characteristic was implemented are presented in Chapter 5.1.6. Figure 8.2 displays longitudinal and transverse horizontal fixed bearing forces along the bridge width for these two models.

It is seen, in Figure 8.2, that adding foundation of piers to the HAST bridge base model did not cause measurable changes. Predicted peak bearing forces by the model with the foundation only reduced by 4% and 1%, respectively, relative to the estimates from the base model.

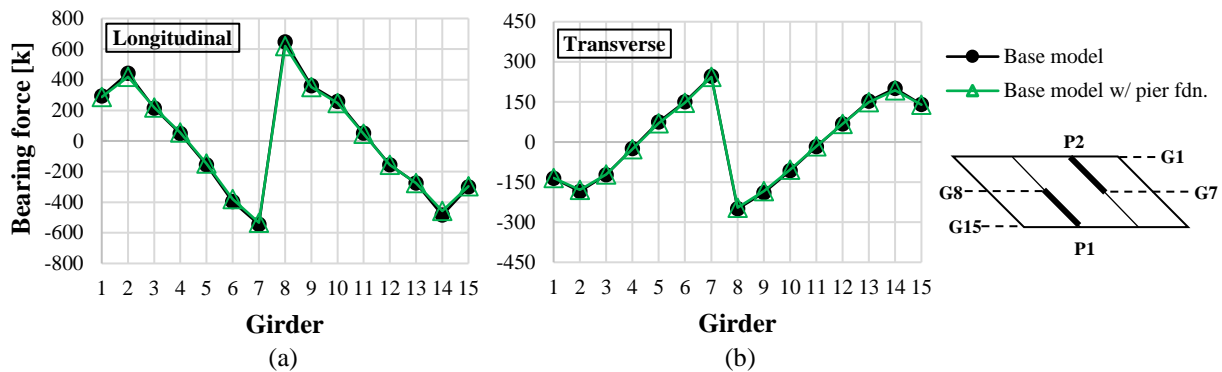


Figure 8.2. Bearing horizontal forces considering pier foundation effects in the (a) longitudinal and (b) transverse bridge directions under thermal loading from finite element models for the HAST bridge.

8.1.3. CAP BEAM AND FIXED BEARINGS CONNECTION EFFECTS

The impact of the rotational flexibility of fixed bearings on fixed bearing forces was assessed. In the base model, fixed bearings are free to rotate relative to piers but are restrained from moving laterally or longitudinally. An additional model was built by restraining translational and rotational degrees of freedom at fixed bearings. Figure 8.3 compares longitudinal and transverse bearing forces from these two models.

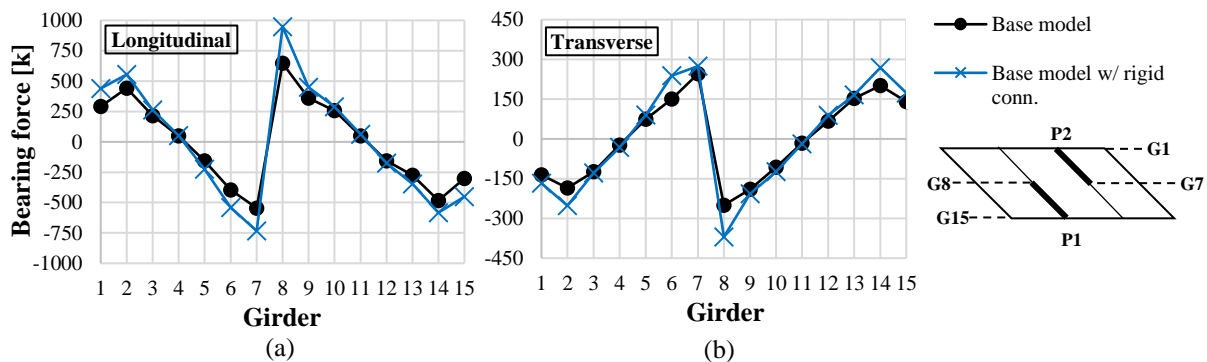


Figure 8.3. Bearing horizontal forces considering cap beam and fixed bearings connection effects in the (a) longitudinal and (b) transverse bridge directions under thermal loading from finite element models for the HAST bridge.

It is clear from Figure 8.3a that the peak longitudinal bearing force predicted by the model with a rigid connection increased considerably. The increase was of 47% with respect to estimates from the base

model. On the other hand, in the transverse direction, the increase was not substantial, and only represented 12% of the peak value coming from the base model. Bearing force trends along the width were essentially unchanged by the inclusion of a fixed connection.

8.1.4. EXPANSION BEARINGS STIFFNESS EFFECTS

Idealized bridge models include expansion bearings that are perfectly free to expand. Including the actual translational flexibility of expansion bearings may create changes in bearing forces. An additional bridge model that included expansion bearing stiffnesses was constructed to study their role on fixed bearing force predictions. Expansion bearings were assigned the upper-bound stiffness value defined by the maximum shear modulus recommended on section 27.2.1 of the WisDOT BM. Figure 8.4 presents horizontal forces on fixed bearings for the base model that does not include stiffnesses on expansion bearings, and the additional model with expansion bearing stiffnesses. This figure displays that including a finite expansion bearings stiffness in models caused negligible changes on horizontal fixed bearing forces. Peak bearing force modifications were below 4% in both directions.

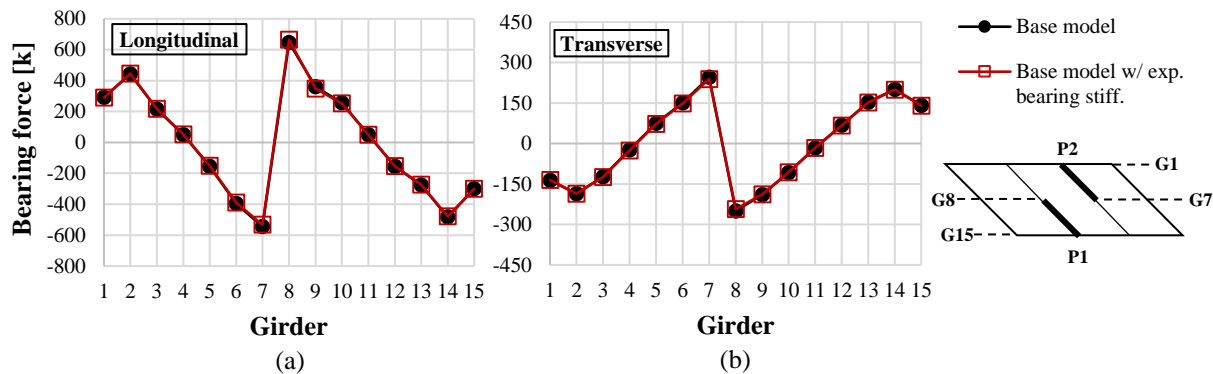


Figure 8.4. Bearing horizontal forces considering expansion bearings stiffness effects in the (a) longitudinal and (b) transverse bridge directions under thermal loading from finite element models for the HAST bridge.

8.1.5. PIER TEMPERATURE CHANGE EFFECTS

Uncertainties exist regarding the spatial distribution of temperature in the superstructure and substructure of any bridge. Similarly, differences in thermal changes occurring concurrently on different bridge components is not well defined. This section evaluated two extreme scenarios: one where piers did not experience thermal changes while the superstructure did (base model); and another where both superstructure and piers underwent the same temperature change. The actual bridge behavior will be in between these two bounds. Figure 8.5 displays the comparison of horizontal (lateral) bearing forces from the two different finite element models.

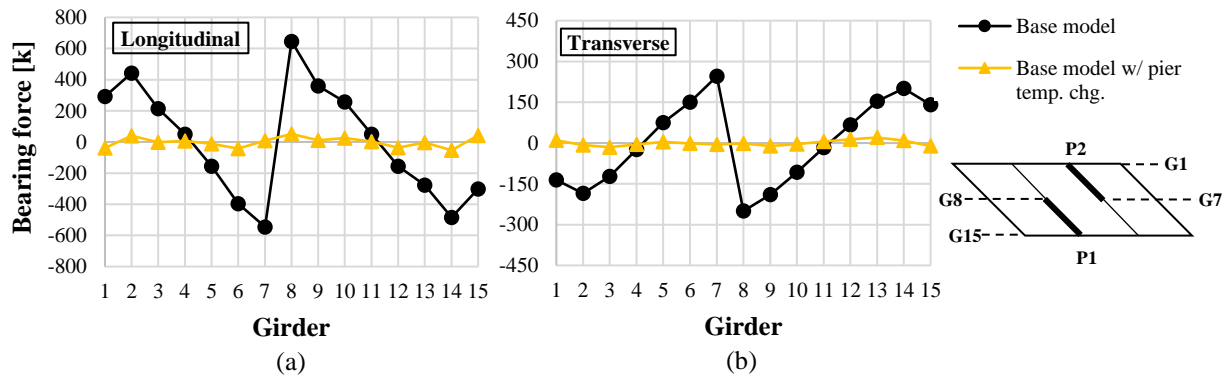


Figure 8.5. Bearing horizontal forces considering pier temperature change effects in the (a) longitudinal and (b) transverse bridge directions under thermal loading from finite element models for the HAST bridge.

It is evident from Figure 8.5 that including the same temperature change on superstructure and piers led to major reductions in bearing forces. As a matter of fact, peak longitudinal and transverse bearing forces predicted by the model that also includes temperature changes on piers reduced by 92% with respect to bearing forces from the base model. The magnitudes of peak bearing force estimates in the longitudinal and transverse directions were of only 51 k and 20 k, respectively, for the former model. Trends along the width were similar between the two models for bearing forces in the longitudinal direction.

Based on the results shown in Chapter 8.1, and in order to stay on the conservative side, the base model features were employed in additional bridge models used to perform parametric studies in the following section. The only exception was the cap beam expansion joint that was used in the HAST bridge models following the actual bridge detail. This detail was not included in the models of bridges presented in the following section.

8.2. BRIDGE DETAILS AFFECTING MAXIMUM FIXED BEARING FORCES

This section consists of parametric studies to explore the effects of skew angle, bridge geometry and bearing fixity arrangement over piers on peak fixed bearing horizontal forces for highly skewed prestressed concrete girder bridges under thermal loading. Temperature was applied to the superstructure. Trends in bearing forces rather than magnitudes of bearing forces should be inferred from the results of this section. As shown in the previous section (Chapter 8.1), fixed bearing forces are highly dependent on the level of refinement introduced to the model.

8.2.1 VARYING SKEW ANGLE

As the base bridge, this section used the visually inspected, two span, 52° skew prestressed concrete bridge (Table 3.1) to investigate the impact of varying skew angles on peak fixed bearing horizontal forces under thermal loading ($\Delta T = -55$ °F). Skew angles used were 0°, 15°, 30°, 45°, and 60°. These bridge models did not include a mixed bearing arrangement over piers.

Figure 8.6 shows peak longitudinal and transverse fixed bearing shear forces for different skew angles. The figure exhibits that with increased skews, both longitudinal and transverse fixed bearing forces noticeably increase. At 60° skew, the peak longitudinal force reached 180 k, while for the non-skewed bridge, longitudinal forces were less than 1 kip. Maximum transverse force at 60° skew increased was 165% of the one from non-skewed bridge. Increases in the transverse direction remained small up to 30° skew.

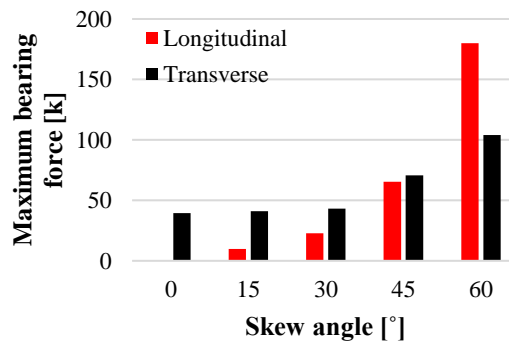


Figure 8.6. Maximum longitudinal and transverse fixed bearing horizontal forces (absolute values) under thermal loading from bridge finite element models with different skew angles for prestressed concrete bridges.

8.2.2 VARYING BRIDGE DETAILS AND GEOMETRY

This section examined the impact of selected bridge details and geometry on peak fixed bearing forces under thermal loading ($\Delta T = -55$ °F) for prestressed concrete bridges. Bridge models (cases) and corresponding details were the ones presented earlier in Table 6.1. Mixed bearing configurations over piers were not used for these analyses.

Figure 8.7 displays maximum longitudinal and transverse fixed bearing forces for these cases. This figure shows that as the number of spans increased (cases 0, 1, and 2), maximum longitudinal and transverse fixed bearing forces increased by 15% and 121%, respectively, for the two-span bridge (case 0) with respect to the single-span bridge (case 1). However, two span (case 0) and three span (case 2) bridges had similar bearing forces.

Increasing the deck width (cases 0, 3, and 4) resulted in significantly higher fixed bearing forces. For the bridge with the widest deck (case 3), longitudinal and transverse forces were 178% and 164% greater, respectively, than the forces on the narrowest bridge (case 4).

As the girder depth increased (cases 0, 5, 6), maximum fixed bearing forces moderately reduced. Peak longitudinal and transverse fixed bearing forces reduced by 28% for the bridge with the greatest girder depths (case 6), relative to the bridge with the shallowest girders (case 5).

Larger girder spacing (cases 0 and 7) led to reductions of 19% in both longitudinal and transverse fixed bearing forces for the bridge with the wider girder spacing (case 7).

Changes to the deck thickness (cases 0 and 8) modified maximum fixed bearing forces. Increases of 38% were found in the maximum longitudinal and transverse forces for the bridge with the thicker deck (case 8).

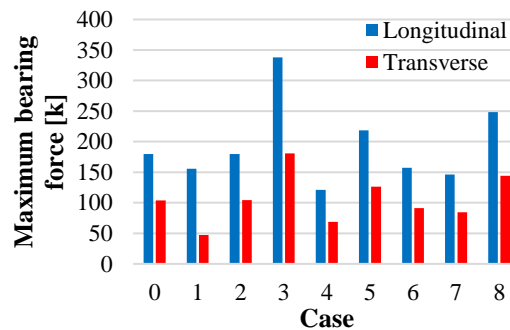


Figure 8.7. Maximum longitudinal and transverse fixed bearing horizontal forces (absolute values) under thermal loading from bridge finite element models with different design details for prestressed concrete bridges.

8.2.3 VARYING BEARING FIXITY ARRANGEMENTS

This final section assessed changes in fixed bearing forces due to mixed bearing configurations over piers. The models of the HAST bridge subject to a thermal load $\Delta T = -55^\circ\text{F}$ was employed to investigate this. Two models were used: one with the actual mixed bearing arrangement (configuration 6 in Figure 7.5), and the other using a regular bearing arrangement (configuration 1 in Figure 7.5). Figure 8.8 compares maximum longitudinal and transverse fixed bearing forces from these two models.

Contrary to expectations, the increase in peak fixed bearing forces was not significant due to the use of a mixed bearing configuration. Increases in bearing forces in the longitudinal and transverse directions were 11% and 8%, respectively, for the bridge with the mixed fixity arrangement with respect to the bridge with a regular bearing configuration.

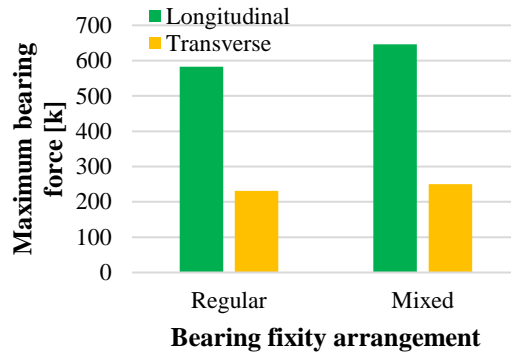


Figure 8.8. Maximum longitudinal and transverse fixed bearing horizontal forces (absolute values) under thermal loading from bridge finite element models with different bearing fixity arrangements over piers for the HAST bridge.

8.3. SUMMARY AND CONCLUSIONS

Trends observed in bearing forces for bridges with or without flexible piers (Chapter 8.1) indicated that pier stiffness could play an important role in predicting horizontal forces on fixed bearings of bridges featuring a mixed arrangement over piers. It was clear that stiffer pier representations lead to greater bearing forces, and that excluding piers from bridge models could result in extremely conservative force estimates. Simulating the foundations of piers did not cause significant changes in bearing forces; however, this change is highly dependent on soil properties and should be considered on a project basis as a source of flexibility that could reduce fixed bearing forces. Adding a rotational restraint to fixed bearings led to greater bearing forces, which was expected due to the increased stiffness of the pier. Including the upper bound of expansion bearing stiffness values did not cause measurable changes on bearing forces, and seems unnecessary for fixed bearing force estimates. Finally, assuming that equal changes in temperature take place in both superstructure and piers lead to smaller forces in fixed bearings compared to cases where temperature changes were different in superstructure and piers. This assumption should be supported by additional field data since it may lead to un-conservative results. Alternatively, temperature analyses can be conservatively performed by assigning temperature changes only to superstructure.

This chapter also showed that fixed bearing forces increase with increasing skew angles. For a non-skewed bridge, this results may be unexpected. However, this effect may be explained by the rotation tendency observed in highly skewed bridges (Chapter 7.1). Several trends in bearing force changes were observed for the various bridge details and geometry considered. In general, increasing number of spans, deck width and girder depth resulted in greater fixed bearing forces. Conversely, greater girder depth and spacing led to reduced bearing forces. The variable that caused the greatest impact on bearing forces was the bridge width, and highlighted that significantly wide bridges could experience large fixed bearing forces at high skew angles. Finally, the mixed bearing arrangement used in the HAST bridge did not cause major increases on fixed bearing forces compared to a regular bearing assignment. This represents another favorable trait of the special mixed fixity configuration.

9. DECK CRACKING UNDER LONG-TERM LOADING

9.1. DECK CRACKS

Several inspection reports described diagonal cracking of concrete decks in highly skewed bridges. The literature search on this crack type suggested that it is mainly caused by the combination of early shrinkage and the restraining effect of girders and end diaphragms at bridge ends [3]. Some studies indicate that diagonal cracking is confined to the acute deck corner regions [58]. Other documents, such as an inspection report shown in Figure 9.1, show diagonal cracks extending beyond acute corners. Understanding the sources and possible mitigating measures of the deck cracking is the motivation of this section.

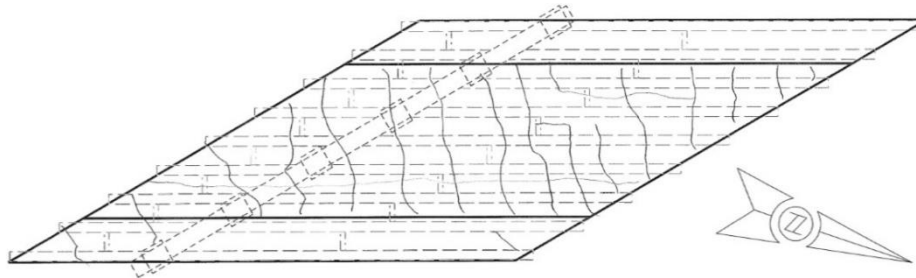


Figure 9.1. Deck crack map of the Old Middleton Bridge. [1]

9.2. DECK CRACKING ANALYSIS METHOD AND PARAMETERS

Deck cracking and its relationship with bridge details were investigated using finite element analyses. All finite element models were detailed 3D models that incorporated concrete material nonlinearity on the deck as described in Chapter 5.1.5 and Chapter 5.2.1. Concrete nonlinearity was confined to a quarter span from the bridge end in order to run models efficiently, as nonlinear analyses are computationally demanding. Parameters investigated were 1) girder end restraint and diaphragm details, 2) bridge skew angle, and 3) deck reinforcement.

End cracking was investigated using the Old Middleton and Chippewa bridges as base models for prestressed concrete and steel girder bridges, respectively. The Old Middleton Bridge was selected because inspection reports showed that it had deck diagonal cracking as shown in Figure 9.1. It is a two-span prestressed concrete girder bridge with a skew of 60°. Concrete nonlinearity was considered for a distance equivalent to one-fourth of the north, and west exterior spans of the Old Middleton and Chippewa bridges, respectively.

Finite element models produce principal tensile strain contour maps. Strains that exceed the theoretically predicted concrete tensile strength are plastic strains, and are indicators of cracking. Design details that have an impact on deck cracking were evaluated by comparing principal tensile strain contour plots obtained from analyses. Plastic strain contour plots were also presented. In addition, the volume of finite elements in the deck with plastic tensile strains (under tension softening) was compared for each model with a varying design detail to quantify the amount of expected cracking. Using volume of finite elements allows accounting for depth of potential cracks into the deck, in addition to length and width. In addition, as a means of having a visual impression of deck cracking caused by the parameters considered in the investigation, contour plots of maximum principal plastic and total strains on deck ends are presented.

9.3. LOADING

Loading considered to investigate deck acute corner cracks were long-term loads, namely temperature and shrinkage. Temperature changes input into models +/- 55 °F and +/- 75 °F for prestressed concrete and steel bridges, respectively. Nonlinear models of both prestressed concrete and steel bridge models showed that when temperature changes are superimposed to dead load, strains increase near deck ends. However, these strains were not plastic, which indicates that under temperature loading the bridge is free to contract or expand. These results showed that decks are unlikely to develop cracking due to temperature loading alone. Therefore, in the analyses presented in this section, the main loading considered was shrinkage.

Shrinkage loading corresponded to the deck ultimate shrinkage estimated using the FIB Model Code 2010 as described in Chapter 5.3.2. The results of temperature analyses are not presented here.

9.4. EFFECT OF BRIDGE END DETAILS ON DECK CRACKS

The following bridge end details were considered for the prestressed concrete bridges to study their impact on deck cracking behavior. The base model was the Old Middleton bridge, which was known to have cracking.

- 1) Full-depth concrete end diaphragms, with lateral restraint on bridge bearings (end diaphragms with shear keys bearing against abutment pedestals). This was the original end configuration for the Old Middleton Bridge.
- 2) Full-depth concrete end diaphragms, no lateral restraint on bridge bearings.
- 3) Partial-depth concrete end diaphragms, no lateral restraint on bridge bearings.
- 4) No end diaphragms, no lateral restraint on bridge bearings.

For the steel girder bridge, the following end details were studied. The base model for these analyses was the Chippewa bridge.

- 1) Steel end diaphragms, with lateral restraint on bridge bearings.
- 2) Steel and partial-depth concrete end diaphragms, no lateral restraint on bridge bearings. This was the original end configuration of the Chippewa bridge.
- 3) Steel end diaphragms, no lateral restraint on bridge bearings.
- 4) Steel end diaphragms, no lateral restraint on bridge bearings, and with mixed bearing fixity over bridge piers. The bearing fixity arrangement was included since experimental (Chapter 4.1.3) and analytical studies (Chapter 7.2) have shown that bridges with this bearing fixity arrangement (i.e., the HAST bridge) may experience a more uniform overall deformation under long-term loading. This could positively impact deck behavior.
- 5) No end diaphragms, no lateral restraint on bridge bearings.

9.4.1. PRESTRESSED CONCRETE BRIDGES WITH VARYING BRIDGE END DETAILS

Figure 9.2 presents the volumetric portion of the deck finite elements exhibiting plastic tensile strains for prestressed concrete bridges with different end details, normalized with respect to the bridge with full-depth concrete end diaphragms, and lateral restraint on bridge bearings. Bearings are laterally restrained when there is shear keys on end diaphragms bearing against pedestals on abutments. Figure 9.2 shows that the detail with full-depth end diaphragms and laterally restrained bearings leads to the most severe cracking, and that removing the lateral restraint from bearings with a full-depth diaphragm did not result in measurable changes. However, partial-depth concrete end diaphragms significantly decreases potential for cracking, as compared to full depth diaphragms. Reduction in the deck volume with plastic tensile strains was beyond 30%. The absence of partial-depth concrete end diaphragm further decreases deck cracking potential, which may be due to a reduction in the restraint on the bottom face of the deck.

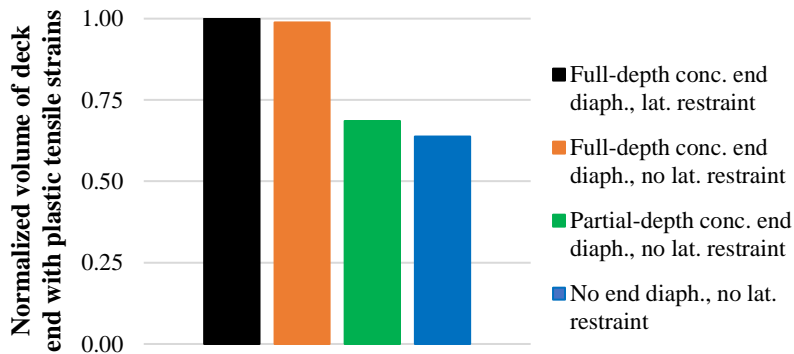


Figure 9.2. Normalized volume of deck finite elements with plastic tensile strains for prestressed concrete bridges with varying end details.

Potential crack patterns caused by shrinkage on these bridges can be observed in Figure 9.3, in which plastic and total principal tensile strains are presented for the top deck surface. Figure 9.4 shows the same for deck bottom surface. The gray areas on total principal tensile strain contour plots show approximate locations of cracked areas. Crack patterns expected have a close resemblance to the cracks documented by the inspection report (Figure 9.1). This qualitatively validates the models. Figure 9.3 and Figure 9.4 indicate that shrinkage alone can lead to diagonal cracking. The cracks were not only limited to acute corners and some cracks did not originate at bridge ends. Similar crack patterns observed on top and bottom deck surfaces indicate that cracking may extend from one face to the other.

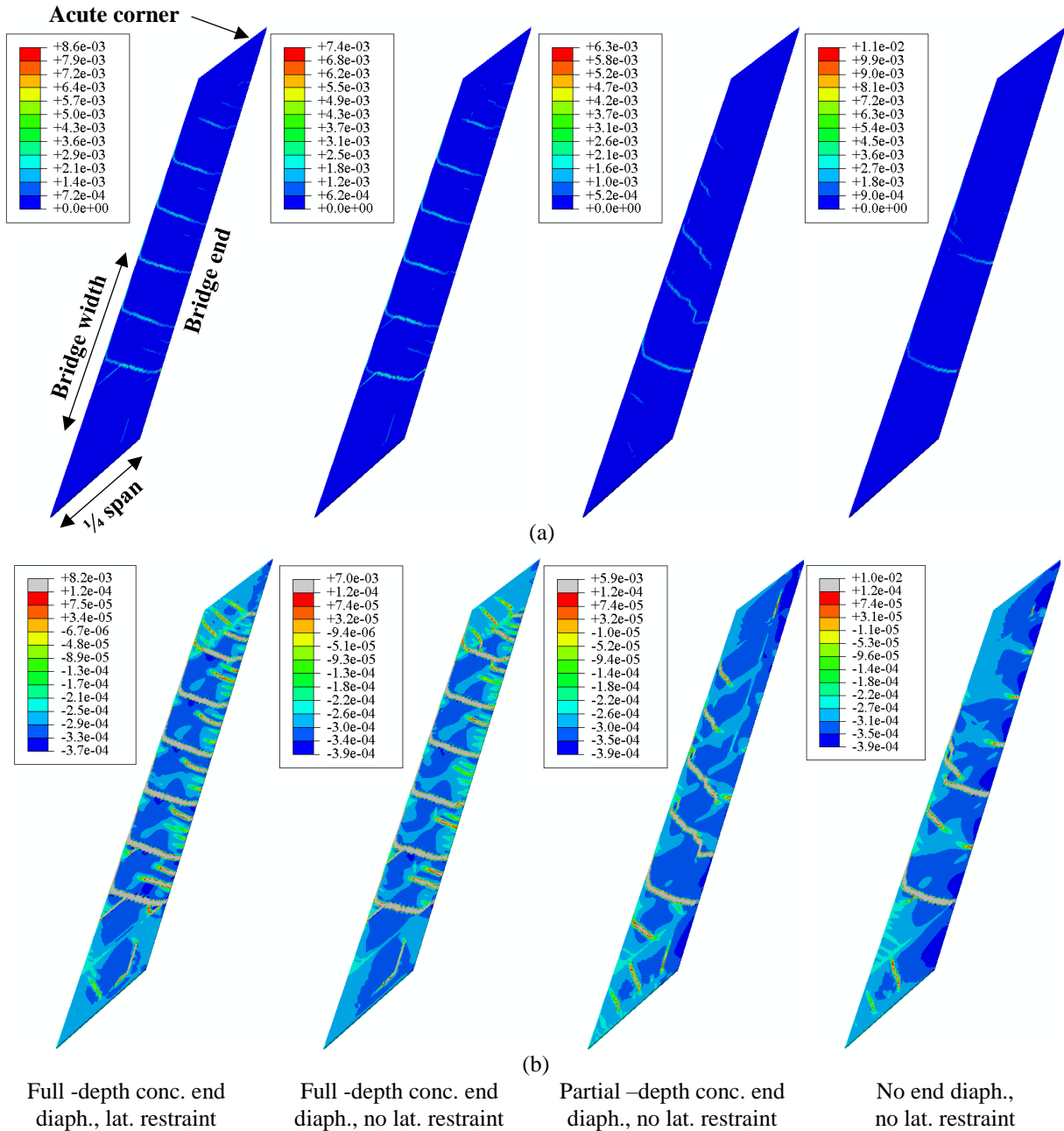


Figure 9.3. Contour plots of principal tensile: (a) plastic and (b) total strains for deck top face of prestressed concrete bridges with varying end details. Tension: (+); compression: (-).

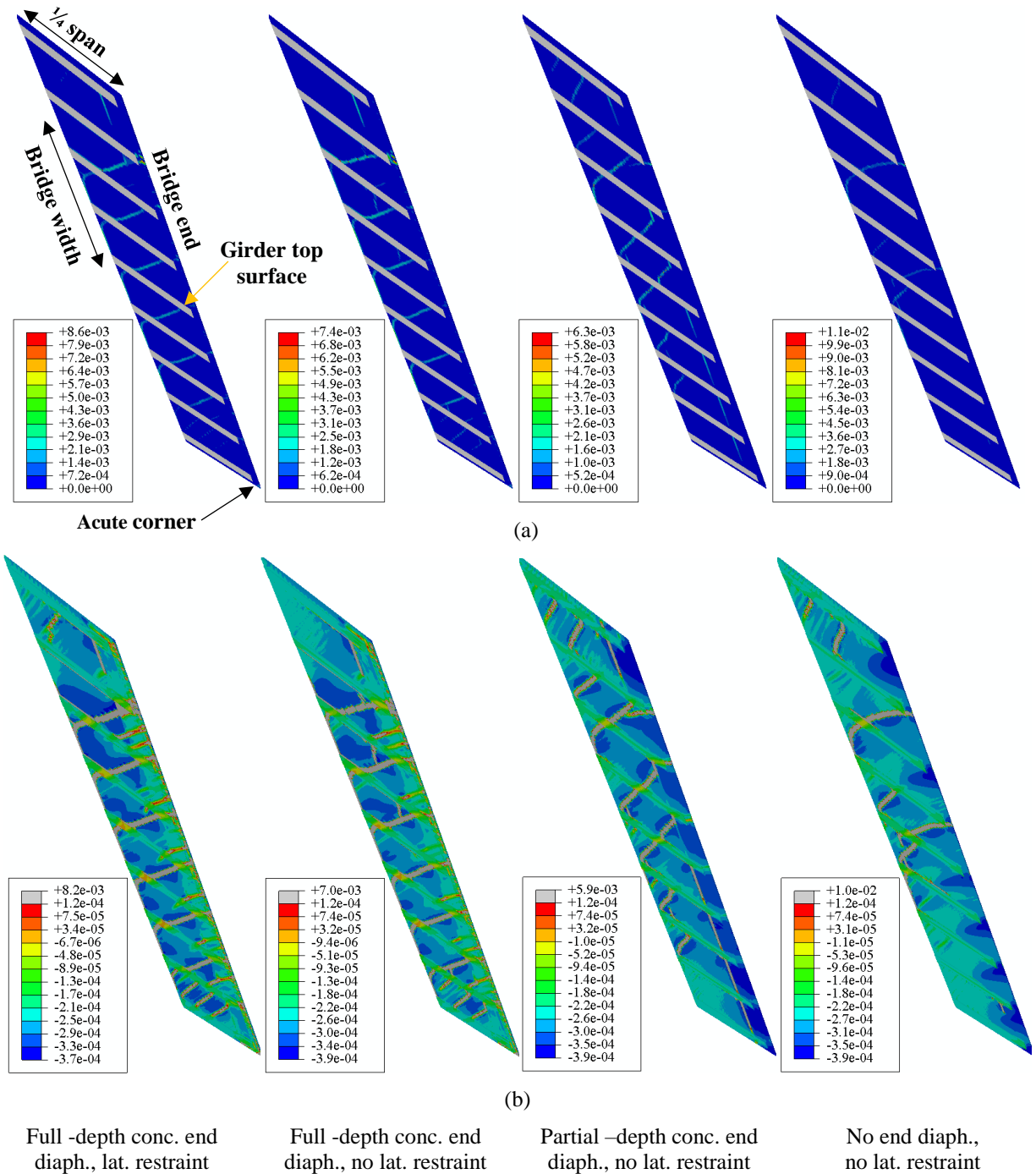


Figure 9.4. Contour plots of principal tensile: (a) plastic and (b) total strains for deck bottom face of prestressed concrete bridges with varying end details. Tension: (+); compression: (-).

9.4.2. STEEL BRIDGES WITH VARYING BRIDGE END DETAILS

Figure 9.5 displays the normalized volumetric ratio of finite elements in plastic tensile strain (cracking) for varying bridge end details for the steel Chippewa bridge. In general, deformations related to restrained shrinkage had a detrimental impact on the deck. The laterally restrained abutment bearings with steel end diaphragms was the detail that created the highest deck tensile plastic strains. An observation from Figure 9.5 is that the deck performance is improved with the mixed bearing fixity arrangement over piers. Crack potential of this bridge is the most similar to the one with no end diaphragms and no lateral restraint.

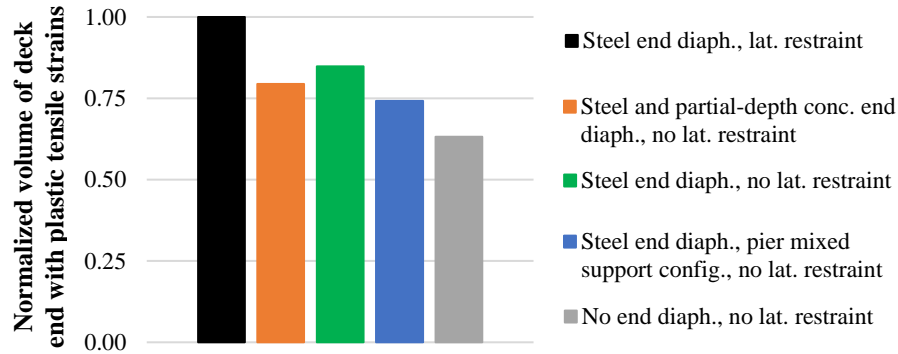


Figure 9.5. Normalized volume of deck finite elements with plastic tensile strains for steel bridges with varying end details.

Contour plots in Figure 9.6 and Figure 9.7 show significantly less cracking than the one seen in prestressed concrete bridges. The cracks were concentrated at bridge ends, on the top face of the deck (Figure 9.6). Acute corner cracking strains were moderately more pronounced than cracking in other locations. Bottom face cracking (Figure 9.7) was less significant than top face cracking, and was observed as few transverse cracks starting near the first three girders adjacent to the acute corner.

The steel bridge with abutment bearings restrained laterally had much more severe cracking on both top (Figure 9.6) and bottom (Figure 9.7) deck surfaces compared to others. For this model, regions of high tensile plastic strains ran through the thickness of the deck, indicating that cracking may not remain superficial. This detail should be avoided to reduce deck shrinkage stresses.

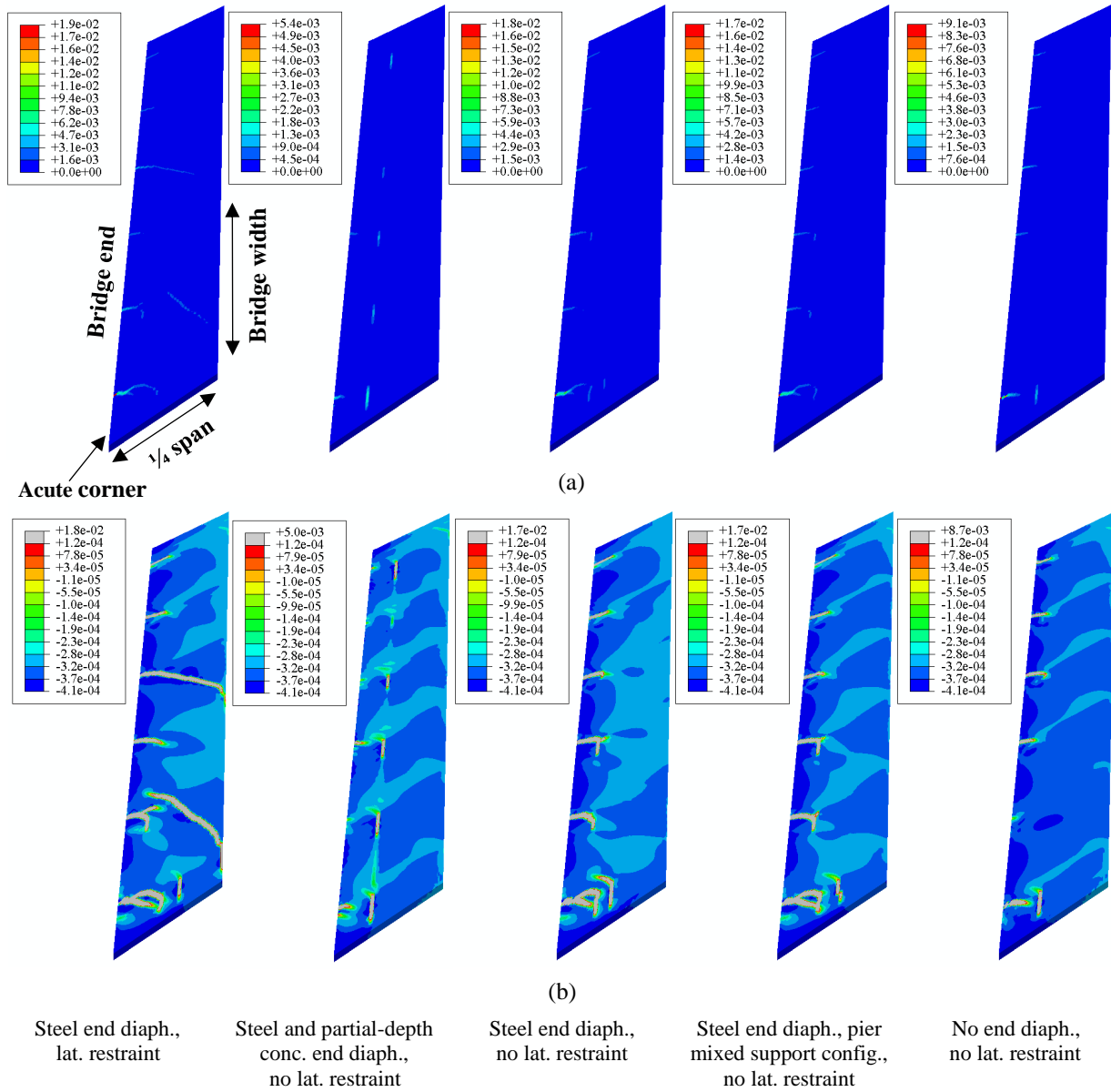


Figure 9.6. Contour plots of principal tensile: (a) plastic and (b) total strains for deck top face of steel bridges with varying end details. Tension: (+); compression: (-).

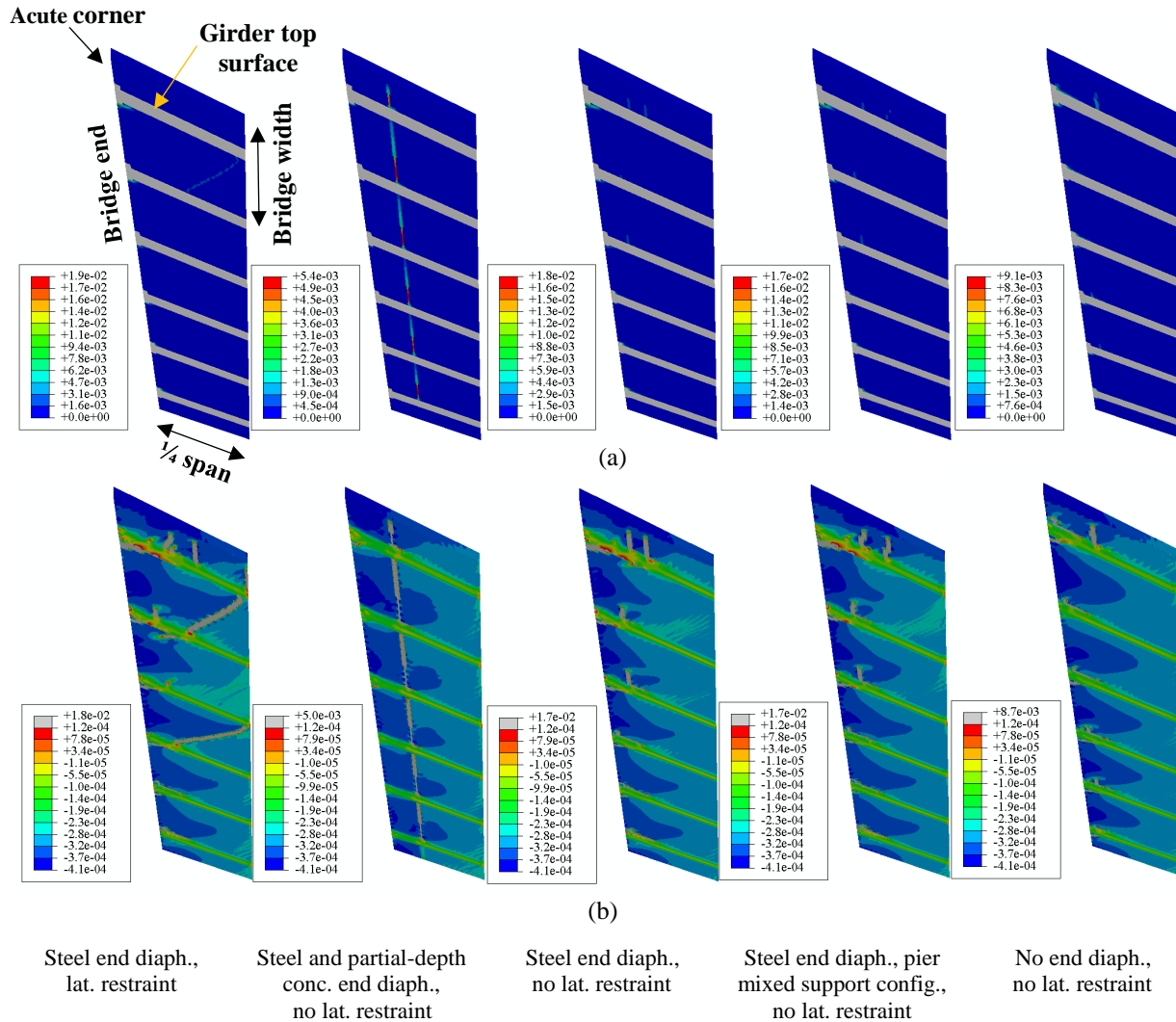


Figure 9.7. Contour plots of principal tensile: (a) plastic and (b) total strains for deck bottom face of steel bridges with varying end details. Tension: (+); compression: (-).

In general, analyses on prestressed concrete and steel bridges indicate that restraint through end diaphragms or lateral restraining of bearings cause a higher tendency for deck cracking. Cracking potential on prestressed concrete bridge decks was greater than the one on the steel bridge decks. Cracking in steel bridges was more concentrated near the acute corner than it was for the prestressed concrete bridges. This might be due to the higher flexibility of steel girders allowing axial displacements compared to prestressed concrete girders. Similarly, prestressed concrete bridge deck plastic strains were not as sensitive to lateral restraint at bearings. This might be due to the higher lateral stiffness of prestressed concrete girders compared to steel girders. It might also be due to the fact that prestressed concrete models with lateral restraint also had a full-depth concrete diaphragm. Full depth concrete diaphragms and lateral restraint at bearings may create similar deformation tendencies.

9.4.3. DISCONNECTED PARTIAL-DEPTH CONCRETE END DIAPHRAGM

Prestressed concrete and steel girder bridges typically feature partial-depth concrete end diaphragms, which as seen previously (Chapter 9.4.1 and Chapter 9.4.2), add some restraining to bridge ends, and may increase potential for cracking due to shrinkage. In order to further reduce the development of shrinkage-related stresses at bridge ends, partial-depth concrete end diaphragms were disconnected from the deck in both the Old Middleton and Chippewa bridges.

Finite element analysis results showed that cracking potential was reduced in both bridges. For the prestressed concrete Old Middleton bridge, the deck volume with plastic tensile strains resulted comparable to the one observed for the bridge without end diaphragms and without lateral restraint (detail 4 in Chapter 9.4). This represented a reduction in cracking potential of 7% with respect to the counterpart with connected partial-depth diaphragms (detail 3 in Chapter 9.4). On the Chippewa bridge, plastic tensile strains became similar to the ones for the bridge with a mixed bearing arrangement over piers (detail 4 in Chapter 9.4). The decrease in cracking tendency was 6% relative to the steel bridge with connected partial-depth diaphragms (detail 2 in Chapter 9.4).

9.5. EFFECT OF BRIDGE SKEW ANGLE ON DECK CRACKS

The effects of bridge skew angle on deck cracking were investigated for prestressed concrete and steel girder bridges. In both cases, bridge end details that were likely to lead to the most severe deck cracking, as shown in Chapter 9.4, were introduced in skewed and corresponding non-skewed bridge finite element models.

To study the skew effects on deck cracking of prestressed concrete girder bridges, two models of the Old Middleton bridge with full-depth concrete end diaphragms and lateral restraint to bearings were used. One had the original skew of 60°, and the other had no skew. A similar approach was followed for steel girder bridges, for which two models of the Chippewa bridge with steel end diaphragms and lateral restraint to bearings were employed. The first had the actual skew of 47°, and the other was the non-skewed counterpart.

9.5.1. SKEW EFFECTS ON DECK CRACKING OF PRESTRESSED CONCRETE BRIDGES

Figure 9.8 shows the volume of finite elements with plastic tensile strains for the highly skewed and non-skewed prestressed concrete bridges, normalized with respect to the bridge with skew. Figure 9.8 reveals differences in deck cracking likelihood due to the presence of skew. The drop in the cracking potential of was significant (60% reduction in volume of deck with plastic strains).

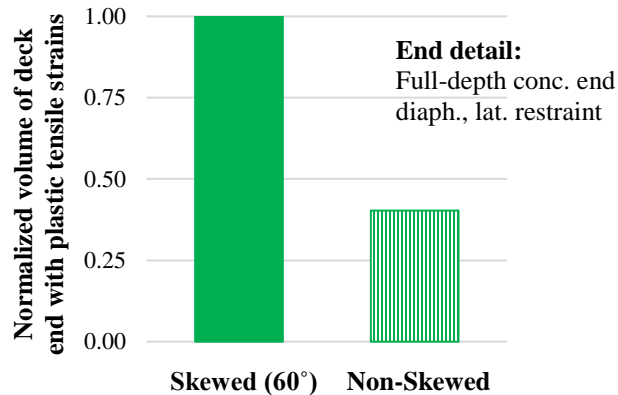


Figure 9.8. Normalized volume of deck finite elements with plastic tensile strains for highly skewed and non-skewed prestressed concrete bridges.

Principal plastic and total tensile strains for the top (Figure 9.9) and bottom (Figure 9.10) deck surfaces are presented to identify differences in potential cracking patterns between these bridges. Figure 9.9 and Figure 9.10 display cracking patterns for the non-skewed bridge that greatly differ from the ones observed on the high skew bridge. First, deck top face longitudinal cracking, approximately running along girders axes, were predominant, and seemed to only reach roughly one eighth of the span (Figure 9.9) for the non-skewed bridge. Some transverse and diagonal cracking were also observed on deck top (Figure 9.9) and bottom faces (Figure 9.10), and appeared mostly confined to bridge ends. Transverse cracking on deck width edges, and beyond deck end regions, probably resulted from the restraining effect of sidewalks that were included in the models.

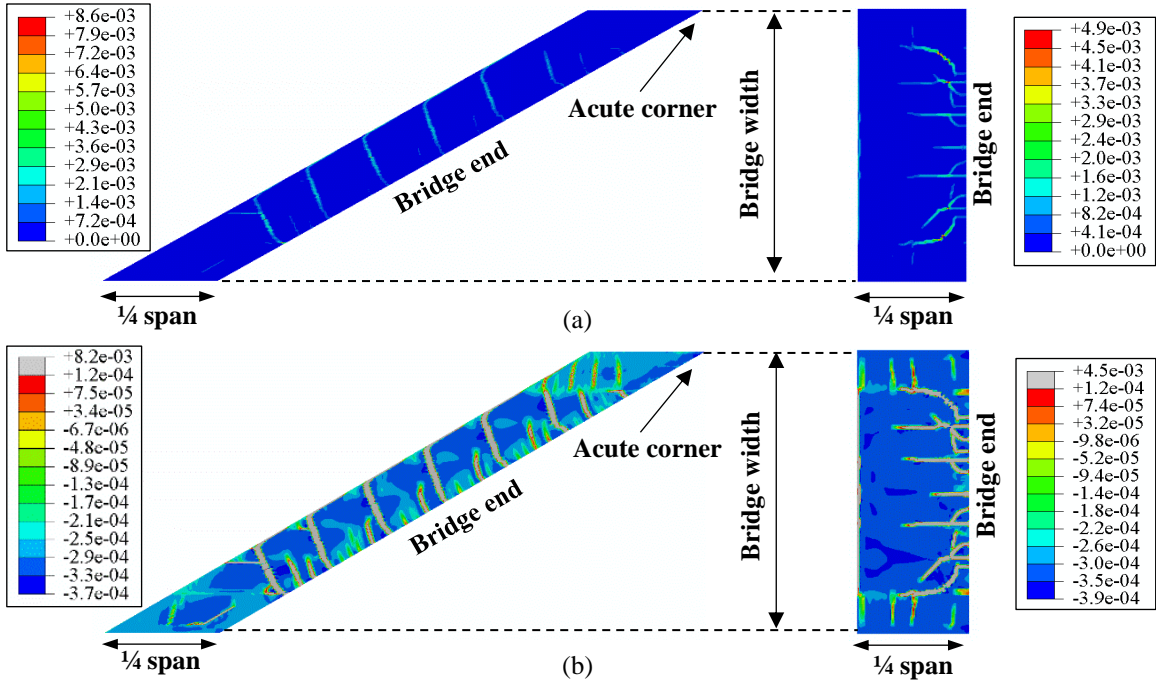


Figure 9.9. Contour plots of principal tensile: (a) plastic and (b) total strains for deck top face of highly skewed (left) and non-skewed (right) prestressed concrete bridges. Tension: (+); compression: (-).

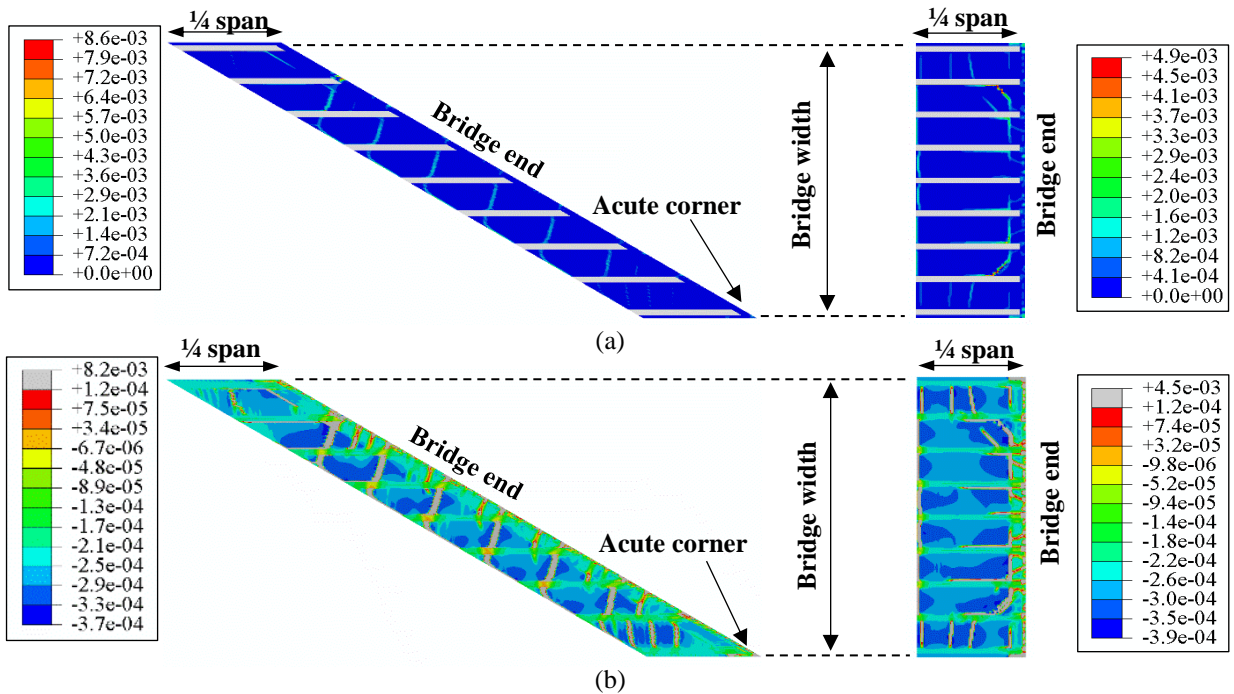


Figure 9.10. Contour plots of principal tensile: (a) plastic and (b) total strains for deck bottom face of highly skewed (left) and non-skewed (right) prestressed concrete bridges. Tension: (+); compression: (-).

9.5.2. SKEW EFFECTS ON DECK CRACKING OF STEEL BRIDGES

The normalized volumetric ratio of finite elements with plastic tensile strains for the highly skewed and non-skewed steel bridges is presented in Figure 9.11 for steel bridges. Similar to what was seen for prestressed concrete bridges (Chapter 9.5.1), Figure 9.11 shows that deck cracking tendency is highly influenced by bridge skew angle, and that the non-skewed bridge could manifest substantially less cracking than its highly skewed counterpart. Deck volume in plastic strains reduced to almost 70% of one with skew when the bridge had no skew.

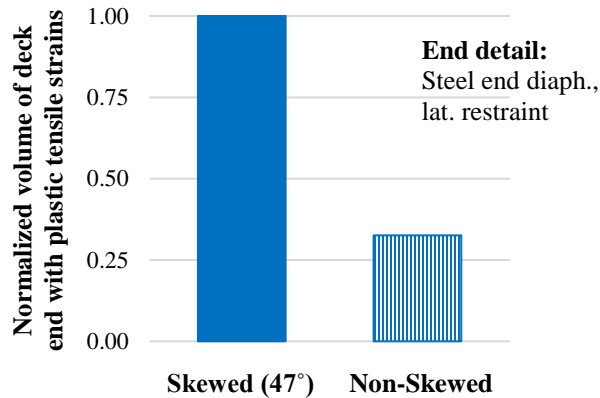


Figure 9.11. Normalized volume of deck finite elements with plastic tensile strains for highly skewed and non-skewed steel bridges.

Contour plots of principal plastic and total tensile strains in Figure 9.12 for the deck top face and in Figure 9.13 for the deck bottom face show the influence of skew angle on cracking patterns. As for prestressed concrete bridges (Chapter 9.5.1), cracking patterns in steel bridges are also impacted by the angle of skew. For instance, the top face of the non-skewed bridge (Figure 9.12) showed short longitudinal cracks initiating at bridge ends, aligned with interior girders axes. The skewed bridge had no diagonal cracking on the obtuse corner. Moreover, cracking on the deck bottom face of the non-skewed bridge was not evident (Figure 9.13), while the skewed bridge displayed diagonal and transverse cracking (Figure 9.13).

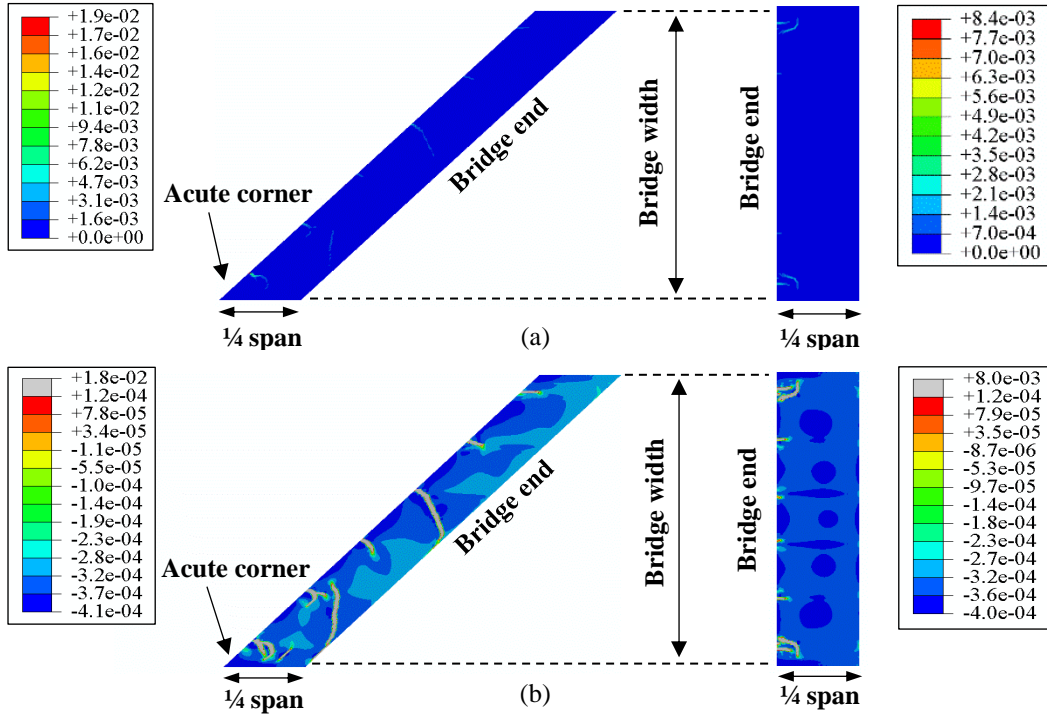


Figure 9.12. Contour plots of principal tensile: (a) plastic and (b) total strains for deck top face of highly skewed (left) and non-skewed (right) steel bridges. Tension: (+); compression: (-).

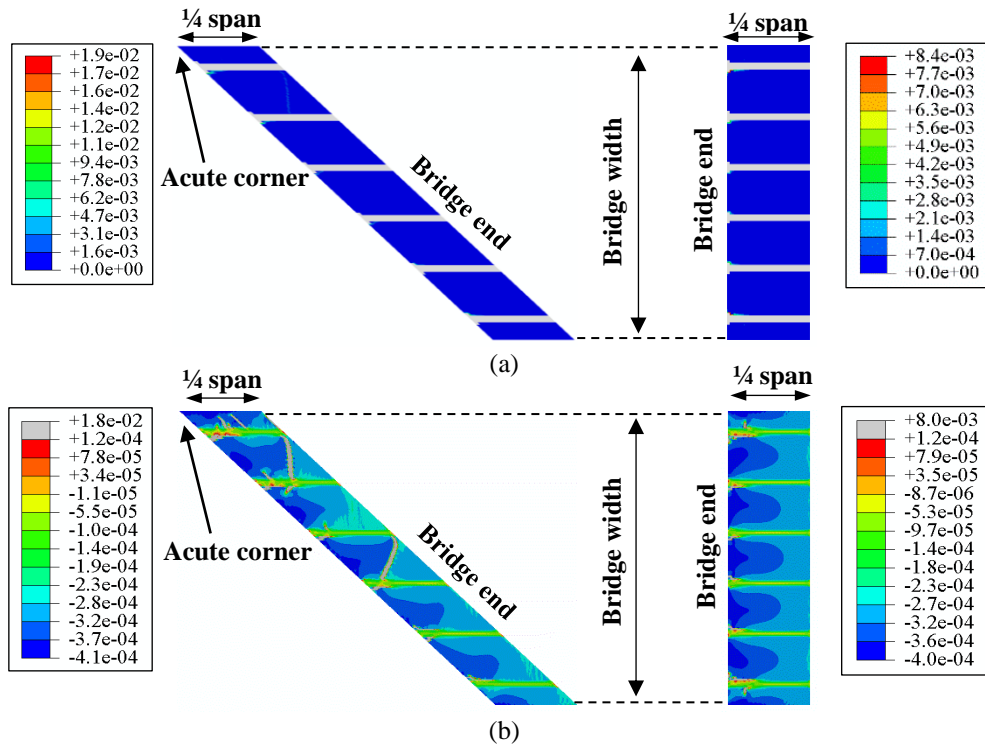


Figure 9.13. Contour plots of principal tensile: (a) plastic and (b) total strains for deck bottom face of highly skewed (left) and non-skewed (right) steel bridges. Tension: (+); compression: (-).

9.6. EFFECT OF DECK REINFORCEMENT ON DECK CRACKS

AASHTO LRFD BDS acknowledges deck end cracking in skewed bridges; however, it only links this behavior to torsion caused by differential deflections at bridge ends. To control bridge end torsional cracks, for bridges with skew angles larger than 25°, AASHTO 9.7.2.5 suggests doubling end zone deck reinforcement area in both directions for a distance equivalent to the effective length of the deck. In these provisions, non-mechanical loads, such as shrinkage and temperature, are not considered as possible sources for cracking [59]. For these non-mechanical loads, additional reinforcement may contribute to restraint and tension in the deck.

In the absence of an AASHTO provision addressing deck cracking due to non-mechanical loading in skewed bridges, the aforementioned recommendation was adopted as the basis for a parametric study on deck end reinforcement. Variables studied were reinforcement orientation and amount within a distance equivalent to the girder spacing from bridge end. These variables are summarized in Table 9.1.

Table 9.1. Deck end reinforcement for cracking control on skewed bridges.

Direction of Transverse Reinforcement	Reinforcement Amount	
	Transverse	Longitudinal
Original (Perpendicular to bridge centerline)	Original	Original
Along-the-skew	Original	Original
Original (Perpendicular to bridge centerline)	Double	Double
Along-the-skew	Double	Double

9.6.1. PRESTRESSED CONCRETE BRIDGES WITH VARYING DECK REINFORCEMENT

The Old Middleton bridge was used as a base model to study deck reinforcement effects on prestressed concrete bridges. Figure 9.14 presents the volume of finite elements in the deck with plastic tensile strains with different deck reinforcement arrangements, normalized with respect to the bridge with the original reinforcement. Orienting the transverse reinforcement along the skew of the bridge is ineffective as it leads to more cracking than the original configuration, which has the transverse reinforcement oriented perpendicular to the bridge longitudinal axis. Similarly, doubling the amount of reinforcement did not decrease deck strains. However, double reinforcement was better than using along-the-skew transverse reinforcement. Finally, doubling the amount of reinforcement and using along-the-skew transverse reinforcement resulted in the highest deck cracking potential of all cases.

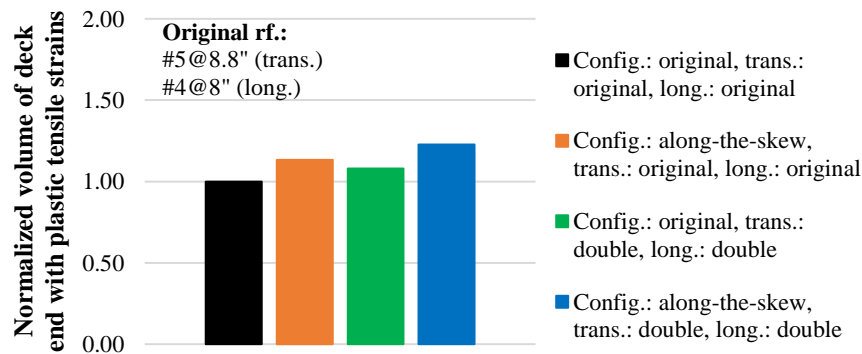


Figure 9.14. Normalized volume of finite elements in the deck with plastic tensile strains for the prestressed concrete bridge with varying reinforcement details.

The contour plots of principal plastic and total tensile strains from the deck top surface are shown in Figure 9.15 for varying reinforcement details. The same contour plots are shown for the deck bottom surface in Figure 9.16.

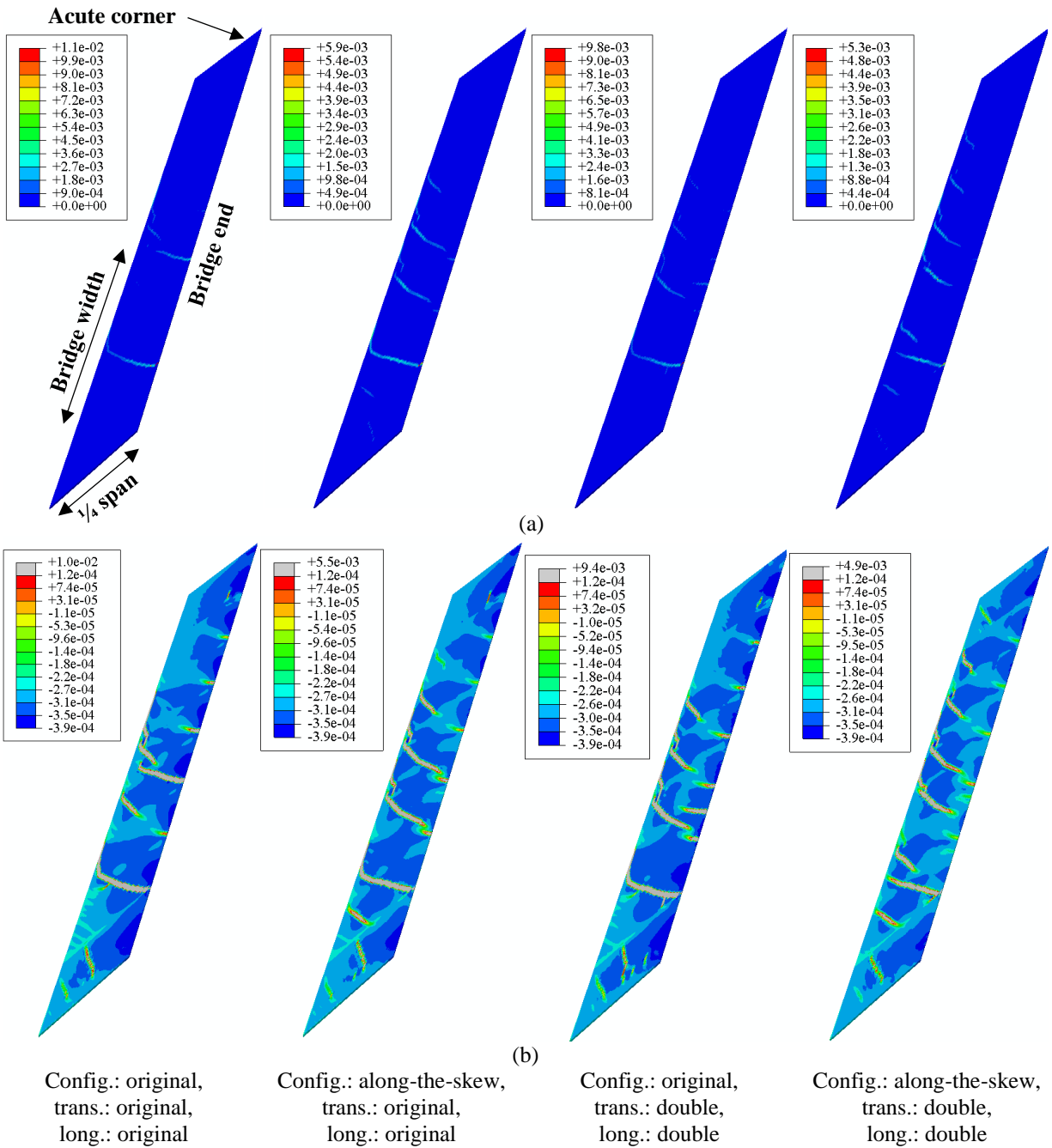


Figure 9.15. Contour plots of principal tensile: (a) plastic and (b) total strains for deck top face for prestressed concrete bridge with varying deck end reinforcement. Tension: (+); compression: (-).

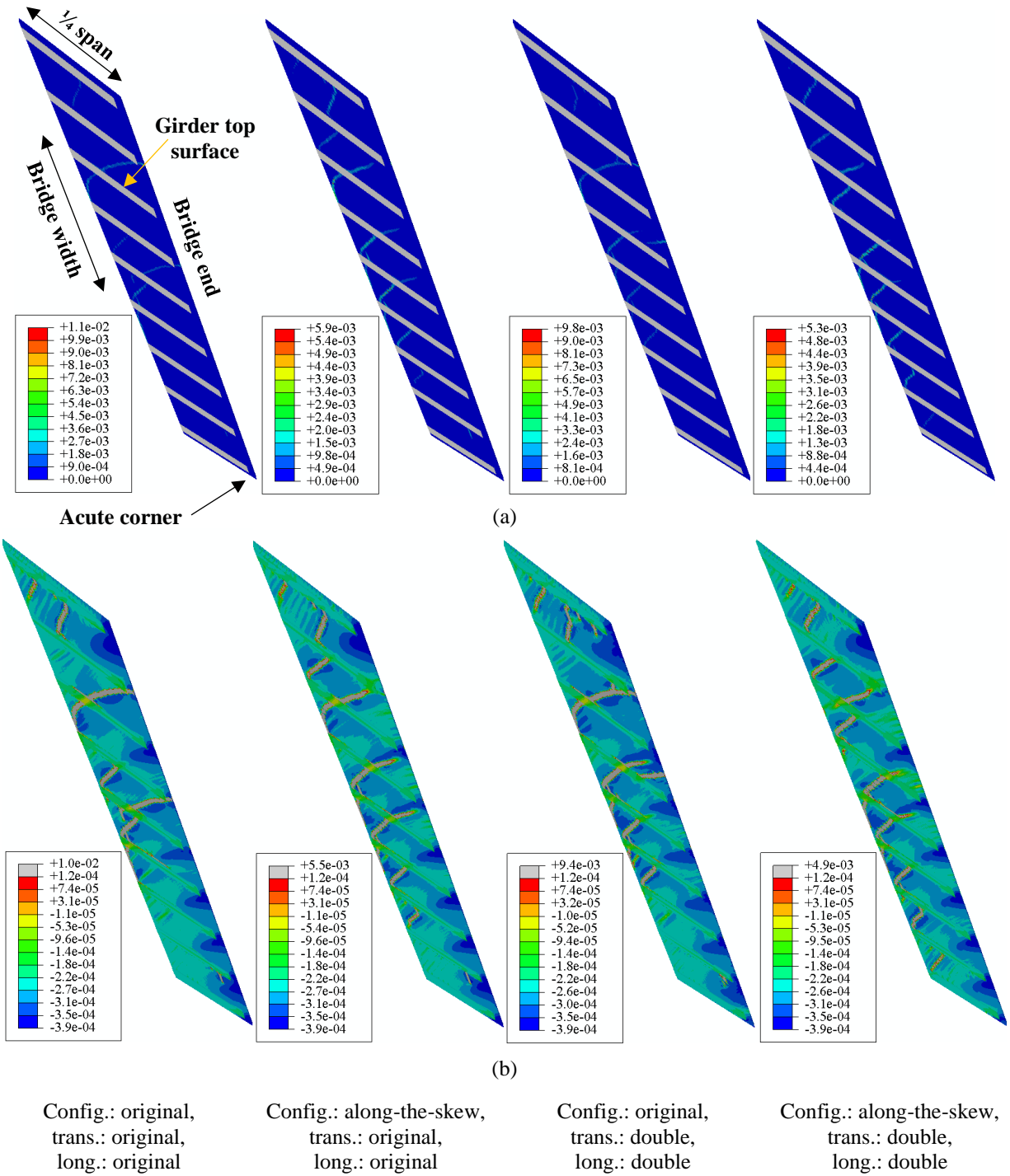


Figure 9.16. Contour plots of principal tensile: (a) plastic and (b) total strains for deck bottom face for prestressed concrete bridge with varying deck end reinforcement. Tension: (+); compression: (-).

9.6.2. STEEL BRIDGES WITH VARYING DECK REINFORCEMENT

Figure 9.17 presents the normalized volume of finite elements with plastic tensile strains for the steel bridge with different deck end reinforcement. Similar to the prestressed concrete bridge, steel girder bridge deck cracking likelihood was the minimum with the original detail. Potential of deck cracking was maximum when deck reinforcement was doubled and placed along the skew. This is more pronounced for the steel bridge, than it is for the prestressed concrete bridge. This might be because the steel bridge had more concentrated cracking near the acute corner than the prestressed concrete bridge. In addition, the higher skew of concrete bridges, 60° compared to 47°, causes reinforcement to cover a smaller portion of the bridge end.

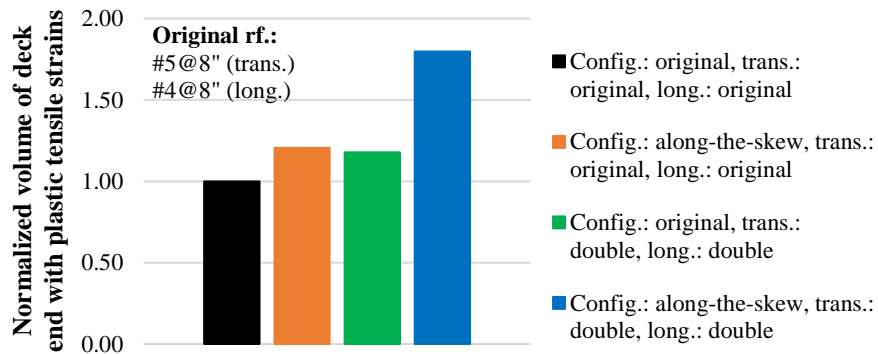
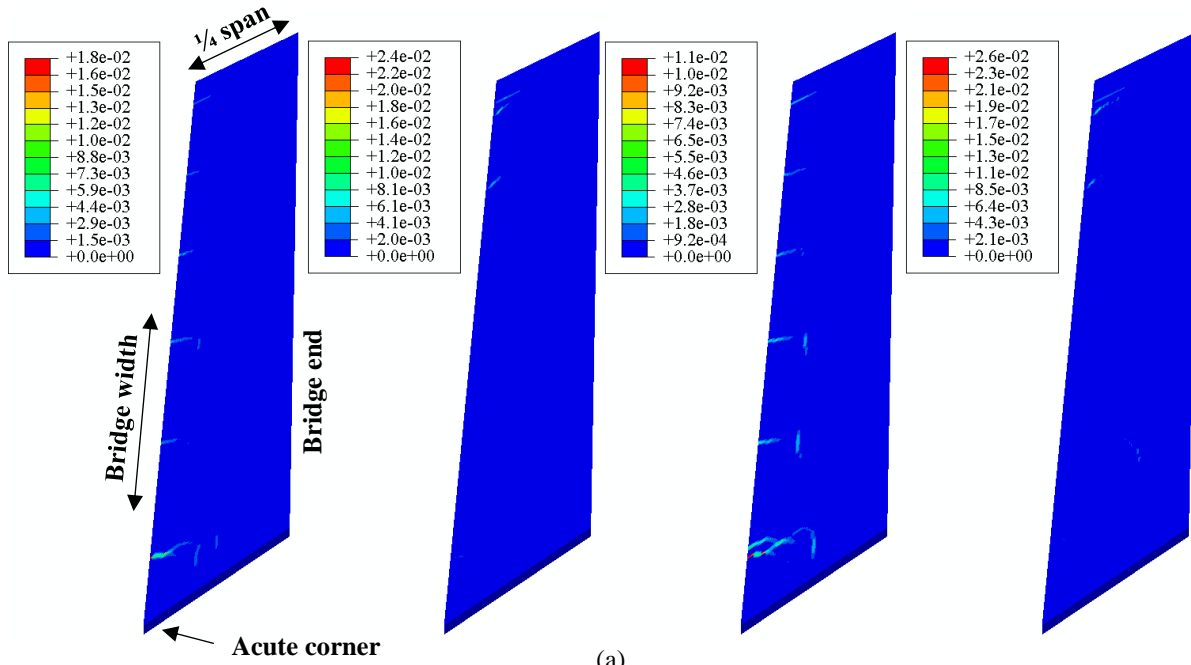
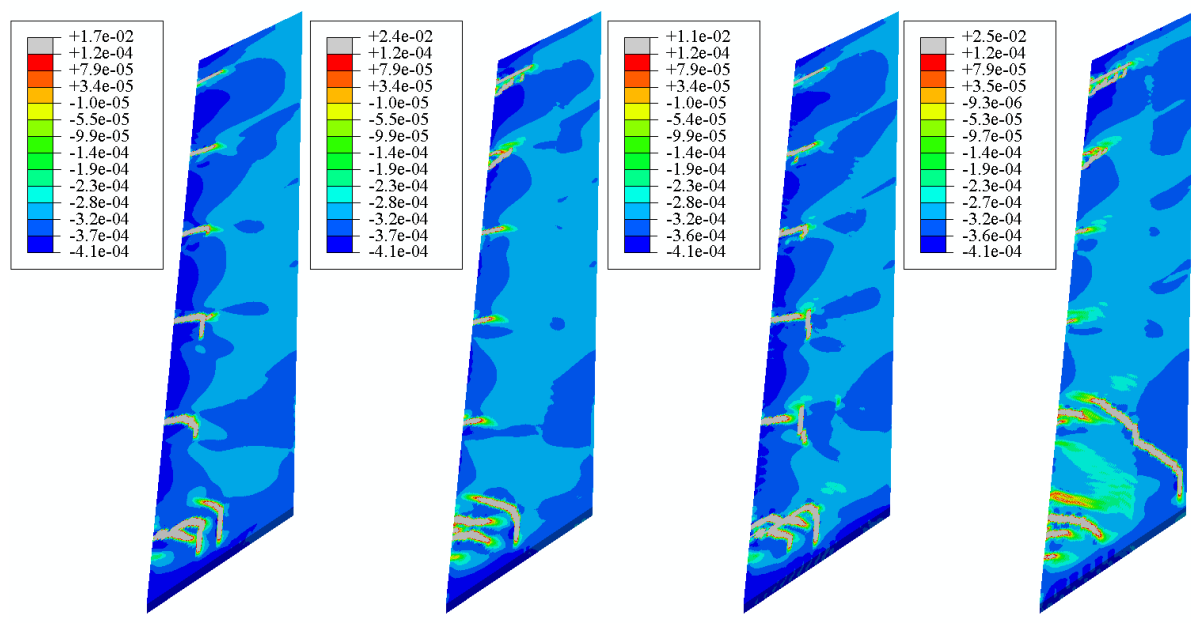


Figure 9.17. Normalized volume of finite elements in the deck with plastic tensile strains for the steel bridge with varying reinforcement details.

Contour plots of principal plastic and total tensile strains are shown in Figure 9.18 for the deck top surface and in Figure 9.19 for the deck bottom surface.



(a)



(b)

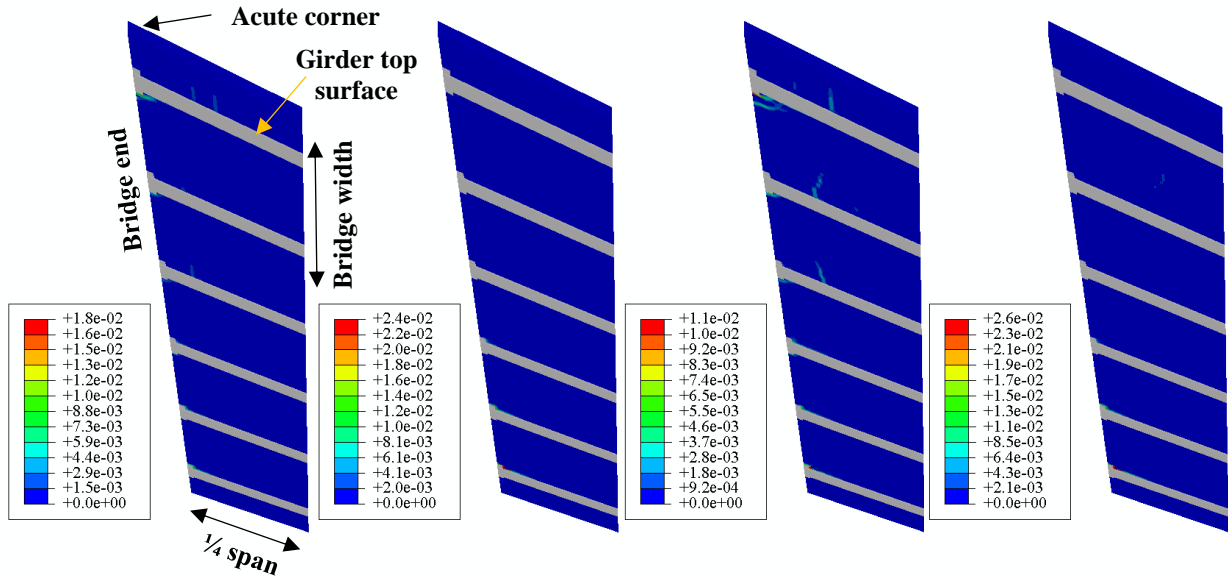
Config.: original,
trans.: original,
long.: original

Config.: along-the-skew,
trans.: original,
long.: original

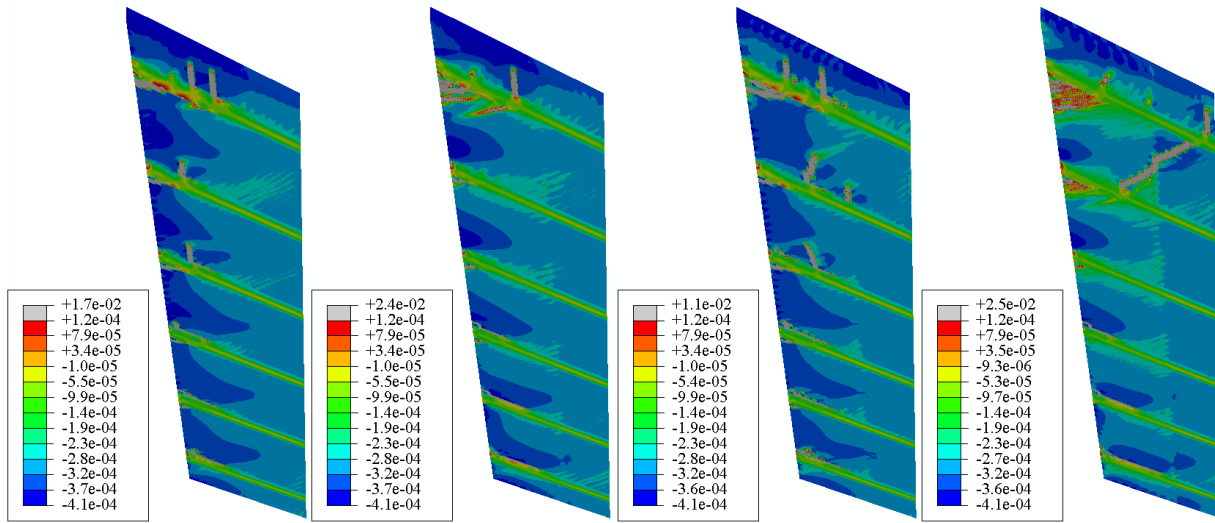
Config.: original,
trans.: double,
long.: double

Config.: along-the-skew,
trans.: double,
long.: double

Figure 9.18. Contour plots of maximum principal: (a) plastic and (b) total strains for deck top face for steel bridge with varying deck end reinforcement. Tension: (+); compression: (-).



(a)



(b)

Config.: original,
trans.: original,
long.: original

Config.: along-the-skew,
trans.: original,
long.: original

Config.: original,
trans.: double,
long.: double

Config.: along-the-skew,
trans.: double,
long.: double

Figure 9.19. Contour plots of maximum principal: (a) plastic and (b) total strains for deck bottom face for steel bridge with varying deck end reinforcement. Tension: (+); compression: (-).

9.7. SUMMARY AND CONCLUSIONS

Finite element models showed that deck, although temperature cycles may widen existing cracks, cracking is unlikely to occur under temperature loading alone. Shrinkage loading alone, on the other hand, can create significant principal plastic strains in concrete decks of skewed bridges. Finite element models were effective in capturing both localized acute corner cracks and global diagonal cracks, both stemming from shrinkage loading. The match between diagonal cracking patterns that extend across the bridge documented in inspection reports and as obtained from finite element models provided qualitative validation of models.

Models revealed that bridge end details affect deck cracking behavior. Reducing deck restraint was key to limiting cracking. Details, such as full-depth concrete end diaphragms and laterally restrained abutment bearings, created the highest deck strains and should be avoided to reduce deck cracking. Using a mixed bearing arrangement over piers showed to not only improve the bearing displacement behavior (Chapter 7.2) but also to control deck cracking for the steel bridge analyzed; and is recommended. The introduction of partial-depth concrete end diaphragms disconnected from the deck did not lead to significant reductions in cracking potential.

Bridge skew angle plays an important role in deck cracking. The severity of cracking in prestressed concrete and steel bridges were similarly exacerbated with increasing skew angles. In addition, deck cracking patterns can be significantly different with skew. It was seen that diagonal cracking in corner regions at bridge ends may also be observed in non-skewed bridges; however, this type of cracking beyond corner areas seemed characteristic of skewed bridges, for which the greatest deformation tendency occurs along the line joining acute corners of the deck.

Increasing the amount of deck reinforcement at bridge ends had no positive effects on deck crack control. This is expected as reinforcement contributes to restraint on deck against shrinkage deformations. Similarly, orienting deck reinforcement along skew (as opposed to orienting it perpendicular to skew) caused higher deck strains; and is not recommended.

10. CONCLUSIONS AND RECOMMENDATIONS

10.1. CONCLUSIONS

The following are the conclusions of this project on the analysis, design and performance of highly skewed bridges. The conclusions are drawn based on literature review and field inspections; load testing of highly skewed bridges; finite element modeling and validation; evaluation of load distribution through finite element analysis; evaluation of displacements under long-term loading; evaluation of deck cracking under long-term loading.

10.1.1. CONCLUSIONS BASED ON THE LITERATURE REVIEW AND FIELD INSPECTIONS

Skew affects shear and moment distribution to girders. For instance, shear forces and reactions on the obtuse corners of the bridge increase and bending moments decrease as the skew angle increases. In addition, negative moments and torsion at bridge ends could develop due to the skew geometry.

Service problems such as lateral horizontal movements of bearings (girder ends) and deck diagonal cracking are associated with temperature and shrinkage loading. However, the relationship between the severity of deck cracking and bridge skew angle is not completely understood.

AASHTO LRFD BDS does not relate typical diagonal cracking on skewed bridges to shrinkage and temperature loading. However, it recognizes bridge end cracking caused by torsion due to girder differential deflections. To address torsion-related cracks, AASHTO provides a crack control provision (A 9.7.2.5).

Design methods related to girder and concrete deck design on skewed bridges given by AASHTO LRFD BDS and State DOT's were in general agreement. Differences between DOT provisions and deviations of DOT provisions from AASHTO LRFD BDS seem to exist mainly due to conservatism and/or DOT bridge maintenance and field experience over the years.

Field visual inspections showed that the condition of high skew bridges was not necessarily worse than similar bridges with no skew. This pointed out the dependence of bridge condition on not only the skew angle of the bridge but also on many other bridge details affecting bridge response. These details may mitigate the negative effects of skew for some bridges.

10.1.2. CONCLUSIONS BASED ON LOAD TESTING

Long-term monitoring of bearing displacements on the HAST bridge showed that longitudinal displacements were highly correlated with temperature changes and that these displacements could be up to 5 times larger than transverse displacements. Transverse displacements were small and did not correlate well with seasonal changes in temperature. The reduced magnitude of transverse displacement component showed that the mixed bearing fixity arrangement over piers of the HAST is capable of controlling lateral displacements of the superstructure. This was later confirmed by finite element modeling.

Even though transverse displacements may be reduced using mixed bearing arrangements, displacement component in the racking direction may still be significant. This is due to the direct relationship between racking displacements, longitudinal displacements and the sine of the skew angle. A similar but smaller displacement is expected in the normal-to-joint displacement (expansion joint), as this displacement is proportional to the longitudinal displacement and the cosine of the skew angle.

Deck strains measured near an acute abutment corner during 1-year after construction were significant and mainly caused by thermal loading and shrinkage. Strains caused by live load were insignificant. Deck strains and "stress-free" gage strains were similar, indicating that the deck was mostly free to move in the location of instrumentation. However, these results should be approached with caution since the finite number of deck monitoring points is not sufficient to characterize the general cracking behavior of the deck.

Bridge load testing showed that steel girders may still exhibit a high degree of composite action with the concrete deck even after more than 20 years in service, with many instrumented locations displaying differences between measured and theoretical neutral axis locations below 15%. In addition, the comparison between measured and predicted AASHTO moment and shear distribution showed that excluding skew reduction factors for moment may be justified for exterior girders, where AASHTO was only slightly conservative. In shear, AASHTO was overly conservative for interior and exterior girders.

10.1.3. CONCLUSIONS BASED ON FINITE ELEMENT MODELING METHODS AND VALIDATION

The 2-D bridge modeling approach, in its simplest version (i.e., no secondary components, design material properties as opposed to tested material properties, etc), was accurate enough to study moment and shear distribution on skewed bridges. Both prestressed concrete and steel bridges tested had reasonable correlations between test and analysis results. However, to adequately reproduce flexural and shear strains measured under truck loading during testing, the inclusion of secondary components and refined material properties on 2-D models, or the use of more advanced 2.5-D or 3-D modeling techniques is required. This is due to the relatively small strains measured in load testing. The effect of discrepancies in individual girder strains between test and modeling on load distribution was minimal.

For bearing displacement response under long-term loading, 2-D bridge models that exclude expansion bearing flexibility lead to reasonable predictions. The influence of horizontal stiffness on bearing displacements is small even for the upper-bound shear modulus of elastomeric rubber. On the other hand, to understand the causes and evolution of deck cracking under shrinkage and thermal loading, linear elastic models, 2-D or 3-D, were not accurate. In order to simulate the deck cracking behavior of skewed bridges, 3-D models that include concrete nonlinear behavior and reinforcement-concrete interaction are necessary.

10.1.4. CONCLUSIONS FOR LOAD DISTRIBUTION UNDER SHORT-TERM LOADS

Parametric studies on the effect of bridge skew angle showed that skew impacts the magnitude of bending moments and shear forces. Bending moments did not reduce significantly with increasing skew angles on prestressed concrete and steel bridges. Reductions were greater for steel bridges. Similarly, the increase in shear forces with greater skew angles was moderate. On exterior girders, the increase was more important for prestressed concrete bridges, while on interior girders, it was more significant for steel bridges. Additional conservatism may be needed for shear forces on exterior girders in prestressed concrete girder bridges, for which AASHTO predictions were slightly smaller than or very close to the ones obtained from base model analyses. Load test results showed that, this conservatism was needed for the moment girder distribution factor of the exterior girder of steel bridges.

Bridge response, in terms of bending moment and shear force distribution, was not affected by intermediate and end diaphragms significantly. The exclusion of these secondary components from girder bridge finite element models could result in slightly conservative bending moment and shear force distributions.

For all geometry and additional design details considered in parametric studies, AASHTO girder line analyses provided conservative results with varying margins of safety (moderate or overly conservative), or slightly under-predicted the response. Accordingly, even though LRFD introduces other factors to account for these variations in load effects, 2-D finite element analyses, which were computationally efficient for every case, should be performed for bridges with high skew to complement girder line analyses. Non-composite action over piers for steel bridges did not have a measurable effect on bending moment and shear force distribution.

10.1.5. CONCLUSIONS FOR GIRDER BEARING DISPLACEMENTS UNDER LONG-TERM LOADS

The investigation on bearing displacement behavior under long-term loading (temperature) displayed that highly skewed bridges move in the horizontal plane (i.e., longitudinally and transversely) of the superstructure.

Studies on the effects of bridge skew angle, on bridges with regular support configurations over piers, showed that increasing skews lead to substantially greater bearing transverse displacements. In addition, at the same bridge end and support, acute corner bearing transverse displacement always surpassed those at the obtuse corner bearing. For negative changes in temperature, bridge rotation was towards obtuse corners, and is expected to be in the opposite for positive changes in temperature. Detected bearing displacement tendencies were representative of both prestressed concrete and steel girder bridges. 2-D finite element modeling to predict bearing transverse displacement response is recommended.

Varying bridge geometry and details affect bearing displacement responses. However, no clear relationship between bridge details and horizontal displacements was observed, possibly due to the limited number of models. All cases had increasing longitudinal deformations with increasing number of spans, slightly different longitudinal displacements by changes in girder depth, girder spacing and deck thickness, and increasing racking deformations with increasing deck width.

Studies on the effect of bearing fixity arrangements over piers on girder end displacements showed that using a mix of fixed and expansion bearings over the same piers substantially reduces transverse bearing displacements under temperature changes, and leads to an approximately uniform global deformation pattern. However, bridge racking may still occur due to the large longitudinal displacements.

The performance of the mixed bearing arrangement over piers could be affected by bridge geometry and details. The effectiveness of this configuration reduced as the skew angle decreased. This configuration is not suitable for non-skewed bridges. The arrangement is recommended for high skew angles of larger than 15 degrees. On bridges with piled encased and multi-column piers, the special fixity arrangement exhibited an excellent performance. For a bridge with hammerhead piers, the mixed configuration was still effective but less beneficial. Including bridge piers in finite element models is recommended to achieve an accurate estimate of the performance of this fixity configuration. Under different length-to-width ratios, the mixed bearing arrangement led to significant reductions in transverse displacements. However, excessively wide or long bridges should be treated with care since the mixed arrangement displayed the smallest reductions in transverse displacements under those geometries.

Bridges with regular fixity configurations over piers exhibited smaller transverse bearing displacements with decreasing bridge width or decreasing bridge span length.

10.1.6. CONCLUSIONS FOR DECK CRACKING UNDER LONG-TERM LOADING

Analyses on deck cracking revealed that shrinkage is the main cause of typical diagonal cracking on high skew bridges. Temperature changes alone were unable to create deck cracking. In addition to localized acute corner cracks, finite element models also showed diagonal cracks extending into the span, which were documented in the field.

The models showed that avoiding bridge details that restrain shrinkage deformations was the best approach to reduce the severity of diagonal cracking. These details include using diaphragms that do not prevent lateral bridge movements such as the ones with shear keys at abutment pedestals, using no end diaphragms or partial depth end diaphragms instead of full depth diaphragms. As an alternative to control shrinkage-related cracking, partial-depth concrete end diaphragms disconnected from the deck were proposed; however, its presence did not lead to significant improvements.

Increasing skew angles could lead to more severe cracking in prestressed concrete and steel bridges. In addition, crack patterns were found to be highly dependent on skew. It was seen that diagonal cracking extending beyond corner areas at bridge ends may only be found on skewed bridges. On the other hand, diagonal cracking confined to corner regions at bridge ends could also be seen on non-skewed bridges.

Parametric studies on the effectiveness of deck reinforcement controlling deck cracking indicated that orienting deck reinforcement with the bridge skew or increasing deck reinforcement amount could adversely affect deck cracking.

10.2. DESIGN RECOMMENDATIONS

The research project led to the following design recommendations:

- 1-D analyses (girder line) of AASHTO LRFD BDS predicted load distribution to girders well for bridges up to 60° skew angle and can be used. However, for some bridges, girder line analyses did not have a reasonable margin of safety (i.e., overly prediction or slight under-prediction of load distribution). For this reason, 2-D bridge analyses should be considered to complement girder line analyses for high skew bridges. 2-D analyses were computationally efficient, in addition to being accurate.
- Excluding secondary components and non-composite action over piers from 2-D bridge models can lead to slightly conservative and similar load distribution predictions, respectively, and may be considered for preliminary design.
- Experimental and analytical results showed that WisDOT practice of excluding moment skew correction factors is reasonable and should continue. In addition, a continuity correction factor for moment and shear may be considered to add a reasonable safety margin for continuous bridges.

- At high skew angles, bearing transverse displacements can be several times the ones occurring in non-skewed bridges. The use of 2-D bridge models is recommended to accurately predict amplified superstructure transverse movements.
- Bridge displacements in racking and normal-to-expansion joint directions should be calculated from geometry and trigonometry using the longitudinal and transverse girder end displacements obtained from temperature loadings. Girder bearing plates and expansion joints should be large enough to prevent unseating of girders and closing of expansion joints, respectively. In addition, a sufficiently large gap that can accommodate temperature displacements should be left between girder ends and abutment back wall to prevent girders being pushed laterally by the abutment back wall.
- Since racking and expansion joint displacements are proportional to larger longitudinal displacements and the sine and cosine of the skew angle, these displacements can be minimized by using prestressed girders that have smaller temperature displacements than steel girders. However, the higher stiffness of prestressed girders may worsen cracking in deck under shrinkage loading.
- The use of a mixed fixity arrangement over piers should be considered on three-span bridges as they can significantly reduce transverse superstructure movements, and lead to uniform deformations in comparison to typical support fixity configurations. The following recommendations should be considered when bearing arrangement is used:
 - The mixed bearing arrangement should be employed on highly skewed bridges ($>30^\circ$), reviewed on a project-by-project basis for bridges with low skew angles ($<30^\circ$), and avoided on non-skewed bridges.
 - Pier stiffness can affect the performance of the special fixity arrangement. Including piers in 2-D models is recommended in order to have a reasonable prediction of the mixed arrangement performance. For high skew angles, control of bearing transverse displacements is expected to be significant regardless of pier type with the use of the mixed bearing arrangement. Hammerhead piers benefit from the mixed bearings the least among all pier types investigated.
 - The mixed bearing configuration should be evaluated on a project-by-project basis for significantly wide or long bridges, as these bridges benefit from the mixed bearing arrangements less than other bridges do. Nevertheless, at high skew angles, the mixed bearing arrangement was effective for all bridge geometries.
- Bridge models that exclude piers to estimate fixed bearing forces should be avoided since they could lead to overly conservative bearing forces. Where appropriate, pier flexibility should be included in bridge models to reduce lateral bearing forces to realistic magnitudes. Assuming that superstructure and piers are subject to equal thermal changes may lead to significantly smaller bearing lateral forces. Since this assumption is not conservative, it should be verified.
- Diagonal cracking on highly skewed bridges may be controlled by incorporating the following recommendations:
 - The main contributor to diagonal cracking is shrinkage. Concrete mixes and construction practices that control shrinkage are recommended.
 - Bridge details that restrain the volumetric concrete contraction caused by shrinkage should be avoided. Full-depth concrete end diaphragms and laterally restrained expansion bearings provide such restraints.
 - The mixed bearing arrangement over the same piers improved deck cracking; and should be considered as a crack control method in three-span girder bridges.
 - Increasing deck reinforcement amount or orienting deck reinforcement along skew are not effective methods to control diagonal cracking and should not be considered. In fact, increased deck reinforcement may lead to more cracking, since reinforcement also restrains shrinkage.

11. REFERENCES

1. WisDOT Bureau of Structures. (2015). "Highway Structures Information (HSI)." <http://on.dot.wi.gov/dtid_bos/extranet/structures/LRFD/index.htm>. (December 2014).
2. Hambly Edmund C. (1991). Bridge Deck Behaviour, Chapman & Hall, London.
3. Fu, G., et al. (2007). "Bridge Deck Corner Cracking on Skewed Structures." Lansing, MI, 153.
4. Bou Diab, F., Mabsout, M., and Tarhini, K. (2011). "Influence of Skew Angle on Live Load Moments in Steel Girder Bridges." Bridge Structures, 7(4), 151-163.
5. Ebeido T. and Kennedy J. B. (1996). "Girder Moments in Continuous Skew Composite Bridges." Journal of Bridge Engineering, 1(1), 37-45.
6. Nutt, R. V., Schamber, R. A., and Zokaie, T. (1988). "Distribution of Wheel Loads on Highway Bridges." National Cooperative Highway Research Program (NCHRP), Project Report 12-26, Washington, DC.
7. Ebeido T. and Kennedy J. B. (1995). "Shear Distribution in Simply Supported Skew Composite Bridges." Canadian journal of civil engineering, 22(6), 1143-1154.
8. Ebeido T. and Kennedy J. B. (1996). "Shear and Reaction Distributions in Continuous Skew Composite Bridges." Journal of Bridge Engineering, 1(4), 155-165.
9. Modjeski and Masters Inc. (2002). "Shear in Skewed Multi-Beam Bridges." National Cooperative Highway Research Program (NCHRP), Project Report 20-7/Task 107, Washington, DC.
10. Huang, H., Shenton, W. H., and Chajes, J. M. (2004). "Load Distribution for a Highly Skewed Bridge: Testing and Analysis." Journal of Bridge Engineering, 9(6), 558-562.
11. Keogh Damien L. and O'Brien Eugene J. (2005). Bridge Deck Analysis, Taylor & Francis Group, New York.
12. Coletti, D., Chavel, B., and Gatti, W. (2005). "The Problems of Skew." Proc., Proceedings of the 2005 World Steel Bridge Symposium.
13. Burke Jr. Martin P. (2009). Integral and Semi-integral Bridges, John Wiley & Sons, Iowa.
14. Larson, T. D., Cady, P. D., and Price, J. T. (1968). "Review of a Three-year Bridge Deck Study in Pennsylvania." Highway Res. Rec. 266, 11-25, Washington, DC.
15. Schmitt, T. R. and Darwin, D. (1995). "Cracking in Concrete Bridge Decks." Rep. K-TRAN:KU-94-1, University of Kansas Center for Research, Inc., Kansas Department of Transportation, Topeka, KS.
16. Krauss, P. D. and Rogalla, E. A. (1996). Transverse Cracking in Newly Constructed Bridge Decks, National Cooperative Highway Research Program, Washington, DC.
17. Saadeghvaziri, M. A. and Hadidi, R. (2002). "Cause and Control of Transverse Cracking in Concrete Bridge Decks." Rep. FHWA-NJ-2002-019, Dept. of Civil and Environmental Engineering, New Jersey Institute of Technology, Newark, NJ.
18. Mokarem, D. W., Russell, H., and Khan, M. (2009). "High Performance Concrete Bridge Deck Investigation." Rep. FHWA-HRT-10-028, U.S. Dept. of Transportation, Federal Highway Administration, McLean, VA.
19. Stringer, D. J. and BURGUEÑO, R. (2012). "Identification of Causes and Solution Strategies for Deck Cracking in Jointless Bridges." Rep. RC-1571. Dept. of Civil and Environmental Engineering, Michigan State Univ., East Lansing, MI.
20. Sonntag, S. and Yoerger, G. (2014). "Inspection Report for B-13-513 Old Middleton Road Over Wisconsin & Southern RR " Insp. Rep. B-13-513, Wisconsin Department of Transportation, Madison, WI.
21. Beckmann, F. and Medlock R. D. (2005). "Skewed Bridges and Girder Movements Due to Rotations and Differential Deflections." Proc., Proceedings of the 2005 World Steel Bridge Symposium.
22. American Association of State Highway and Transportation Officials (2014). "AASHTO LRFD Bridge Design Specifications". Washington, DC.
23. Wisconsin Department of Transportation (WisDOT) (2015). "Bridge Manual." Madison, WI.
24. New York State Department of Transportation (NYSDOT) (2006). "Bridge Manual." Albany, NY.
25. Connecticut Department of Transportation (ConnDOT) (2003). "Bridge Design Manual." Newington, CT.
26. Minnesota Department of Transportation (MnDOT) (2003). "LRFD Bridge Design Manual." Oakdale, MN.
27. Ohio Department of Transportation (ODOT) (2007). "Bridge Design Manual." Columbus, OH.
28. Michigan Department of Transportation (MDOT). "Bridge Design Manual." Lansing, MI.
29. Vermont Agency of Transportation (VTrans) (2010). "VTrans Structures Design Manual." Montpelier, VT.

30. Massachusetts Department of Transportation (MassDOT) (2013). "LRFD Bridge Manual." Boston, MA.
31. New Jersey Department of Transportation (NJDOT) (2009). "Design Manual for Bridges and Structures." Ewing Township, NJ.
32. Indiana Department of Transportation (INDOT) (2013). "Design Manual." Indianapolis, IN.
33. New Hampshire Department of Transportation (NHDOT) (2015). "Bridge Design Manual." Concord, NH.
34. Maine Department of Transportation (MaineDOT) (2003). "Bridge Design Guide." Augusta, ME.
35. Illinois Department of Transportation (IDOT) (2012). "Bridge Manual." Springfield, IL.
36. Pennsylvania Department of Transportation (PennDOT) (2015). "Design Manual, Part 4: Structures." Harrisburg, PA.
37. State of Rhode Island Department of Transportation (RIDOT) (2007). "LRFD Bridge Design Manual." Providence, RI.
38. Texas Department of Transportation (TxDOT) (2013). "Bridge Design Manual - LRFD." Austin, TX.
39. Washington State Department of Transportation (WSDOT) (2015). "Bridge Design Manual." Olympia, WA.
40. Puckett, J. A., et al. (2006). "Simplified Live Load Distribution Factor Equations." National Cooperative Highway Research Program (NCHRP), Project Report 12-62, Washington, DC.
41. Walpole, E. R., et al. (2012). Probability & Statistics for Engineers & Scientists, Prentice Hall, Boston, MA.
42. Computers and Structures, I. (2014). CSiBridge 16.1, Version 16.1.
43. Dassault Systèmes Simulia Corporation. (2016). ABAQUS 6.16-1, Version 6.16, Providence, RI.
44. Computers and Structures Inc. (2016). "CSI Analysis Reference Manual." Berkeley, CA, 534.
45. Dassault Systèmes Simulia Corporation (2009). "RI USA Dassault Systmes Abaqus Analysis Users Manual."
46. The International Federation for Structural Concrete (2013). "FIB Model Code for Concrete Structures 2010." 434.
47. Okumus, P., Oliva, M. G., and Becker, S. (2012). "Nonlinear Finite Element Modeling of Cracking at Ends of Pretensioned Bridge Girders." Engineering Structures, 40(0), 267-275, <http://dx.doi.org/10.1016/j.engstruct.2012.02.033>.
48. Oliva, M. G. and Okumus, P. (2011). "Finite Element Analysis of Deep Wide-Flanged Pre-stressed Girders to Understand and Control End Cracking." WHPR 11-06. Wisconsin Department of Transportation, Madison, WI, 128.
49. Okumus, P. and Oliva, M. G. (2013). "Evaluation of Crack Control Methods for End Zone Cracking in Prestressed Concrete Bridge Girders." PCI Journal, 58(2), 91-105.
50. Diaz Arancibia, M. and Okumus, P. (2017). "Causes of Excessive Detensioning Stresses in Northeast Extreme Tee (NEXT) Beams." PCI Journal, 62(3), 31-45.
51. Okumus, P., Kristam, R., and Diaz Arancibia, M. (2016). "Sources of Crack Growth in Pretensioned Concrete-Bridge Girder Anchorage Zones after Detensioning." Journal of Bridge Engineering, 04016072, 10.1061/(ASCE)BE.1943-5592.0000928.
52. Okumus, P. and Oliva, M. G. (2014). "Strand Debonding for Pretensioned Bridge Girders to Control End Cracks." ACI Structural Journal, 111(1), 201-210.
53. Okumus, P., Kizilarslan, E., and Oliva, M. G. (2016). "Anchorage Zone Cracking Evaluations in Debonded Deep Bulb-Tee Bridge Girders." Proc., PCI Convention and National Bridge Conference, Nashville, TN, March 3-6, Paper 34: 11.
54. Okumus, P. (2012). "Nonlinear Analysis of Pretensioned Bridge Girder Ends to Understand and Control Cracking at Prestress Release." PhD Dissertation, University of Wisconsin-Madison, Madison, WI, 199.
55. Mindess, S., Young, F., and Darwin, D. (2003). "Concrete." Upper Saddle River, NJ, 644.
56. ACI Committee 209 (2008). "209.2R-08 Guide for Modeling and Calculating Shrinkage and Creep in Hardened Concrete."
57. Diaz Arancibia, M. and Okumus, P. (2018). "Load Testing of Highly Skewed Concrete Bridges." ACI Special Publication, SP-323: Evaluation of Concrete Bridge Behavior through Load Testing - International Perspectives, 2.1-2.18.
58. Wan, B., Foley, C., and Komp, J. (2010). "Concrete Cracking in New Bridge Decks and Overlays." 142.
59. Diaz Arancibia, M., Okumus, P., and Oliva, M. G. (2017). "Review of Skew Effects on Prestressed Concrete Girder Bridges: Problems and Current Practices." Proc., PCI Convention and National Bridge Conference, Cleveland, OH, February 28-March 4, Paper 50: 18.